An extensive review of various technologies for enhancing the thermal and optical performances of parabolic trough collectors

DOI:
10.1002/er.5271

Document Version
Final published version

Received: 9 October 2019 | Revised: 19 January 2020 | Accepted: 20 January 2020

DOI: 10.1002/er.5271

INTERNATIONAL JOURNAL OF ENERGY RESEARCH WILEY

REVIEW PAPER

An extensive review of various technologies for enhancing the thermal and optical performances of parabolic trough collectors

Nabeel Abed[1,2] | **Imran Afgan**[1,3]

[1]Department of Mechanical, Aerospace and Civil Engineering, School of Engineering, University of Manchester, UK

[2]Mechanical Technical Department, Technical Institute of Anbar, Middle Technical University, Anbar, Iraq

[3]Department of Mechanical Engineering, College of Engineering, Khalifa University, Abu Dhabi, UAE

Correspondence
Nabeel Abed, Department of Mechanical, Aerospace and Civil Engineering, School of Engineering, University of Manchester, Manchester M13 9PL, UK.
Email: nabeel.abed@postgrad.manchester.ac.uk

Funding information
Engineering Sustainable Solar Energy and Thermocline Alternatives-ESSEnTiAl, Grant/Award Number: 332271136

Summary

A wide range of engineering industrial applications require both the thermal and optical efficiencies of the system to be maximized with a reasonable low penalty for the friction factor and subsequently low losses in pressure. Among the family of concentrated solar power systems, parabolic trough collectors (PTCs), which have recently received significant attention, face similar challenges. The current work presents an extensive review of the PTC systems comparing recent and past technologies, which are widely being used to improve and enhance the thermal and optical efficiencies. Furthermore, the techniques used for single and two-phase flow modeling in numerical simulations, design variables, and experimental processes have been discussed in detail. The article also presents different numerical methods and analytical approaches of implementing the nonuniform solar distribution with different design parameters. Four main technologies are comprehensively addressed to effectively enhance the thermal performance of the PTCs; changing working heat transfer fluids, replacing the working fluids by nanofluids (single and hybrid) that have higher thermal–physical properties than those of base working fluids, inserting different tabulators with various design configurations, and finally combining the advantages of nanofluids and swirl generators in the same application. The article also critically summarizes the studies investigating the enhancement of thermal performance: use of novel design of PTCs and passive heat transfer enhancement techniques. Finally, a wide range of numerical and experimental studies are proposed for the future work related to the aforementioned main technologies.

KEYWORDS

heat transfer enhancements, nanofluids, parabolic trough solar collectors, solar thermal energy, tabulators, thermal and optical performances

1 | INTRODUCTION

1.1 | Concentrated solar power technology

It is widely known that global warming has become a defining issue of our time, with consequences that include shifting weather patterns, rising sea levels, and compromised food production. To address global warming, clean, renewable, and sustainable sources of energy should be identified to reduce the amount of CO_2 emissions. Solar thermal energy is one of the viable solutions to reduce reliance on fossil fuels, decrease the level of greenhouse-gas emissions, and meet the requirements of human societies with electrical power, water heating systems, and other industrial processes. Concentrated solar power (CSP) plants, in particular, rely on the direct normal irradiance, which can be described as the amount of solar energy received per unit area on the surface held normal to the rays of the sun. CSP plant technology can be categorized into four main families depending on the method used to collect and concentrate the solar radiant energy: (a) parabolic trough collectors (PTCs), (b) linear Fresnel reflectors, (c) parabolic dishes, and (d) solar towers. The operating principle of each technology is shown in Figure 1 (Blanco and Miller[1]), while their main properties are listed in Table 1 (Philibert and Frankl[2]). Presently, the most cost-effective and commercially developed technology among CSPs is the PTC system, particularly for medium-temperature applications, thus these systems are the subject of the present review.

1.2 | Fundamentals of PTC

As shown in Figures 2 and 3, PTC systems can be basically regarded as large heat exchangers, with the major components being the solar absorber, the glass envelope, the positioning system, the support structure, and the reflector surface; some of the main components of PTC systems are described below.

1.2.1 | Reflectors

This element consists of high specular reflectance (more than 88%) mirrors and structural components used to reflect the solar energy onto the receiver. Mirrors are

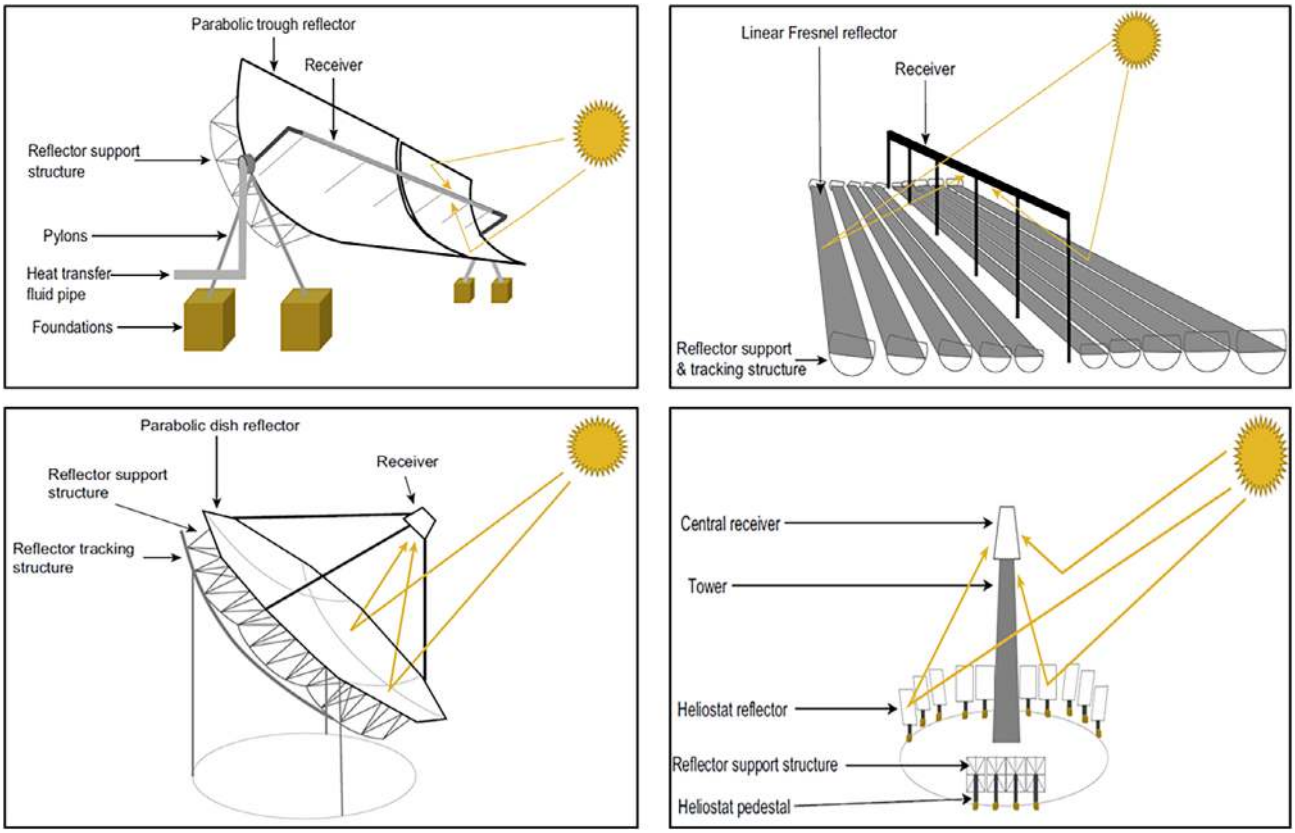

FIGURE 1 Current concentrated solar power technologies, Blanco and Miller,[1] license number: 4751880835903 [Colour figure can be viewed at wileyonlinelibrary.com]

TABLE 1 The main properties of the four concentrated solar power technologies, Philibert and Frankl[2]

Focus category		Line focus	Point focus
Absorber category		The sun is tracked along a single axis by collectors with focusing the irradiance only on a linear absorber making the tracking sun simpler.	The sun is tracked along two axes by collectors with focusing the irradiance only on a single point absorber allowing for larger temperature.
Fixed	A fixed absorber is a stationary tool and it is independent of the focusing apparatus. However, the transfer of the collected thermal energy to the power section is easier.	Linear Fresnel reflectors	Central receiver
Mobile	The mobile absorber moves together with the concentrating apparatus. However, more energy can be collected by both mechanisms (point focus and line focus).	Parabolic trough collectors	Parabolic dishes

normally made from low-iron float glass (approximately 4 mm thickness) of large solar transmittance, silvered from the back, and coated with selective coatings to maximize their solar reflectance (SR = 0.93) and durability. The installation, as well as the mounting of the structures, has a large effect on the overall performance of the plant (Kreith and Goswami[3]).

1.2.2 | Absorber tube

The solar receiver converts the absorbed incident solar radiation into the thermal energy which is carried through the absorber via the heat transfer fluid (HTF; described below). This component (also called a heat collection element [HCE] or receiver) is the most important element in the PTC system, and is made typically from a steel tube that is coated with a multilayer cermet coating to provide very good optical properties, low thermal emissivity, and large solar absorptivity. Its length is generally 4 m between the two support braces and might be extended to 150 m. The inner and outer diameters of the absorber tube are typically of about 66 mm and 70 mm, respectively, whereas the inner and outer diameters of the glass envelope are of about 115 mm and 120 mm (Price et al[4]). The annular space between the absorber tube and the glass envelope is generally kept at vacuum conditions (air pressure in the gap typically maintained at 0.013 Pa) to further reduce the heat losses (Hachicha et al[5]).

1.2.3 | Heat transfer fluid

The function of the HTF is to collect the thermal energy absorbed by the receiver and to transport it to the storage system or directly to the power block in the case of solar thermal power plant (STPP) application. Selecting the appropriate HTF is application-specific and depends on the operating conditions and design peculiarities of each installation. Ideally, HTFs should have good thermal stability, should be able to operate safely throughout the range of temperatures of interest, should have good chemical compatibility with the tubing wall materials, and finally should be low cost and environmentally friendly. Additionally, a high thermal conductivity, high heat capacity, and large heat transfer coefficient are normally desired to maximize the heat transfer effectiveness, together with a low viscosity and a small thermal expansion coefficient to reduce pumping power and thermal expansion concern (Nahhas et al[6]).

The main objective of this article is to critically review experimental and numerical investigations carried out on the thermal and optical performances of PTC systems, focusing specifically on reducing the thermal losses, reducing pumping power requirements, and enhancing the thermal efficiency by changing the working fluid, using nanofluids (single and hybrid) or by inserting swirl generators inside the absorber tubes. Another important objective is to discuss in details the effect of collector design on the thermal and optical performances taking into account shape parameters, mirror structure, absorber design, tracking system, absorber ends, absorber materials, and envelope characteristics. In comparison with recently published review papers on solar thermal energy, such as Jebasingh and Herbert,[7] Abdulhamed et al,[8] and Bellos and Tzivanidis,[9] this article differs in terms of scope, focus, and coverage. In particular:

- The scope is here restricted to PTC systems and their applications, as documented in available experimental

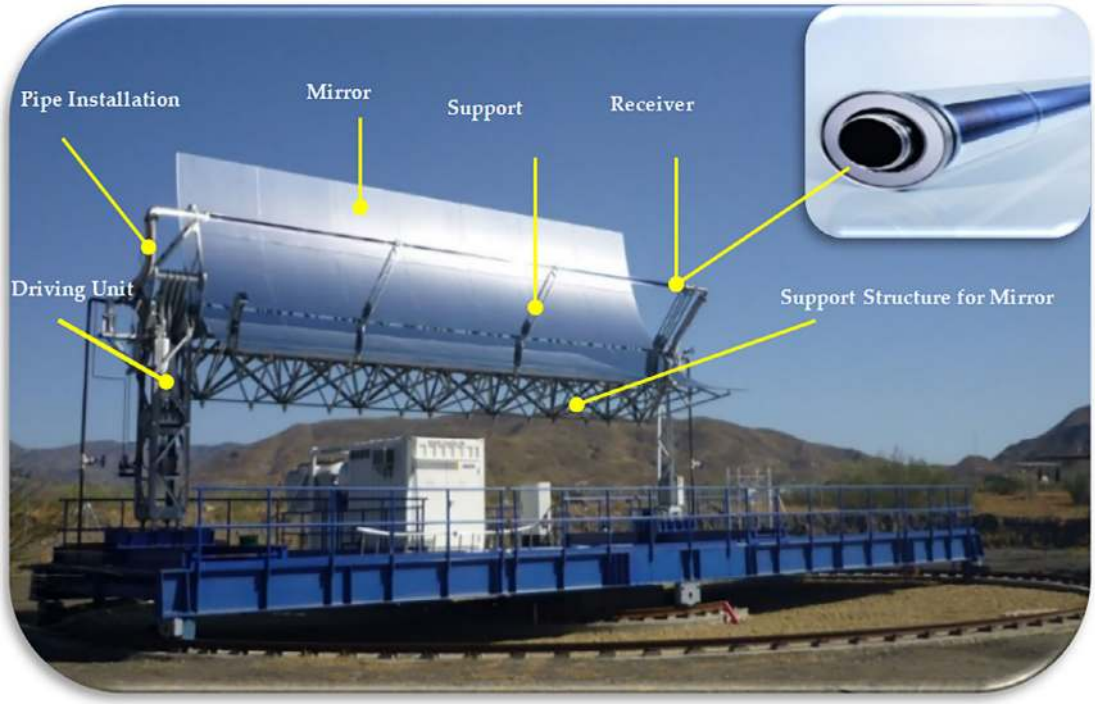

FIGURE 2 The structure and elements of parabolic trough collector, from www.dlr.de.com[12] [Colour figure can be viewed at wileyonlinelibrary.com]

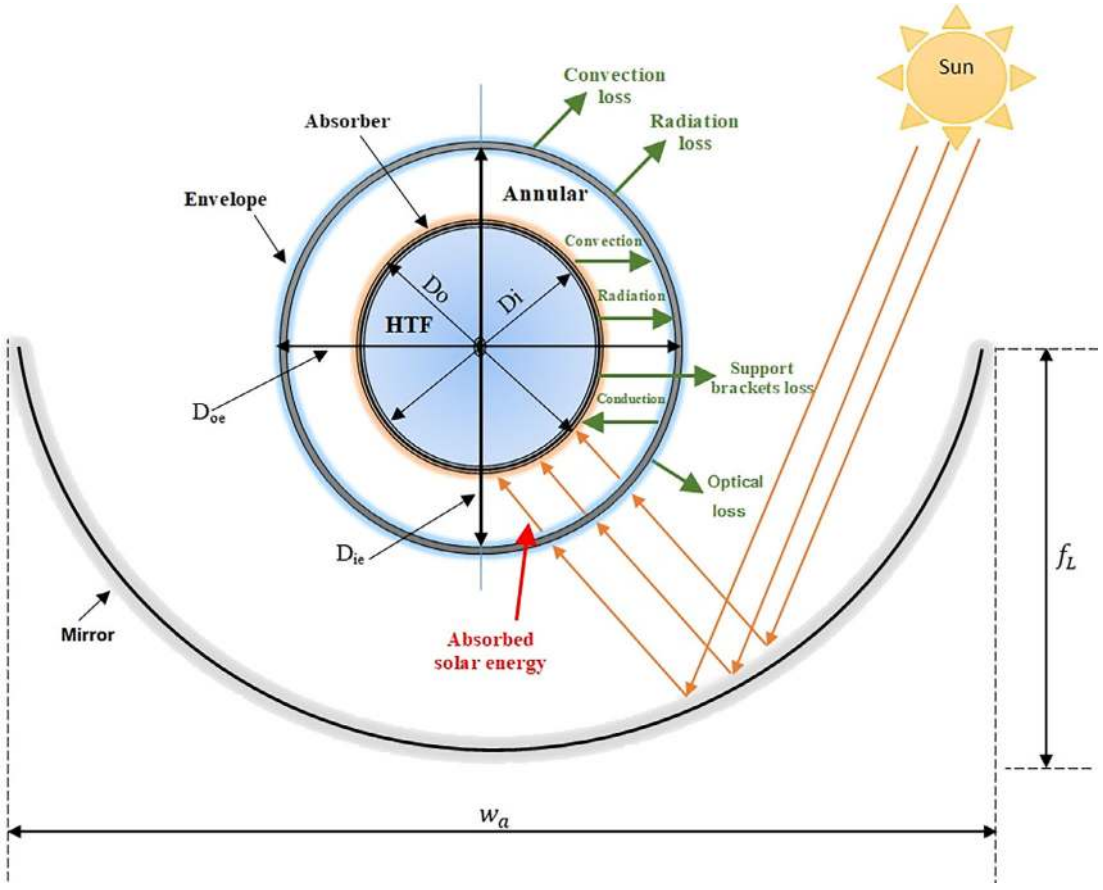

FIGURE 3 The schematic cross section of a typical parabolic trough collector [Colour figure can be viewed at wileyonlinelibrary.com]

and numerical scientific studies dating as far back as 1986.
- The present work provides a comprehensive account of promising technologies that can be used to improve the thermal performance of PTC systems (notably, nanofluids and swirl generators), and includes a critical assessment of the techniques that have been devised to take into account the nonuniform heat flux distribution of solar receivers.
- The present work includes a comprehensive account of available models for estimating the thermo-physical properties of nanofluids for use in practical applications.
- Providing important data for thermo-physical properties of single and hybrid nanofluids over a range of fluid inlet temperature and different particle sizes.

The practical significance of PTC systems is rather broad: to date, PTC systems have been successfully used in a range of applications, including power generation, water treatment (desalination and/or pasteurization), air conditioning and refrigeration, and hot water production, as summarized in Table 2 where selected key reference studies are also included.

2 | MATHEMATICAL FORMULATIONS OF PTCs

Figure 3 schematically illustrates a typical PTC system, which consists of a tubular receiver located along the focal line of the parabolic trough (mirrors). The receiver includes a metallic tube (externally covered by a selective coating) where the HTF flows, which is contained within an annular envelope usually made from glass. The heat transfer models for PTC systems are based on the thermal energy balance between the working fluid and the surrounding. Radiant energy from the sun is concentrated onto the receiver: part of this energy is absorbed by the HTF. Some of this energy is sent back to the glass envelope by radiation and natural convection, and some of it is lost via the support brackets by conduction mode. The last part (lost energy) can cross to the glass envelope by conduction as well and then from the glass envelope would pass it to the ambient by convection and to the sky by radiation.

TABLE 2 Main engineering and industrial applications of parabolic trough collectors utilized in the preceding studies

No.	Main application type	References
1	Electrical power generation	Larrain et al,[10] Hachicha et al[5]
2	Water desalination process	Jafari et al,[11] Raja and Vijay[12]
3	Water pasteurization process	Bigoni et al[13]
4	Air-conditioning and solar refrigeration	Fadar et al,[14] Al-Alili et al[15]
5	Hot water production	Hewett et al[16]
6	Pumping irrigation water	Larson[17]
7	Solar cooker	Noman et al[18]
8	Industrial processes	Larcher et al,[19] Kizilkan et al[20]

2.1 | Mathematical analysis of the geometrical design

The geometrical profile of the typical PTC can be described by the following expression (Duffie and Beckman[21]):

$$x^2 = 4yf_L. \tag{1}$$

The parameter f_L is the focal line, which represents the position of the solar receiver. This parameter is determined by the following formula:

$$f_L = \frac{w_a}{4\tan\left(\frac{\varphi}{2}\right)}. \tag{2}$$

In the equation above, w_a is the width of the collector's aperture and φ_r represents the rim angle. This angle can be calculated by the following expression:

$$\varphi_r = tan^{-1}\left[\frac{8\left(\frac{f}{w_a}\right)}{16\left(\frac{f_L}{w_a}\right)^2 - 1}\right] = sin^{-1}\left(\frac{w_a}{2r_r}\right). \tag{3}$$

The variable r_r is the rim radius which can be obtained from the following formula:

$$r_r = \frac{2f_L}{1 + cos\varphi_r}. \tag{4}$$

Other important parameters related to the collector's geometry are the total collector aperture area A_a and the outer surface area of the solar absorber A_o, which can be calculated as follows:

$$A_a = w_a L \tag{5}$$

$$A_o = \pi D_o L. \tag{6}$$

The parameter L is the length of the collector aperture. From the above equations, the geometrical

concentration ratio (GCR) represents the collector's aperture area to the outer surface area of the absorber as following:

$$\mathrm{GCR} = \frac{A_a}{A_o}. \tag{7}$$

2.2 | Optical analysis of PTC's design

In this section, the optical efficiency and other related parameters are discussed. Based on the energy balance concept, the solar irradiation absorbed (Q_{abs}) by the collector is divided into two main parts; useful energy (Q_u) and heat losses (Q_{loss}) as follows:

$$Q_{\mathrm{abs}} = Q_u + Q_{\mathrm{loss}}. \tag{8}$$

The typical optical efficiency (η_o) of the PTC is calculated from the absorbed solar energy (Q_{abs}) divided by the available solar energy (Q_s) as given below:

$$\eta_o = \frac{Q_{\mathrm{abs}}}{Q_s}. \tag{9}$$

The typical optical efficiency (η_o) varies with changing the incidence angle (θ) of the solar irradiation which can also be modeled and obtained depending on the incidence angle modifier (K) from the following expression:

$$K(\theta) = \frac{\eta_o(\theta)}{\eta_{o,\max}}. \tag{10}$$

The modifier $K(\theta)$ is a function of geometrical parameters of the PTC additional to the incidence angle, which can be given by the following formula derived by Gaul and Rabl[22]:

$$K(\theta) = \cos(\theta) - \frac{f_L}{L}\left(1 + \frac{w_a^2}{48 f_L^2}\right)\sin(\theta). \tag{11}$$

The previous expression considered the end loss of the PTC and cosine loss leads to calculating an accurate expression of the optical efficiency. The parameter ($\eta_{o,\max}$) represents the maximum optical efficiency of the typical PTC, which is given by:

$$\eta_{o,\max} = \rho_{\mathrm{opt}}\gamma\tau\alpha. \tag{12}$$

The parameters (ρ_{opt}, γ, τ, and α) are the optical reflectance, the intercept factor, the envelope transmittance and the receiver absorbance, respectively. For the optimum design of the commercial PTC, the intercept factor value is close to 1. However, the envelope transmittance and the receiver absorbance are design-specific variables that usually vary between 0.9 and 0.95. The optical reflectance takes usually values between 0.9 and 0.93 depending on all possible optical errors such as tracking error, shading coefficient, and so forth. Therefore, the maximum optical efficiency of a conventional PTC with a zero incidence angle is approximately 75% (Behar et al[23]).

2.3 | Thermal analysis of PTC's system

In this section, the main parameters related to the thermal performance of the PTC are presented. These include the thermal efficiency, the thermal exergy, the solar available radiation, the useful exergy and useful energy, the heat transfer behavior, the friction factor, and the related pressure drop. The useful thermal energy (Q_u [W]) carried by the HTF is determined by using the thermal energy balance on its control volume, which is given in the following equation (Duffie and Beckman[21]):

$$Q_u = \dot{m} C_p (T_{\mathrm{out}} - T_{\mathrm{in}}). \tag{13}$$

The solar energy (Q_s [W]) that is absorbed by the solar collector can be determined as the solar beam radiation (G_b [W/m^2]) multiplied by the reflector aperture area (A_a) as reported in the equation below:

$$Q_s = A_a G_b. \tag{14}$$

Then, the collector thermal efficiency is the ratio of the useful thermal energy to the absorbed solar energy, which can be given in the following expression:

$$\eta_{\mathrm{th}} = \frac{Q_u}{Q_s}. \tag{15}$$

However, the overall collector efficiency is the ratio of the useful thermal energy to the absorbed solar energy taking the effect of pumping power into consideration, as suggested by Wirz et al[24] as follows:

$$\eta_{\mathrm{overall}} = \frac{Q_u - W_p/\eta_{\mathrm{el}}}{Q_s}, \tag{16}$$

where η_{el} is the electrical efficiency of the power block which was taken as 32.7%. However, W_p is pumping power (W) and can be calculated by the following equations:

$$W_p = \Delta P \dot{V}, \tag{17}$$

where $\dot{V}$ is volumetric flow rate (m^3/s) and ΔP is the pressure drop (Pa) which can be calculated by using the Darcy–Weisbach equation as follows:

$$\Delta P = f \frac{L}{D_i} \frac{\rho U^2}{2} \tag{18}$$

$$f = \frac{8\tau}{\rho U^2}, \tag{19}$$

where f is friction factor, U is the fluid velocity (m/s), L is the absorber length (m), D_i is the inner absorber diameter (m), ρ is the fluid density (kg/m^3), and τ is the wall shear stress (Pa). The useful thermal exergy (E_u [W]) output from the solar collector can be calculated from the following equation (Yazdanpanahi et al[25]):

$$E_u = Q_u - \dot{m} C_p T_{\text{am}} \ln\left(\frac{T_{\text{out}}}{T_{\text{in}}}\right) - \dot{m} T_{\text{am}} \frac{\Delta P}{\rho T_f}, \tag{20}$$

where T_f represent the average fluid temperature (K) and T_{am} is the ambient temperature (K). The last term of pressure drop is typically very small in practical applications, especially with liquids working fluids, and can therefore be neglected.

The available solar exergy (E_s [W]) can be calculated from the following equation suggested by Petela[26]:

$$E_s = Q_s \left[1 - \frac{4}{3}\left(\frac{T_{\text{am}}}{T_{\text{sun}}}\right) + \frac{1}{3}\left(\frac{T_{\text{am}}}{T_{\text{sun}}}\right)^4\right]. \tag{21}$$

The sun temperature in the above equation is (5800 K) which is the real temperature in its outer layer. The exergetic efficiency then can be calculated as the ratio of the useful exergy to the input exergy, as follows:

$$\eta_{\text{ex}} = \frac{E_u}{E_s}. \tag{22}$$

It is very important to take the exergetic efficiency into account because it is related to the maximum possible produced work. However, the thermal losses (Q_{loss} [W]) from the outer surface of the absorber tube to the inner surface of the glass envelope are represented by the thermal radiation and thermal natural convection which can be written as follows (Bhowmik and Mullick[27]):

$$Q_{\text{loss}} = \frac{\pi D_o L \sigma\left(T_o^4 - T_{\text{ie}}^4\right)}{\frac{1}{\varepsilon_o} + \frac{1-\varepsilon_{\text{ie}}}{\varepsilon_{\text{ie}}}\frac{D_o}{D_{\text{ie}}}} + \frac{2\pi L k_{\text{eff}}}{\ln\left(\frac{D_{\text{ie}}}{D_o}\right)}(T_o - T_{\text{ie}}). \tag{23}$$

The variable k_{eff} is the effective thermal conductivity, which can be calculated from the following expression:

$$k_{\text{eff}} = k\left\{0.386[Pr/(0.861+Pr)]^{0.25}\left[\frac{(\ln(D_{\text{ie}}/D_o)^4}{b^3\left[D_o^{-0.6} + D_{\text{ie}}^{-0.6}\right]^5} Ra_b\right]^{0.25}\right\}, \tag{24}$$

where b in the above equation is $(0.5(D_{\text{ie}} - D_o))$, and Ra_b represents the Rayleigh number based on the gap between the absorber tube and glass envelope, and can be expressed by:

$$Ra_b = \frac{g\beta(T_o - T_{\text{ie}})b^3}{\nu^2} Pr. \tag{25}$$

The parameter β represents the thermal expansion coefficient $1/K$ and g is the gravitational acceleration (m/s^2). Nevertheless, the thermal losses in the annular space when operated under vacuum conditions are represented by only radiation mode since the pressure is too low and the free molecular convective heat transfer can be neglected. Thus, the radiation heat loss from the outer surface of the solar absorber to the inner surface of the glass envelope can be given in the following equation (Duffie and Beckman[21]):

$$Q_{\text{loss}} = \frac{\pi D_o L \sigma\left(T_o^4 - T_{\text{ie}}^4\right)}{\frac{1}{\varepsilon_o} + \frac{1-\varepsilon_{\text{ie}}}{\varepsilon_{\text{ie}}}\frac{D_o}{D_{\text{ie}}}}. \tag{26}$$

The subscripts i and o refer to the inner and outer surfaces of the absorber tube, respectively, while ie and oe refer to the inner and outer surfaces of the glass envelope, respectively, and ε is the surface emissivity. Depending on the concept of energy balance on the solar collector, it is obvious that the heat losses from the solar receiver to the glass envelope is the same as the thermal energy transferred by conduction through the glass envelope and from the glass envelope to the surroundings by radiation and to the ambient by convection. As such, the thermal losses from the glass envelope can also be calculated as follows (Bhowmik and Mullick[27]):

$$Q_{\text{loss}} = L\pi D_{\text{oe}} h_{\text{out}}(T_{\text{oe}} - T_{\text{am}}) + L\pi D_{\text{oe}} \sigma \varepsilon_{\text{oe}}\left(T_{\text{oe}}^4 - T_{\text{sky}}^4\right), \tag{27}$$

where σ is Stefan–Boltzmann constant which is approximately 5.67×10^{-8} W/m^2 K^4 and ε_{oe} represents the emissivity of the glass envelope which depends strongly on the temperature of the outer surface of the glass envelope and its material made from. The convection heat transfer coefficient of the ambient can be calculated from the equation below, as suggested by Bhowmik and Mullick[27]:

$$h_{out} = 4V_w^{0.58} D_{oe}^{-0.42}. \quad (28)$$

The parameter V_w is the wind speed, which is normal to the axis of the solar receiver. However, the sky temperature is a function of ambient temperature and can be given by the following equation (Swinbank[28]):

$$T_{sky} = 0.0552\, T_{am}^{1.5}. \quad (29)$$

It should be noted that in the case of removing the glass envelope entirely from the PTC system, the thermal losses would transfer directly from the absorber tube to the ambient and surrounding, that is, the parameters of absorber tube should be used instead of those of the glass envelope in the thermal losses expression (Equation (27)) resulted in the following formulation:

$$Q_{loss} = L\pi D_o h_{out}(T_o - T_{am}) + L\pi D_o \sigma \varepsilon_o \left(T_o^4 - T_{sky}^4\right). \quad (30)$$

The emissivity of the solar receiver ε_o depends strongly on the temperature of the outer surface of the solar receiver, receiver materials, and selective coatings. However, the convection heat transfer coefficient of the ambient in the case of removing the glass envelope can be calculated from the following formulation:

$$h_{out} = 4V_w^{0.58} D_o^{-0.42} \quad (31)$$

In addition to the previous equations of the useful thermal energy, the thermal energy transferred from the wall absorber to HTF is the main parameter of heat transfer analysis, which strongly depends on the convection heat transfer coefficient. Therefore, the useful thermal energy can also be given in the form below (Duffie and Beckman[21]):

$$Q_u = h A_i (T_i - T_f). \quad (32)$$

The parameter A_i is the inner surface area of the absorber tube. However, the convection heat transfer coefficient is determined from the Nusselt number Nu, which depends on the absorber geometry and flow conditions. Besides, two important nondimensional numbers are involved in the calculation of Nu number: the Reynolds number Re and Prandtl number Pr. For the case of solar absorber, these numbers (Nu, Re, and Pr) are given in the equations below (Incropera et al[29]):

$$Nu = \frac{hD_i}{k} \quad (33)$$

$$Re = \frac{\rho U D_i}{\mu} \quad (34)$$

$$Pr = \frac{\mu C_p}{k}. \quad (35)$$

The variables k, ρ, U, μ, and C_p are fluid thermal conductivity (W/m K), fluid density (kg/m^3), fluid velocity (m/s), fluid dynamic viscosity (Pa s), and fluid specific heat capacity (J/kg K), respectively. In the solar absorber, the turbulent flow occurs with Re number greater than or equal to 4000 and Nu number can be predicted with empirical correlations for turbulent pipe flow, such as those of Petukhov[30] or Gnielinski[31] reproduced below:

$$Nu = \frac{\left(\frac{f}{8}\right) Re\, Pr}{1.07 + 12.7\left(\frac{f}{8}\right)^{0.5}\left(Pr^{\frac{2}{3}} - 1\right)} \text{ for } \left\{ \begin{array}{r} 0.5 \le Pr \le 2000 \\ 10^4 < Re < 5 \times 10^6 \end{array} \right\} \quad (36)$$

$$Nu = \frac{\left(\frac{f}{8}\right)(Re - 1000)\, Pr}{1 + 12.7\left(\frac{f}{8}\right)^{0.5}\left(Pr^{\frac{2}{3}} - 1\right)} \text{ for } \left\{ \begin{array}{r} 0.5 \le Pr \le 2000 \\ 3 \times 10^3 < Re < 5 \times 10^6 \end{array} \right\}. \quad (37)$$

Either of these two equations can be used for the validation (the latter is in fact a modification of the former to extend its range of validity to lower Reynolds number values; where the ranges of applicability overlap the two correlations provide comparable predictions). The variable f is the friction factor, which strongly depends on the Re number and can be given by the turbulent flow correlation of Petukhov[30] or that of Mwesigye et al[32]:

$$f = \left(0.75\, Ln\, Re^{-1.64}\right)^{-2} \text{ for } \left\{3000 < Re < 5 \times 10^6\right\} \quad (38)$$

$$f = 0.173\, Re^{-0.1974} \text{ for } \left\{1.02 \times 10^4 < Re < 7.38 \times 10^5\right\}. \quad (39)$$

However, for tubular flow in laminar conditions when Re $\le$ 2300, the Nu number (at constant heat flux) and friction factor can be predicted as follows (Incropera et al[29]):

$$Nu = 4.36 \tag{40}$$

$$f = \frac{64}{Re}. \tag{41}$$

3 | LITERATURE REVIEW OF PTCS

3.1 | Experimental studies

This section discusses only the most important experimental studies showing the experimental set up, main findings, design parameters, and operational conditions under different climates such as United States, United Kingdom, France, India, China, Iran, Algeria, Morocco, Greece, and so forth. Dudley et al[33] studied experimentally the effect of thermal losses on the solar collector efficiency through the parabolic solar collector of Solar Electric Generating System plants using different coating materials for the collectors and Syltherm 800 oil as HTF. They proposed experimental correlations of the collector thermal efficiency for all types of annular cases and selective coatings under considerations as summarized in Table 3, where ΔT is the average fluid temperature above the ambient temperature (°C) and I is the solar irradiation (W/m^2).

To estimate the maximum efficiency under dynamic conditions, Xu et al[34] tested an outdoor rig and compared the results with a simple multiple linear regression solver. The reported maximum efficiency for the outdoor rig was around 42%. To further understand the receiver heat losses in the PTC system, Lei et al[35] performed measurements for a new design solar receiver using energy balance for steady and quasi-steady-state equilibrium conditions. Results revealed that the thermal emittance and the receiver temperature, which are very important parameters in the calculation of thermal losses, were both affected by nonuniform heat flux. Moreover, experimental correlations have been proposed of total thermal losses per meter of absorber length for any collector with a glass envelope and restricted to some limitations as clarified in Table 4.

Coccia et al[36] manufactured a low-cost PTC system called UNIVPM.01 to evaluate the thermal efficiency of the collector. Under different operating conditions, they were able to conclude that the thermal efficiency of the collector deteriorated with an increase in the thermal input (the slope efficiency was found to be around −0.683). To study the end losses, Li et al[37] undertook an experimental study with different geometries using the method of reduction; lengthening the receiver, adding end plane mirrors, inclining the PTC, and so forth. Moreover, Wu et al[38] also performed an experimental research to measure thermal losses from the PTC system using a new molten salt characterized with a low melting point of 86°C and operation temperature of 550°C. The working fluid was circulated over 1000 hours in the thermal system; Figure 4 shows the experimental rig equipment. This new molten salt resulted in lower risk at start-up, operation, and shut down of the system, as compared with working fluids with higher melting point. On the other hand, higher thermal loss was obtained compared with the PTC using thermal oil due to higher working temperature of molten salt.

Researchers mentioned in the preceding studies considered the typical type of solar absorber material (ie, steel) whereas Geete et al[39] examined the thermal performance of the fabricated PTC using four arrangements: copper-engine oil (a pipe is made from copper and engine oil is the working fluid), copper-water, mild steel-engine oil, and mild steel-water combinations. According to their results, the highest temperature difference was 59°C using mild steel-engine oil arrangement operated at 12:30 PM with a mass flow rate of 0.0024 kg/s. To study the performance of the solar field as a whole, Kumaresan et al[40] and Sivaram et al[41] investigated experimentally the performance of a PTC with a storage system during the charge process. They measured the solar irradiation intensity using a pyrheliometer at every 15 minutes and temperatures of HTF (water) at inlet and outlet using thermocouples connected with a data acquisition system. Moreover, they measured errors related to the fundamental data, that is, mass flow rate, temperature, and solar insolation using the root sum square approach in order

TABLE 3 Experimental correlations of the collector thermal efficiency proposed by Dudley et al[33]

Parameter	Annular	Coating	Correlations
Thermal efficiency (%)	Vacuum	Cermet	$\eta = 73.3 - 0.007276(\Delta T) - 0.496\left(\frac{\Delta T}{I}\right) - 0.0691\left(\frac{\Delta T^2}{I}\right)$
	Air	Cermet	$\eta = 73.4 - 0.00803(\Delta T) - 9.68\left(\frac{\Delta T}{I}\right) - 0.0669\left(\frac{\Delta T^2}{I}\right)$
	Vacuum	Black chrome	$\eta = 73.6 - 0.004206(\Delta T) + 7.44\left(\frac{\Delta T}{I}\right) - 0.0958\left(\frac{\Delta T^2}{I}\right)$
	Air	Black chrome	$\eta = 73.8 - 0.00646(\Delta T) - 12.16\left(\frac{\Delta T}{I}\right) - 0.0641\left(\frac{\Delta T^2}{I}\right)$

Variable	Limitations	Experimental correlations
$T_{absorber}$	T_{amb}: 10°C-30°C, wind: 0-2 m/s and T_{abs}: 200°C-410°C	$Q_{loss} = 0.1479T_{abs} + 8.1786 \times 10^{-9}T_{abs}^4$
$\Delta T = (T_{glass} - T_{ambient})$	Negligible wind velocity	$Q_{loss} = 5.2057\Delta T + 2.0916 \times 10^{-5}\Delta T^4$

TABLE 4 Experimental correlations of the total heat losses proposed by Lei et al[35]

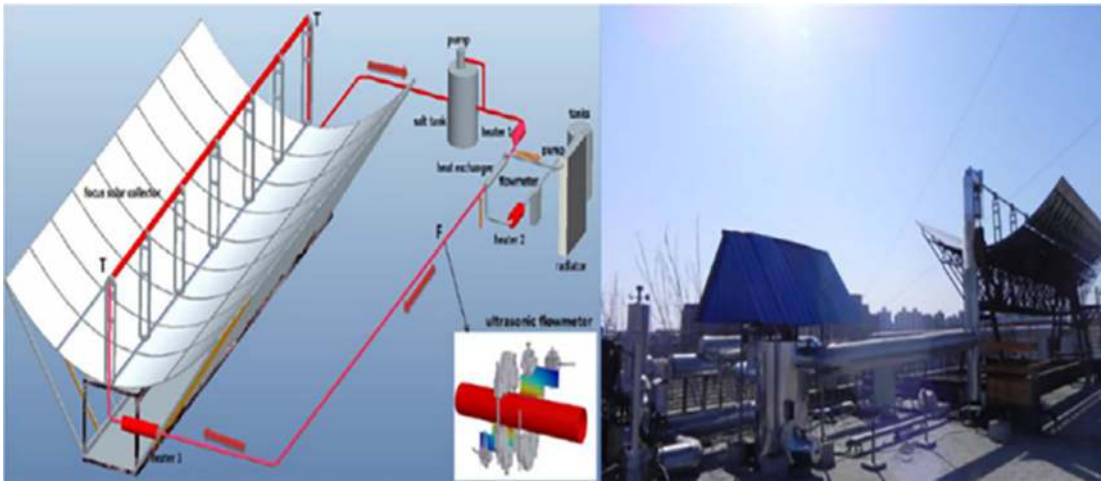

FIGURE 4 The parabolic trough collector system with molten salt as heat transfer fluid, Wu et al,[38] license number: 4742720693544 [Colour figure can be viewed at wileyonlinelibrary.com]

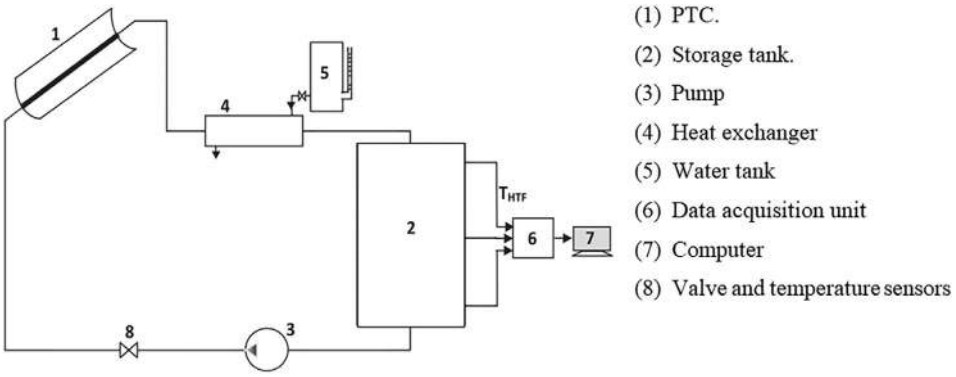

FIGURE 5 Experimental set up of Kumaresan et al,[40] license number: 4742720908250

to determine the collector efficiency. It was pointed out that the instantaneous collector efficiency is highly dependent on two important factors: useful heat gain and incident beam irradiation; the experimental set up Kumaresan et al[40] is presented in Figure 5.

To gain more understanding about the PTC mechanisms, Kumar and Kumar in [42] used two different modes: tracking and south facing under the Indian climate with and without a glass envelope. As a consequence, the maximum outlet temperature was observed at the minimum mass flow rate ($T = 54.7°C$ at $m = 0.001$ kg/s of the south facing orientation and $T = 45.6°C$ in the mode of tracking). Furthermore, by increasing the mass flow rate for all the south facing cases (0.024 kg/s), the thermal efficiency was increased to 53.33% with glazing and to 46.17% without glazing. The interesting observation noticed from this research is that there is no significant change in the thermal efficiency by further increasing the mass flow rate beyond 0.024 kg/s.

Tajik et al[43] investigated experimentally the thermal efficiency of the solar PTC using porous medium instead of classical working fluids. Three different fill cases have been examined; free absorber, partly filled with copper foam and fully filled copper foam, see Figure 6 for more details. Results revealed that the overall thermal loss coefficient with fully filled copper foam case has reduced

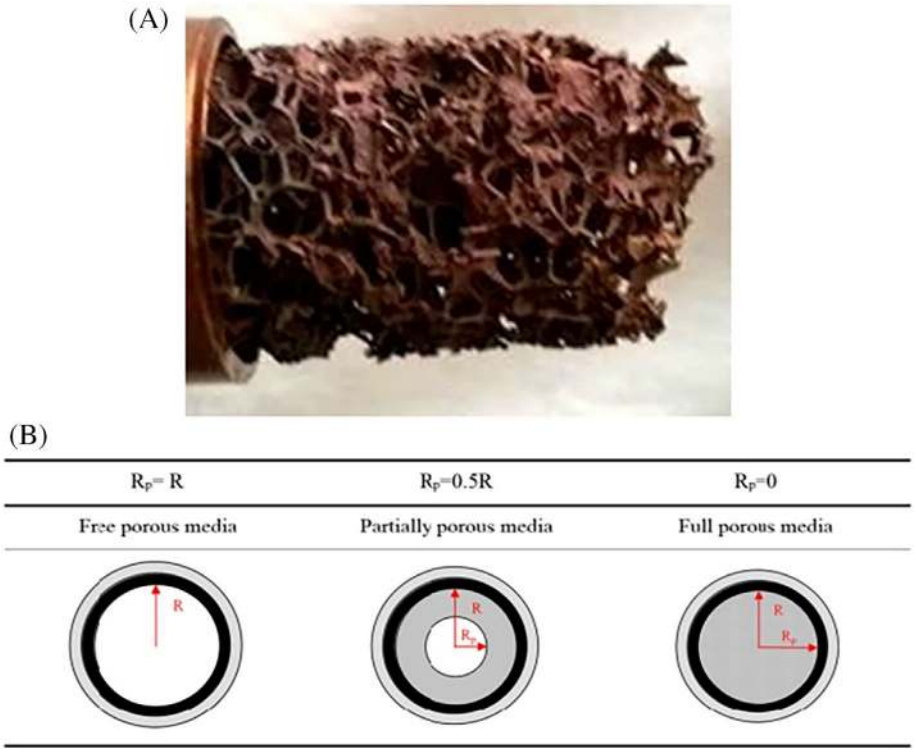

FIGURE 6 A, Copper foam and, B, configurations of absorber, Tajik et al,[43] ID: 72092616 [Colour figure can be viewed at wileyonlinelibrary.com]

to 45% and thus the thermal efficiency increased accordingly.

Recently, Agagna et al[44] experimentally investigated the optical and thermal performances of a small-scale parabolic trough power plant called (MicroSol-R) with a single storage tank system, the system diagram is presented in Figure 7. Three PTCs are installed in this platform in different directions: one of them is oriented in North-South direction whereas others are oriented in East-West directions. The optical efficiency range obtained was between 40% on December (13:00) and 77% on June (8:00-16:00). Mouaky et al[45] studied the thermal performance of the 186 kWth PTC under a semi-arid climate in Morocco concerning the effect of soiling on the energy production of the system. Results revealed that the proposed design can produce 388 Tons of steam at 500 kPa.

Regarding the exergy performance in PTCs, the huge amount of exergy destruction results from the concentration of sunrays on the absorber coatings. One possible solution has been provided recently by Wang et al[46] by comparing experimentally the exergy destruction considering the rotatable axis performance and a fixed axis oriented in North-South direction under the Chinese climate. The proposed idea of rotatable axis has reduced the exergy destruction and thus the exergy efficiency of the PTC could be enhanced by 3% annually. This is because the angle of the PTC can be easily perpendicular to the sun location with rotatable axis compared with the fixed one; the diagrams of both configurations are illustrated in Figure 8. However, Bakos[47] studied experimentally the effect of performing tow-axes tracking system compared with a fixed-axis system oriented in the South direction under the Greece climate. The solar energy collected has enhanced up to 46.46% with the proposed system.

3.2 | Analytical and numerical investigations

The mathematical models in the early time of PTC technologies were simplified and therefore not adequate for predicting the effective thermal performance, for informing design procedure analysis, or for controlling the accuracy of numerical predictions. Therefore, the numerical computation of the collector thermal performance and the assessment of the optical efficiency were really difficult to accurately obtained (Jeter[48]). Researchers paid attention after that and significantly improved the mathematical models and combined both optical and thermal features besides all components of the PTC system in order to effectively assess their behavior (Price et al[4]). Advances in the modeling and simulation of engineering applications have led to tremendous growth in modeling capability of PTC systems, where extensive elaborate information can now be achieved computationally. Experimental investigations, on the other hand, are

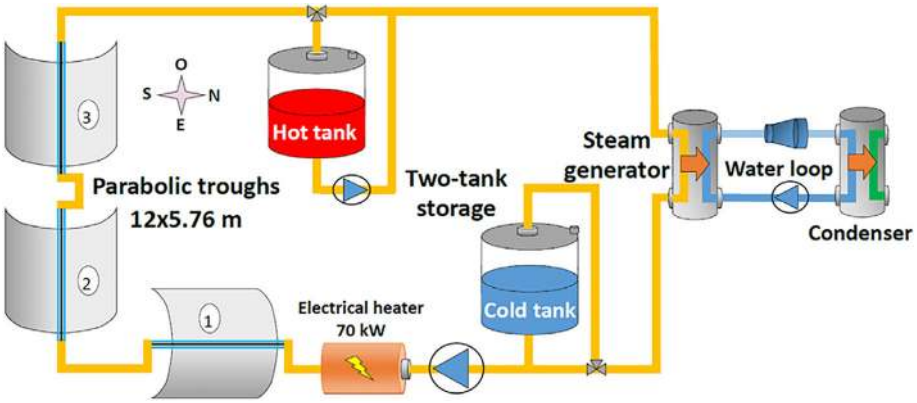

FIGURE 7 Diagram of MicroSol-R parabolic trough collector power plant, Agagna et al,[44] license number: 4742720124627 [Colour figure can be viewed at wileyonlinelibrary.com]

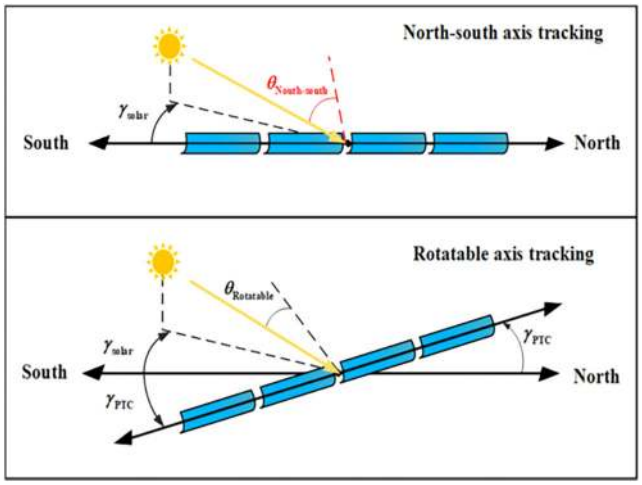

FIGURE 8 Diagrams of fixed axis and rotatable one of the parabolic trough collector, Wang et al,[46] license number: 4742721462079 [Colour figure can be viewed at wileyonlinelibrary.com]

considerably more expensive and time consuming than numerical simulations, and not all parameters of interest can be easily measured. In this section, different works are presented showing the main modeling approach and their achievements. Within a PTC system, there still remain a number of issues that needs addressing, one of them being the performance of the solar collector tube receiver. Due to the inherent design of the solar collector tube (one side always exposed to the direct sunlight and the other to reflect light through mirrors), the heat flux around the periphery is never uniform. This nonuniform heating within the pipe leads to local stratification and other heat flux mixing problems, eventually reducing the operational efficiency of the whole plant. Various methodologies currently exist to mathematically address this problem of nonuniform heat flux distribution around a solar receiver. Jeter[49] studied this problem with an analytical model where he derived a semi-finite formulation from the first integral of the concentrated flux density differential equations for the types of trough collectors. Thomas and Guven[50] also studied the effect of the heat flux distribution around the receiver of a PTC system for several optical configurations. It was deduced that the heat flux around the collector receiver is nonuniform in the circumferential direction for the horizontal tubes but symmetrical for the vertical receivers.

3.2.1 | Ray-tracing method

To really understand the nonuniform heat flux distribution around the absorber tube numerically and how to apply the nonuniform heat flux distribution in Computational fluid dynamics (CFD) solvers, the Ray-tracing technique is very common tool used to analyze and design the optical optimization and performance of the PTC. This technology provides detailed information about the optical features of the PTC with many surface options of imaging equations (Gaussian, Newtonian, etc.). In the literature, several tools use the ray-tracing technology, including SimulTrough, Opticad, SolTrace, TracePro, and ASAP (Advanced Systems Analysis Program); some visualization examples found in literature are presented in Figure 9. However, for the analysis of the optical characteristics of the PTC system, researchers in the numerical field have used extensively the Monte Carlo Ray Tracing (MCRT) model by either writing their own codes or utilizing the previous tools.

Grena[51] reported optical simulation of the PTC with and without glass envelope under realistic solar irradiation using a ray-tracing approach in three dimensions. The optical properties were considered as wavelength-dependent and the light-ray was taken as the basic element of simulations. More aspects have been also modeled realistically such as investigating the effect of tracking error and studying the intensity absorbed by the solar receiver. Yang et al[52] performed their own MCRT code considering different parameters: GCR, rim angle,

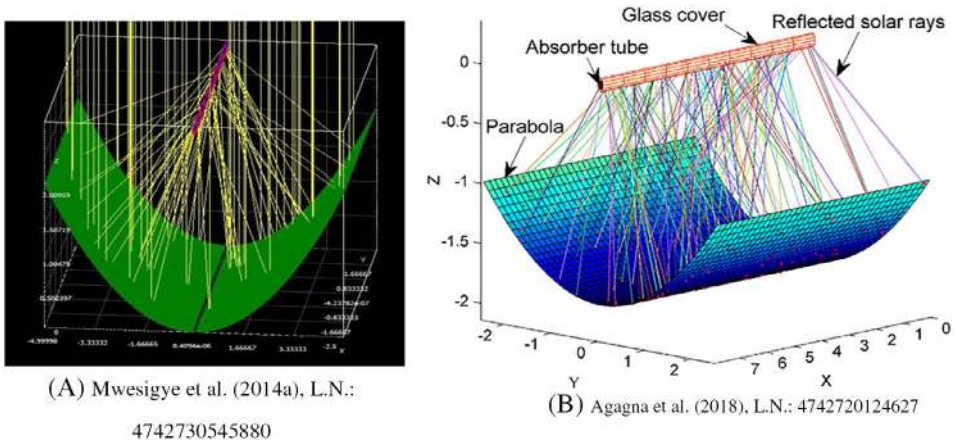

FIGURE 9 Visualization of the parabolic trough collector under nonuniform solar energy using ray-tracing model [Colour figure can be viewed at wileyonlinelibrary.com]

and tracking errors, whereas the solar rays were assumed to be nonparallel. The obtained result is the local concentration ratio (LCR) profile of an ideal PTC which was compared with the analytical results of Jeter.[49] The resulting curve showed the same trend as Jeter's.

He et al[53] produced an optical model based on combining the MCRT model with finite volume method (FVM) to solve the conjugated heat transfer models in the PTC considering the effect of various geometric concentration ratios and different ring angles on the optical performance. Their results have been compared with the analytical results of Jeter,[49] finding less than 2% average errors. They found also that the heat flux distribution curve was divided into four regions: direct radiation region, heat flux decreasing region, heat flux rinsing region and the region of shadow influence. Cheng et al[54] performed a CFD simulation on the receiver tube in three dimensions using the k–ε turbulence model. The MCRT model was combined with CFD solver in order to apply the nonuniform heat flux distribution. The authors compared results with the measurements of Dudley et al[33] and reported a difference of roughly 2%.

Cheng et al[55] developed their own MCRT code for a general-purpose numerical model of concentrating solar collectors (CSC). The model investigated and analyzed the photo-thermal conversion procedures in three different applications of the CSC (ie, PTC systems, parabolic dish collectors, and pressurized volumetric receiver systems). The reliability of the output curves was also compared with Jeter[49] results and good agreement was shown. Another numerical attempt to apply the nonuniform heat flux distribution was proposed by Hachicha et al,[5] where the authors performed a finite volume based numerical investigation with the Ray Trace model to develop an optical model for determining the nonuniform heat flux distribution around the solar receiver. The results were compared with analytical results of Jeter[49] with a maximum deviation of less than 8%.

Later, Zhao et al[56] developed their own MCRT simulation code to optimize and calculate the heat/density flux distributions on the solar receiver, considering in their simulations rim angles, GCRs, glass envelope transmittance, receiver absorption, envelope reflectivity, mirror reflectivity and nonparallelism of the sun rays (using cone optics). Their results yielded good agreement with Jeter.[49] Moreover, Kaloudis et al[57] represented the approximated LCR by using 7-curve fitting equations compared with the MCRT model suggested by Cheng et al.[54] The curves generated are third degree polynomial functions in a form of: $\mathrm{LCR} = b_3\emptyset^3 + b_2\emptyset^2 + b_1\emptyset + b_0$, where $\emptyset$ is an absorber angle and b_3, b_2, b_1, b_0 are constants have different values depending on the range of the absorber angle, given in Table 5.

Liang et al[58] proposed their own code for three different optical models based on the ray-tracing method. Each model has its own optical approach: the first model is based on the MCRT method, the second model is based on the initialization of the photon distribution with Finite Volume approach, while the third model is based initially on the FVM to determine the ray locations and then by multiplying reflectivity, transmissivity and absorptivity changed to the photon energy method. The third model was superior where the computational effort was less than this of the first model by 60% and the running time was shorter than that of the first model by 40%. Liang et al[59] extended their own previous code to present four different optical models using the Monte Carlo Method and finite volume approach, combined with a novel approach to initialize the profile of photons and to describe the reflecting, absorbing, and transmitting processes; the photon distribution in both cases is presented in Figure 10. The finding results yielded good accordance compared with Jeter[49] findings.

Houcine et al[60] established their new code using a numerical approach based on ray-tracing 3-Dimensions 4-rays (RT3D-4R) under realistic optical properties and

Part	∅ range (°)	b_3	b_2	b_1	b_0
1	0-75	0.0	−1.071170E−4	−8.100954E−4	1.112046
2	75-104	−2.544403E−3	6.878607E−1	−5.974390E1	1.685403E3
3	104-171.2	−6.602394E−5	3.196692E−2	−5.280388	3.275329E2
4	171.2-188.8	0.0	1.524597E−1	−5.488588E1	4.957224E3
5	188.8-256	5.961826E−5	−3.504845E−2	6.979938	−4.403785E2
6	256-285	2.493475E−3	−2.019052	5.427366E2	−4.840387E4
7	285-360	0.0	−7.511141E−5	2.688045E−2	−9.606886

TABLE 5 Coefficients of the local concentration ratio curves, Kaloudis et al[57]

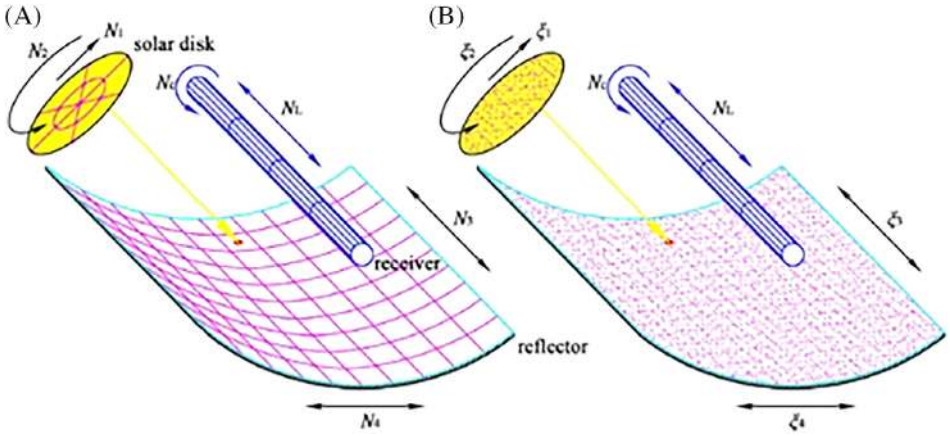

FIGURE 10 Visualization of photon distributions in, A, finite volume method and, B, MCM, Liang et al,[58] license number: 4742730812455 [Colour figure can be viewed at wileyonlinelibrary.com]

solar coordinates (one axis and dual tracking system) of the PTC system. Moreover, they also studied the effects of the rim angle and geometric concentration ratio on the overall gain solar energy reflected on the solar receiver. Results showed good agreement compared with findings of Jeter,[49] He et al,[53] and Hachicha et al.[5]

Agagna et al[44] introduced three different models of variable degree of sophistication for PTCs using the MCRT: model 1 is a simple one-dimensional model and simpler, model 2 is a two-dimensional model that can be used to predict the thermal characteristics of the PTC system, while model 3 is the most accurate and can provide detailed information about the realistic nonuniform heat flux distribution on the solar receiver. Hoseinzadeh et al[61] also introduced their own code based on MCRT method to produce optical and thermal models in MATLAB with optimizing three different design parameters: the collector aperture, the solar absorber diameter, and the rim angle. The maximal optical efficiency obtained was 65% for the PTC with 0.6 m aperture width, 100° rim angle and 0.025 m absorber diameter. Cheng et al[62] proposed a novel computational approach of producing a fitting formula of an optical efficiency of the PTC based on combining the MCRT model with the population-based particle swarm optimization algorithm. Results are in good agreement with Jeter.[49]

From the scenario explained previously, the main objective of all researchers is to produce the distribution of the LCR, which represents the heat flux distribution around the solar receiver after multiplying it by the direct normal irradiation. Once that is applied properly, there is no need to take the parabolic structure into account. Moreover, all preceding findings have been compared with those of Jeter[49] and presented in Figure 11 over a period of time between 1986 and 2018.

3.2.2 | Design parametric investigations of PTCs

As explained previously, the heat flux distribution is nonuniform over the glass envelope in the circumferential direction of the conventional PTC design. This property, in addition to the thermal performance and optical properties, can be affected by different design parameters such as optical errors, rim angle, material deflection, reflector mirrors, aperture width, receiver geometry, GCR, tracking system, tracking orientation, incidence angle, Re number, inlet temperature of working fluid, and so forth. Therefore, in this section, the numerical and analytical studies concerned these issues are presented.

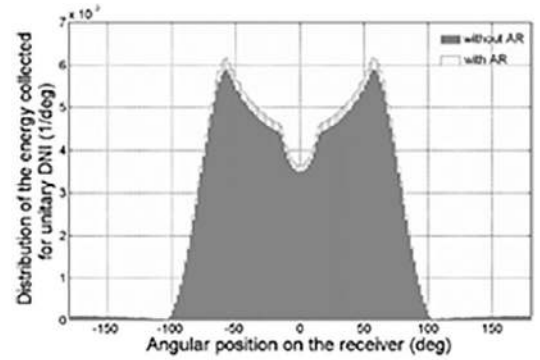

(A) Grena (2009), ID: 72092593

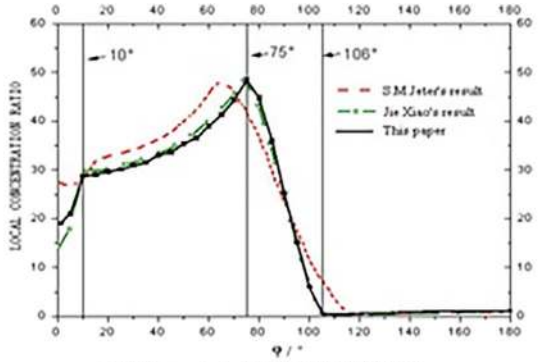

(B) Yang et al. (2010), ID: 72092588

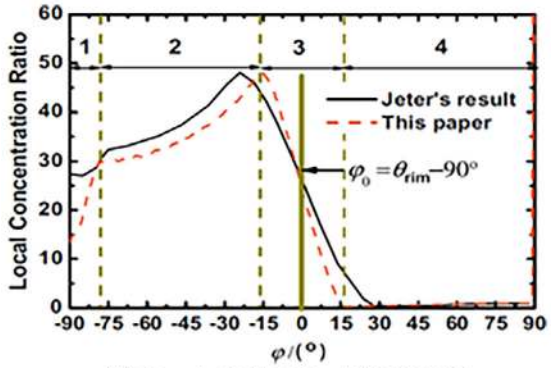

(C) He et al. (2011), L.N.: 4742731170430

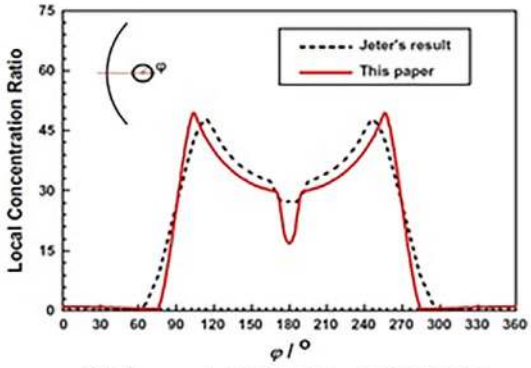

(D) Cheng et al. (2012a), L.N.: 4742731431445

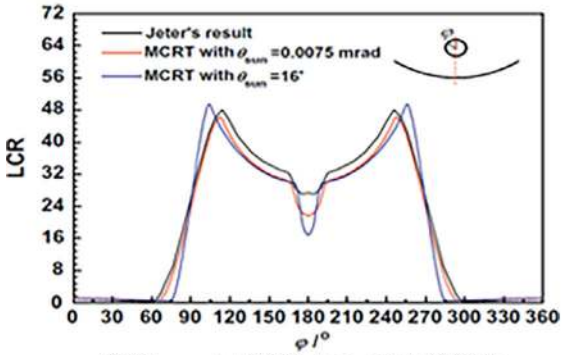

(E) Cheng et al. (2013), L.N.: 4742740092556

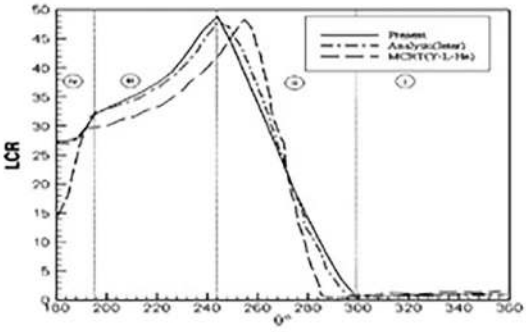

(F) Hachicha et al. (2013), L.N.: 4742890786848

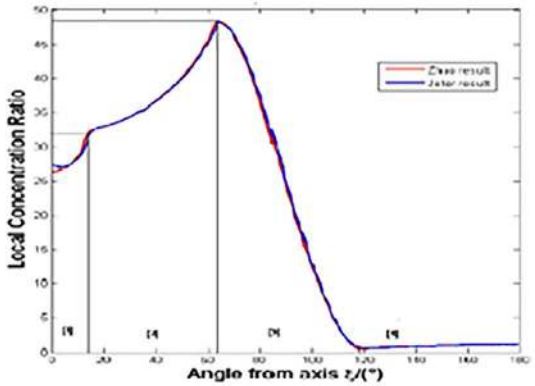

(G) Zhao et al. (2015), L.N.: 4742890978358

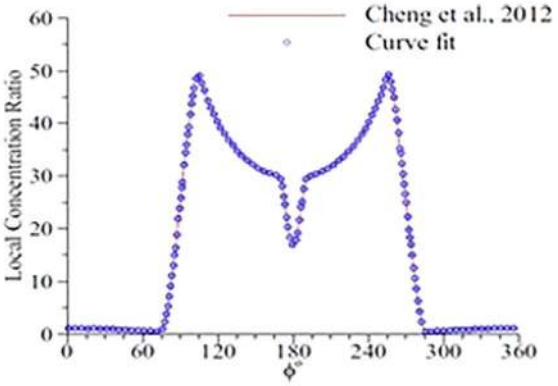

(H) Kaloudis et al. (2016), L.N.: 4742891136317

FIGURE 11 The local concentration ratio distribution presented in previous studies [Colour figure can be viewed at wileyonlinelibrary.com]

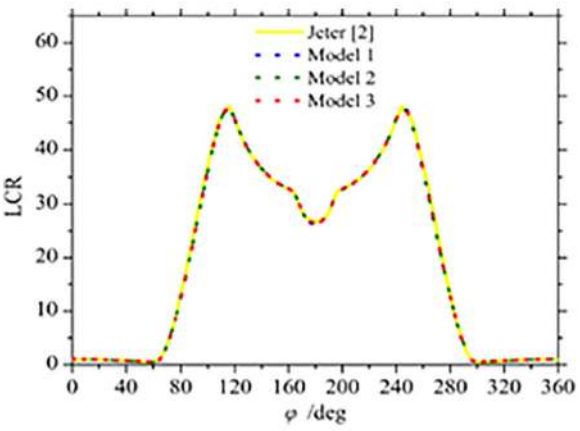

(I) Liang et al. (2016), L.N.: 4742891318987

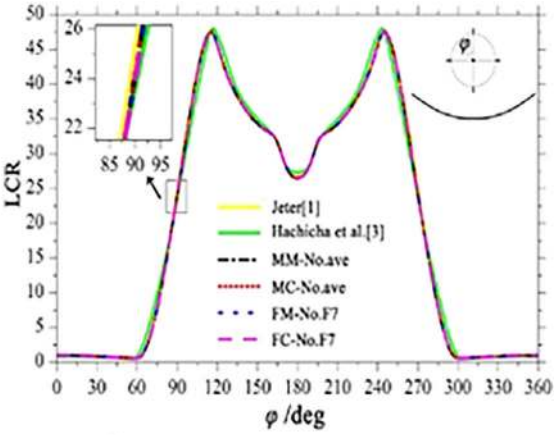

(J) Liang et al. (2017), L.N.: 4742730812455

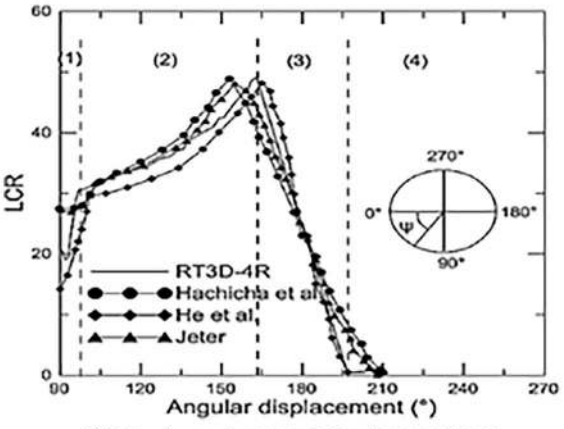

(K) Houcine et al. (2017), L.N.: 4742900283692

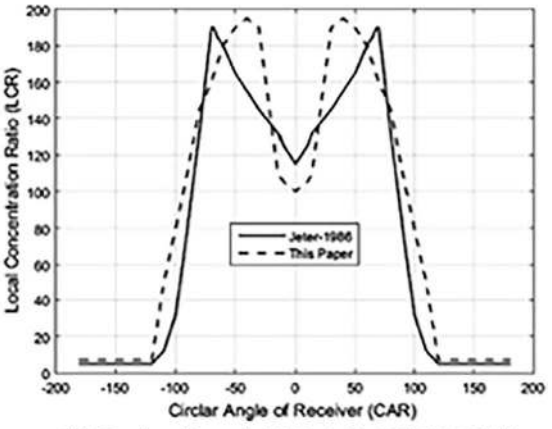

(L) Hoseinzadeh et al. (2018), L.N.: 4742921187340

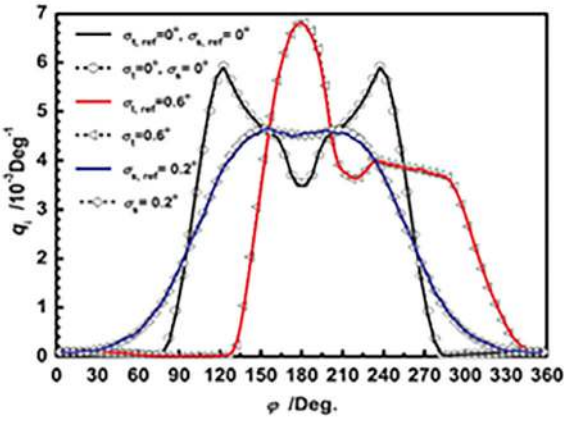

(M) Cheng et al. (2018), L.N.: 4742740286799

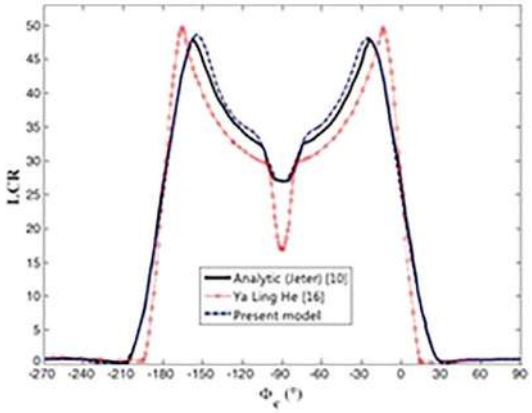

(N) Agagna et al. (2018), L.N.: 4742720124627

FIGURE 11 (Continued)

The effect of the rim angle on the PTC performance plays a key role in the thermal heat flux behavior, bending deflection in the absorber tube and entropy generation. Khanna et al[63] investigated the effect of deflection, optical errors, and rim angle on the circumferential heat flux distribution. Results showed that the heat flux distribution increased and became more distributed on the circumference with decreasing the wall deflection while the heat flux became more distributed on the circumference with zero optical errors. The optimum rim angle was suggested to be 110° so as to maximize the total heat flux. Wirz et al[24] studied the effect of changing the rim angle on the thermal efficiency using several secondary mirrors and receiver diameters. Results showed that the optimum rim angle which led to the maximum thermal efficiency was also 110°. Moreover, the thermal efficiency was found to increase of 0.8% to 1.6% by applying the secondary mirrors compared with the benchmark design.

Mwesigye et al[64] investigated the effect of rim angle and concentration ratio on the heat transfer and entropy generation. They pointed out that the entropy generation heat transfer, increased with reducing the rim angle and slightly increased with increasing the concentration ratio. Khanna et al[65] found that by increasing the rim angle from 60° to 140°, the maximum temperature difference of the receiver in the circumferential direction was reduced from 16°C to 7°C, and the maximum receiver deflection was also reduced from −9 mm to −1.7 mm. Khanna and Sharma[66] examined also the effect of rim angle, aperture width and optical errors on the total flux availability and solar flux distribution. By increasing the rim angle from 60° to 135°, the maximum difference in solar flux reduced from 46 to 22 kW/m^2. However, increasing the aperture width led to further increase in the heat flux nonuniformity in the circumferential direction. The same trend has been noticed with increasing the optical error in which the flux availability has also reduced from 45 to 30 kW/m^2. The authors finally concluded that the rim angle could not be the independent variable to evaluate the thermal performance.

Forristall[67] developed a comprehensive study of heat transfer model using engineering equation solver (EES) by utilizing both one- and two-dimensional heat transfer models. It was concluded that the predicted performance of heat collector was in good agreement with the experimental data of AZTRAK (Dudley et al[33]). It was also determined that the best material for the absorber tube was type 321 hours stainless steel due to its strength and reduction in the bending problem. Furthermore, the coating type (its emittance is 0.07@ 400°C proposed coating) increased the efficiency by 8.5% whereas the vacuum annulus type led to the best performance. However, the heat flux distribution cannot be implemented as nonuniform distribution in EES. Tao and He[68] studied the heat transfer and fluid flow behavior inside the solar collector and inside the annular gap as well for different Rayleigh numbers and tube diameter ratios (inner absorber diameter/inner envelope diameter). They found that with increasing the tube diameter ratio, the Nusselt number in the annular gap dropped gradually while increasing in the inner tube diameter. They also highlighted that the natural convection process in the annular gap must be considered when the Rayleigh number is higher than 10^5.

To calculate the optical efficiency of PTCs, Huang et al[69] proposed a new analytical model which was modified and integrated to study the collector performance of a PTC with a vacuumed tube envelope using a numerical integration algorithm program considering the effect of different tracking error and different displacement error. Lu et al[70] investigated analytically the effect of both uniform and nonuniform heat transfer distributions on the thermal performance under on-sun and off-sun conditions. They reported that the receiver heat transfer was nonuniform with a larger heat loss and surface temperature under on-sun conditions, while the receiver heat transfer was more or less uniform with only slight differences in surface temperature and heat loss coefficient under off-sun conditions (zero beam irradiation); therefore, the better performance for the solar PTC was evaluated to be under the nonuniform heat flux distribution. Another numerical approach proposed by Cheng et al[71] was aimed at combining the MCRT model with the FVM in a parametric study on the heat flux density and temperature distribution. It was suggested by the authors that the solar heat flux distribution curves should not be divided into four areas as indicated by other researchers; He et al.[53]

Wu et al[72] examined the heat loss from a PTC with annular gap in conjugated heat transfer configuration using the FVM coupled with the (MCRT) model and the standard k–ε turbulence model. It was concluded that the thermal loss resulted from bellows is about 7% of the total thermal loss. Moreover, it was found that an inverse relation exists between the HTF velocity and the temperature gradient of the absorber metal. However, an alternative numerical approach to represent the nonuniform heat flux was presented by Okafor et al[73] using the sine equation expression in terms of concentrated base-level heat flux under laminar flow regime. Different Re numbers, different receiver diameters, and different fluid inlet temperatures have been considered to study their effect on the secondary flow. Ray et al[74] preformed numerical 3D simulations considering the glass envelope as semi-transparent and modeling the selective coating on the outer surface of the solar absorber with a range of DNI (750-1000 W/m^2) and different mass flow rate of the working fluid (1.7-17.6 kg/s). Results showed that the temperature difference in the circumferential direction decreased by 71.95% with increasing the mass flow rate from 1.7 to 17.6 kg/s and the thermal efficiency has been affected slightly with increasing the DNI as well as mass flow rate.

Tripathy et al[75] examined the effect of different absorber materials on the thermal and mechanical performances using steel, copper, Bimetallic and Tetra-layered laminate with different flow rates. According to their results, the effect of changing the absorber material on the transferred energy to HTF is quite small and can be neglected. However, it has a considerable influence on the bending owing to the thermal expansion and self-weight. They found that steel causes poor temperature distribution in the circumferential direction due to its lower thermal conductivity, whereas copper behaves

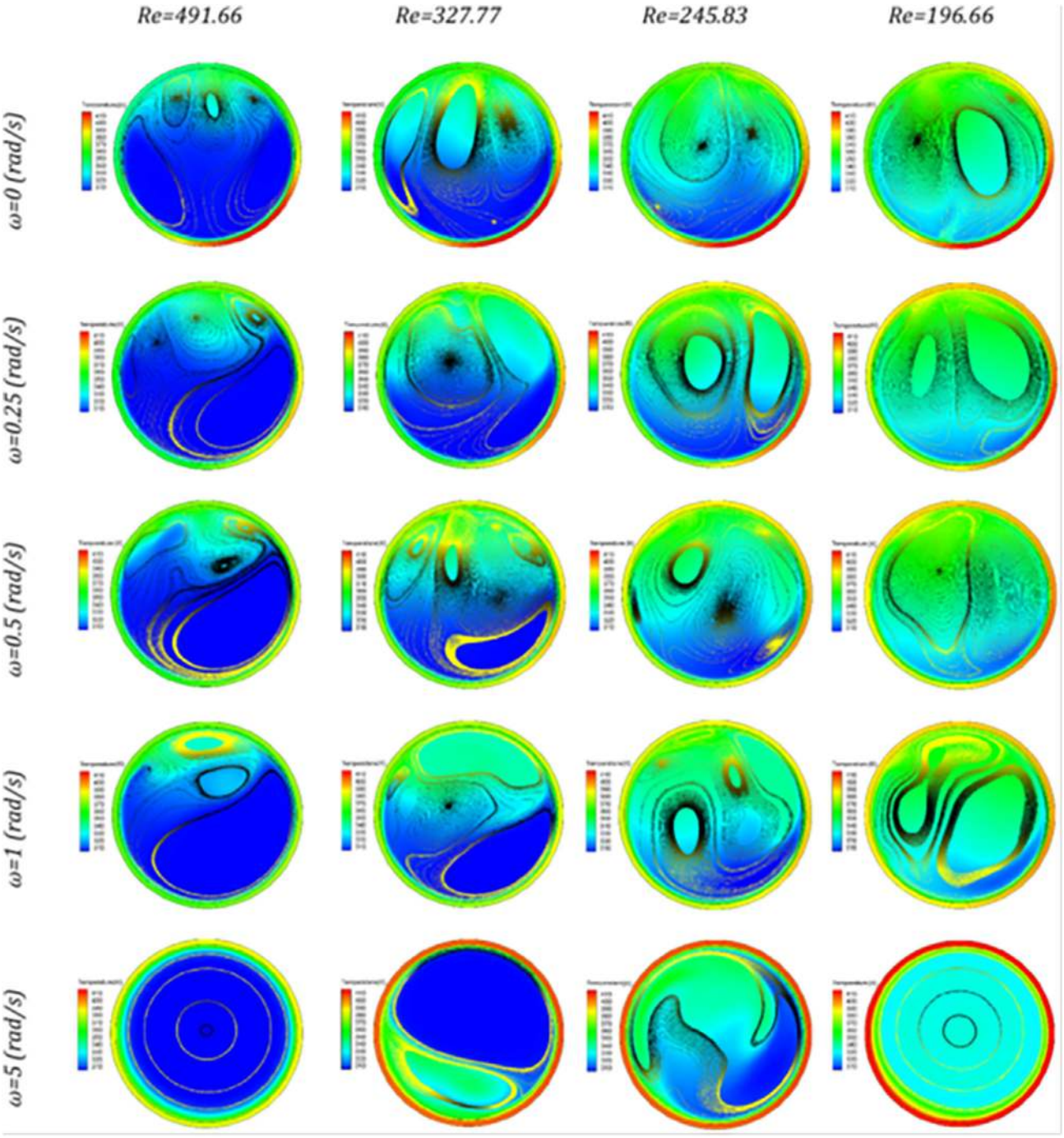

FIGURE 12 The effect of rotational velocities on temperature profiles, Norouzi et al,[81] license number: 4742921336468 [Colour figure can be viewed at wileyonlinelibrary.com]

better, but has heavier self-weight. Finally, the Tetra-layered laminate provided the best temperature distribution and reduced the maximum deflection by 45% to 49% as compared with steel.

Donga and Kumar[76] studied the thermal performance of the PTC with absorber tube misalignment at a range of volumetric flow rate (5.65-33.9 m^3/h), slope error range of (0-3 mrad) and two different receiver diameters of 70 mm and 80 mm. It was pointed out that the thermal efficiency is only affected slightly (reduction up to 3%) by receiver dislocation in the presence of slope errors. Moreover, there was insignificant effect on the thermal efficiency by the receiver misalignment with zero slope error. The effect of incidence angle on the PTC performance has been addressed recently by Zou et al,[77] where they investigated the thermal performance of the PTC

TABLE 6 Some solutions proposed in the previous studies might affect the heat losses

References	Study type	Used techniques	Achievements
Odeh et al[83]	Numerical	Using water instead of Syltherm 800 oil as heat transfer fluid.	Reduction in thermal losses when using water as working fluid.
Forristall[67]	Numerical	Testing the effect of different working fluids on the thermal performance.	Selected (Xceltherm 600 and Syltherm 800) as the best candidates which led to noticeable increase in the thermal efficiency and reduction in the heat losses.
Gong et al[84]	Experimental	The ends of absorber were covered by heat insulator.	46.18% reduction in heat losses.
Roesle et al[85]	Numerical	Keeping low pressure in the gap between the receiver and the glass jacket using a vacuum pump.	If the operating temperature increases to more than 400°C, the absorber tube would suffer from extreme heat losses.
Lei et al[35]	Experimental	Using a new solar receiver with a high vacuum system and a vacuum gauge.	The new design provided better thermal performance since the heat losses drastically reduced.
Yaghoubi et al[86]	Experimental and numerical	Three types of cover used in parabolic trough collector; vacuum, lost vacuum, and broken glass tube.	Heat losses in cases of lost vacuum and broken glass tube were 46% and 58.5%, respectively, larger than that of vacuum tube leading to a drop of 3%-5% and 19%, respectively, in the overall system performance.
Zhang et al[87]	Experimental	A new structure of the solar absorber in U-type shape with a double-glazing vacuum.	Thermal efficiency increased from 79.1% to 79.2% on a calm day and 47.2% to 66.3% on a windy day where the heat losses increased from 0.183 to 0.255 kW.
Wu et al[38]	Experimental	Using molten-salt to achieve the heat loss of the solar collector as the temperature of heat transfer fluid changed.	The thermal losses at the joints increase from 5% to 18% with removing the thermal insulation.
Sanchez and Rosengarten[88]	Numerical	Reducing the absorber diameter.	Thermal losses reduced gradually with increasing the pressure drop and accordingly pumping power.
Khandelwal et al[80]	Numerical	Using liquid sodium as heat transfer fluid instead of Molten salt, Therminol oil VP1, and NaK78.	Significant reduction in thermal losses from 11 times to 3 times.
Osorio and Rivera-Alvarez[89]	Numerical	Using double glass envelops outside the absorber tube.	Both optical and thermal efficiencies enhanced especially under partially cloudy climate. More reduction in thermal losses compared with typical parabolic trough collector.

depending on nonideal optical parameters including sunshape, incidence angle, tracking error, slope error, and absorber alignment error. Results illustrated that the thermal efficiency has significantly dropped by 41.11% as the incidence angle increased from 0° to 60°. Moreover, increasing slope errors and tracking errors caused considerable reduction in the thermal efficiency.

Recently, Xu et al[78] introduced a mathematical model to study the unsteady thermal performance of the PTC under different fluid inlet temperatures and DNIs. It was concluded that the working fluid motion has no strong effect on the receiver temperatures. García et al[79] studied the temperature distribution on the solar receiver and thermal efficiency of the PTC by developing a reduced-order mathematical model based on the steady-state heat transfer behavior. After comparing results with previous references, less than 10% relative error was recorded. Khandelwal et al[80] studied the PTC thermal performance under different geometrical and operational parameters, various aperture diameters, different mass flow rates, and various working fluids. A considerable drop in the temperature gradient has been

TABLE 7 Advantages and limitations of alternative heat transfer fluids compared with thermal oils, Blanco and Miller[1]

Heat transfer fluid type	Temperature (°C)	Advantages	Drawbacks
Direct steam generation	250 ($P = 0.4$ MPa)	• The plant configuration is simpler. • The steam temperature is larger. • No pollution and no fire hazard.	• No thermal storage system. • The solar field control is more complex. • Pressure in the solar field is larger.
Compressed gases	More than 500	• The steam temperature is larger. • Thermal storage is cheaper. • No pollution and no fire hazard.	• Heat transfer coefficient is smaller. • The solar field control is complex. • Higher pressure in the solar field. • Pumping power required is larger.
Molten salts	230-600	• The plant configuration is simpler. • The steam temperature is larger. • Thermal storage is cheaper. • No pollution and no fire hazard.	• Electricity self-consumption is larger. • Freezing hazard. • Design of solar field is complicated.

noticed when using liquid sodium compared with other fluids and the temperature profile on the circumferential direction became more uniform. Moreover, the PTC with larger aperture performed better than this with smaller in terms of absorbing more energy and reducing the thermal gradient.

Norouzi et al[81] studied numerically the effect of different parameters on the collector's performance including absorber materials, Re numbers, nanofluids, and rotational speed of the absorber in 2D and 3D unsteady models. It was concluded the collector's efficiency using Aluminum absorber material is 25% larger than any other materials with rotational speed of 0.25 rad/s and volume fraction of 3%. It was also suggested that, because the thermal efficiency could either increase or decrease as the rotational speed is changed due to the fluctuating performance of the thermal efficiency, the rotational speed should be chosen properly. Figure 12 shows the effect of rotational speeds.

4 | THERMAL LOSSES

The most important issue in PTC systems is how to minimize the overall heat losses which would act to greatly improve the thermal performance of PTCs which in turn leads to gradually enhance the overall collector efficiency. On the other hand, the absorber heat loss has a negative effect on decreasing some parameters, thermal properties, flow quantity, and the HTF temperature delivered by the solar field. For this reason, the HCE should be effectively designed to minimize heat losses to the free air. The process of covering the receiver tube with a glass envelope acts to reduce the radiative and convective heat losses to the environment. Furthermore, coating the absorber tube with a selective coating (having large absorption rates, more than 0.95) helps also in reduction of radiative heat losses. To seek a further reduction in the thermal losses, the gap between the receiver and glass envelope can be operated under vacuum conditions with very small air pressure (0.013 Pa), which helps to significantly reduce the natural convection heat loss. Another possible approach is designing the absorber tube to be long ($L \geq 4$ m) and choosing the absorber diameter to be small relative to the collecting aperture, which leads to minimization of conduction heat losses at the absorber ends (Burkholder and Kutscher[82]). A summary of various techniques to improve the thermal performance of the PTC system is provided in Table 6.

5 | EFFECT OF CHANGING HTFS ON THERMAL AND HYDRAULIC PERFORMANCES

The working fluid is one of the most important elements in determining the thermal performance of PTC systems. Recent estimates until reported that there are about 63 fully operational STPPs with PTC systems around the world. Sixty-one of these plants use thermal oils as the working HTF with the maximum working temperature of 398°C. The main reasons for the use of thermal oils are: low vapor pressure, affordable price, long life, and thermal stability. However, this does not in any way mean that thermal oils are the best candidates for the working fluid as they also have some key drawbacks, including the limitation of temperature (around 400°C), and environmental toxicity and flammability (Blanco and Miller[1]). There are currently three alternative HTFs that have been examined in the literature: liquid-water/steam (referred to direct steam generation), pressurized gases, and molten salts. Each of these working fluids has its own advantages

TABLE 8 Summery of the heat transfer fluid studies presented in the available literature

References	Study type	Working fluid	Details of findings
Odeh et al[83]	Numerical	Syltherm 800 oil and water.	Water shows a lower thermal loss coefficient than Syltherm 800 oil.
Forristall [67]	Numerical	Therminol VP1, Xceltherm 600, Syltherm 800, 60-40 salt, and Hitec XL salt.	Effect of working fluid smaller than other parameters. The maximum thermal efficiency was observed when using Xceltherm 600 and Syltherm 800; however, these fluids are relatively expensive.
Montes et al[90]	Numerical	Molten salt, water, and oil.	Optimum system efficiency achieved with water as the working fluid.
Ouagued and Khellaf[91]	Numerical	Syltherm 800, Syltherm XLT, Santotherm 59, Marlotherm X, and Therminol D12.	The Syltherm 800 can be operated at a temperature higher than 700 K, while the working fluids Marlotherm X and Syltherm XLT can only be operated at temperatures less than 700 K; other working fluids tested could be operated between 650 K and 750 K.
Ouagued et al[92]	Numerical	Syltherm 800, Santotherm 59, Marlotherm X, Therminol D12, Syltherm XLT, Santotherm LT, and Marlotherm SH.	The maximum range was recorded for Syltherm 800 700-800 K, which was deemed as the most appropriate choice from a thermal capacity point of view. The highest cost was with the Santotherm LT which was U.S. $129 kWh/day.
Biencinto et al[93]	Numerical	Pressurized nitrogen and synthetic oil.	Slight differences observed in the net electrical power between fluids, only (less than 0.91%), while the gross electrical production per year was found to be the same.
Good et al[94]	Experimental	Air.	The operating temperature has exceeded 600°C.
Wang et al[95]	Numerical	Molten salt and thermal oil.	Using molten salt provided higher pressure drop and lower thermal efficiency.
Selvakumar et al[96]	Experimental	Therminol D-12 and hot water.	Therminol D-12 performed better and stable for more than 100 cycles of operation.
Wu et al[38]	Experimental	Molten-salt compared with the results of PTR70.	The heat losses resulted from the fluid of PTR70 are smaller than those resulted from molten-salt.
Qiu et al[97]	Numerical	Supercritical CO_2 (S-CO_2) under two different cases; Rankine and Brayton cycles.	The collector efficiency in two cycles increased to 81.93%-84.7% (Rankine) and 18.78%-84.17% (Brayton).
Tahtah et al[98]	Experimental	Thermal oil and water.	A rapid increase was noticed in the temperature evaluation using the thermal oil compared with water. Thus, water was found to be good in terms of heat storage medium.
Bellos et al[99]	Numerical	Pressurized water, Therminol VP-1, nitrate molten salt, sodium liquid, air, carbon dioxide, and helium.	The performance of liquid fluids is generally higher than this of gas fluids.
Aguilar et al[100]	Numerical	Synthetic oil, subcritical carbon dioxide, and super-critical carbon dioxide.	Larger solar irradiation has been absorbed when using super-critical carbon dioxide.

and disadvantages when compared with thermal oils. A brief comparison between different working fluids is presented in Table 7. It can be clearly observed from this table that none of the considered fluids is a perfect solution as they all have some constraints or technical issues that need to be resolved.

A further comprehensive review of the different HTFs used in the PTC systems is summarized in Table 8.

TABLE 9 Thermal properties of particles used in previous studies

Type		T (K)	ρ (kg/m^3)	C_p (J/kg K)	k (W/m K)	Size (nm)	References
Metallic particles	Cu	400	8933	397	393	50	Mwesigye and Meyer[101]
	Al	300	2702	903	237	–	Incropera et al[29]
	Au	300	19 300	129	317	–	Incropera et al[29]
	Ag	400	10 500	239	425	50	Mwesigye and Meyer[101]
	Fe	300	7870	447	80.2	–	Incropera et al[29]
	Ni	300	8900	444	90.7	–	Incropera et al[29]
	Graphene	–	2200	710	1000-5000	0.515	Natividade et al[102]
	Si	300	2330	712	148	–	Incropera et al[29]
	Zn	300	7140	389	116	–	Incropera et al[29]
Non-metallic particles	Al_2O_3	300	3600	765	36	20	Al-damook et al[103]
	Al_2O_3	400	3970	940	32.4	–	Mwesigye and Meyer[101]
	CuO	298	6400	620	76.5	33	Turkyilmazoglu et al[104]
	CeO_2	298	7220	460	12	<30	Sharafeldin and Gyula[105]
	CeO_2	400	6757	392.5	5.86	–	Nelson et al[106]
	TiO_2	298	4250	686.2	8.95	10	Turkyilmazoglu et al[104]
	NiO	298	6670	850	41	–	Myers et al[107]
	SiO_2	300	2220	745	1.4	20	Al-damook et al[108]
	γ-Al_2O_3	298	3880	773	36	13	Pak and Cho[109]
	BeO	300	3000	1030	272	–	Incropera et al[29]
	Cu_2O	–	6080	474	42	–	Sadeghi et al[110]
	ThO_2	300	9110	235	13	–	Incropera et al[29]
	Fe_2O_3	400	5180	670	6.9	–	Bellos and Tzivanidis[9]
	ZnO	–	7133	383	111	50	Abu-Hamdeh and Almitani[111]
	Fe_3O_4	–	5180	670	80.4	36	Abu-Hamdeh and Almitani[111]
	γ-Fe_2O_3	–	5242	679	161	4-5	Huminic and Huminic[112]
	MgO	293	7035	554.5	242	–	Minea et al[113]
	Co_3O_4	293	6110	460	69	–	Sundar et al[114]
	GO	293	1910	710	1000	–	Sundar et al[114]
CNT	CNT	–	2100	709	3000	80	Peng et al[115]
	SWCNT	298	2600	425	6600	–	Khan et al[116]
	MWCNT	–	1600	796	3000	–	Ghadikolaei et al[117]

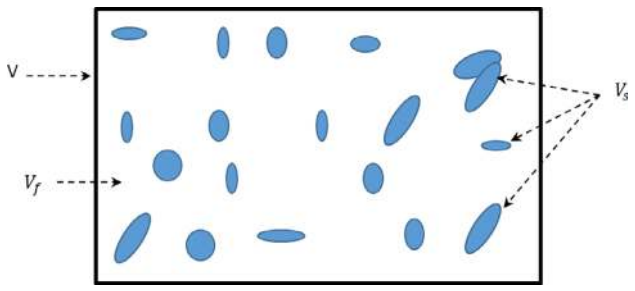

FIGURE 13 Heterogeneous mixture of fluid and nanoparticles [Colour figure can be viewed at wileyonlinelibrary.com]

6 | THERMAL PERFORMANCE IMPROVEMENT BY ADDING NANOPARTICLES

One of the most useful techniques to improve the thermal performance in PTCs is to add metallic or nonmetallic nanoparticles to the base working fluid which leads to the creation of a so-called nanofluid. The added nanoparticles having different thermal properties than those of the base working fluid make the working fluid mixture more efficient and effective; in particular, the higher thermal conductivity and lower specific heat

capacity which leads to enhance the overall performance of the absorber tube. Furthermore, the presence of nanoparticles in the base fluid helps also in a notable decrease in effective thermal stresses on the absorber tube. However, a further increase in nanoparticle volume fractions can lead to the agglomeration and clustering of the nanoparticles inside the solar receiver thereby resulting in increasing the requirement of pumping power. For this reason, the nanoparticle volume fraction has to be optimized for an efficient heat transfer augmentation and reasonable friction factor and accordingly pressure drop. The nanoparticles utilized currently in the PTC applications can be metallic (like Al, Ag, Au, Cu, Fe, etc.), nonmetallic (such as Al_2O_3, CuO, Fe_2O_3, SiO_2, TiO_2, NiO, ZnO, etc.), or carbon nanotubes (CNT) includes single-walled nanotubes (SWCNT) and multi-walled carbon nanotubes (MWCNT). The thermal properties of a wide range of nanoparticles are described in Table 9 over a range of inlet temperatures and different particle sizes.

6.1 | Proposed correlations of thermophysical properties

From a numerical modeling perspective, a nanofluid can be simulated using either as a single-phase or a two-phase model. Both of these approaches have been used in literature with the two-phase model approach being the more accurate one. However, the selection of the thermophysical properties is critical, when it comes to ensuring acceptable predictions via modeling nanofluids. For this reason, various models and correlations from the literature are presented below.

6.1.1 | Density of nanofluid, ρ_{nf} (kg/m^3)

The mixture of base fluid and nanoparticles is considered to be a heterogeneous mixture which can be composed of different parts and can easily be distinguished either by the naked eyes or by a microscope, see Figure 13.

The total mass of both solid and fluid materials can be introduced in the heterogeneous mixture in terms of densities as expressed below (Pak and Cho[109]):

$$\rho_{\mathrm{nf}} = \frac{m}{V} = \rho_s\varphi + \rho_f(1-\varphi). \tag{42}$$

6.1.2 | Specific heat capacity of nanofluid, $C_{p,\,nf}$ (J/kg K)

This property can be derived based on the energy balance for incompressible substances which is expressed in the following way (Xuan and Wilfried[118]), which is used very commonly in the literature:

$$C_{p,\mathrm{nf}} = \frac{1}{\rho_{nf}}\left[\rho_s C_{p,c}\varphi + C_{p,f}\rho_f(1-\varphi)\right]. \tag{43}$$

Another correlation was proposed by Pak and Cho[109] based on the volume fraction of two substances is given by the following formulation:

$$C_{p,\mathrm{nf}} = C_{p,s}\varphi + C_{p,f}(1-\varphi). \tag{44}$$

It should be noted that the correlation proposed by Xuan and Wilfried[118] (Equation [43]) is widely applicable and more accurate than the one given by Pak and Cho[109] (Equation [44]) as the latter correlation is based on a universally representing property, that is, the nanofluid density. Further evidence is provided by O'Hanley et al,[119] which compare the results from both the correlations with the experimental data of different nanofluids. O'Hanley et al,[119] reported that the results predicted by the Xuan and Wilfried[118] correlation were much closer to the experimental data than those predicted through the Pak and Cho[109] correlation for all nanofluids.

6.1.3 | Dynamic viscosity of nanofluid, μ_{nf} (kg/m s)

The dynamic viscosity of solid–fluid suspension was first proposed analytically by Einstein[120] and Einstein[121] based on the molecular model, which considered the solid particles as noninteracting spheres as follows:

$$\mu_{\mathrm{nf}} = \mu_f(1+2.5\varphi). \tag{45}$$

This model is only applicable to nanofluids with low volume fraction ≤2%. After that, Brinkman[122] developed the previous analytical model by adding the effect of the velocity modification resulted from the presence of sphere particles and giving the following formulation for uniform mixture:

$$\mu_{\mathrm{nf}} = \mu_f\frac{1}{(1-\varphi)^{2.5}}. \tag{46}$$

This model is assumed to be applicable for high concentration ratio, $\varphi \le 4\%$. However, this model has been extended further by Batchelor[123] to take the Brownian motion effect into account in addition to the hydrodynamic interactions of the sphere particles with a volume fraction less than 10%:

$$\mu_{\mathrm{nf}} = \mu_f\left(1 + 2.5\varphi + 6.2\varphi^2\right). \quad (47)$$

For a typical volume fraction, the last three models would produce almost identical results. For example, at 1% (0.01) volume fraction, the effective viscosity (μ_{nf}/μ_f) of the last three models are 1.025, 1.0254, and 1.0256, respectively. Another analytical attempt was performed by Happel[124] considering the tangential stress resulted from the presence of solid particles under creeping flow conditions:

$$\mu_{\mathrm{nf}} = \mu_f(1 + 5.5\varphi). \quad (48)$$

However, this expression produces very high nanofluid viscosity compared with the preceding models. On the other hand, experimental studies have also contributed different expressions of dynamic viscosity of nanofluid, one being performed by Buongiorno[125] where the author used the experimental data of Pak and Cho[109] and correlated the dynamic viscosity for both γ-Al_2O_3-water and TiO_2-water and presented in the following expressions, respectively:

$$\mu_{\mathrm{nf}} = \mu_f\left(1 + 39.11\varphi + 534\varphi^2\right) \quad (49)$$

$$\mu_{\mathrm{nf}} = \mu_f\left(1 + 5.45\varphi + 108\varphi^2\right). \quad (50)$$

Khanafer and Vafai[126] considered the same experimental data of Pak and Cho[109] and derived the following formulations of the dynamic viscosity for both nanofluids (γ-Al_2O_3-water and TiO_2-water), respectively:

$$\mu_{\mathrm{nf}} = \mu_f\left(1 + 23.1\varphi + 1525\varphi^2\right) \quad (51)$$

$$\mu_{\mathrm{nf}} = \mu_f\left(1 + 3.54\varphi + 169\varphi^2\right). \quad (52)$$

Although all four previous viscosity models are based on the same experimental data, the factors in the corresponding expressions are apparently different. However, the resulted viscosity values for the same nanofluid are comparable. Another experimental study was performed by Wang et al[127] where they measured the viscosity of Al_2O_3-water, which was higher than that measured by the Pak and Cho[109] by 2.5 times. That could be due to the effect of particle size and shape or might be due to the effect of non-Newtonian flow behavior, which has a vital role in nanofluid measurements. However, Maiga et al[128] used the same data of Wang et al[127] and derived the following expression:

$$\mu_{\mathrm{nf}} = \mu_f\left(1 + 7.3\varphi + 123\varphi^2\right). \quad (53)$$

It is noticeable that factors of this model are considerably smaller than those of Pak and Cho[109] but clearly larger than those of analytical correlation proposed by Batchelor.[123] This model is very common and widely used in the available literature and it can be recommended for more accurate results. Chen et al[129] measured experimentally the effective viscosity of another nanofluid (TiO_2-ethyl glycol) and derived the following correlation:

$$\mu_{\mathrm{nf}} = \mu_f\left(1 + 10.6\varphi + 112\varphi^2\right). \quad (54)$$

This correlation is valid for a volume fraction up to about 10%. It is noticeable from the correlations presented previously that the viscosity equation is currently modeled with a polynomial expression of degree two. However, some authors, including Mooney[130] followed by Tseng and Chen[131] and Tseng and Lin,[132] proposed a viscosity equation in the exponential form as below:

$$\mu_{\mathrm{nf}} = A\mu_f \exp^{(B\varphi)}, \quad (55)$$

where A and B are empirically determined factors which are considerably different in all studies. On the other hand, Nguyen et al[133] derived and supplied two correlations in two different functions (exponential and polynomial) for the same nanofluid (Al_2O_3-water) in the following expressions, respectively:

$$\mu_{\mathrm{nf}} = \mu_f\left(1 + 2.5\varphi + 150\varphi^2\right) \quad (56)$$

$$\mu_{\mathrm{nf}} = 0.904\,\mu_f \exp^{(14.8\varphi)}. \quad (57)$$

It is worth noting that the coefficient value of the second term of the polynomial model of Nguyen et al[133] is equal to the results of analytical expressions for spherical particles (2.5). Moreover, this model proposes non-Newtonian behavior of the resulted nanofluids. Whereas the exponential correlation proposed by Tseng and Lin[132] was given by:

$$\mu_{\mathrm{nf}} = 13.47\,\mu_f \exp^{(35.98\varphi)} \quad (58)$$

To conclude, the exponential expression for the nanofluid viscosity is not recommended due to higher values predicted as compared with the polynomial

expressions. Moreover, a small error in volume fraction calculation would lead to significant error in the viscosity value when using the exponential function. Therefore, it is currently recommended to utilize the polynomial function with degree two based on the temperature-dependent base fluid viscosity (Michaelides[134]).

6.1.4 | Thermal conductivity of nanofluid, k_{nf} (W/m K)

The first model for calculating the electrical conductivity of a heterogeneous solid–fluid mixture of spherical particles was proposed by Maxwell[135] in the following expression:

$$k_{nf} = k_f \left[1 + \frac{3(k_s - k_f)\varphi}{(k_s + 2k_f) - (k_s - k_f)\varphi}\right]. \quad (59)$$

This model is only applicable for a volume fraction less than 1%. The same analytical investigation had been proposed by Bruggeman[136] to derive an expression of thermal conductivity of nanofluid with different regular shapes. The resulted correlation is given by:

$$k_{nf} = k_f \left[1 + \frac{n(k_s - k_f)\varphi}{k_s + (n-1)k_f - (k_s - k_f)\varphi}\right]. \quad (60)$$

The coefficient n represents the particle shape. It is 3 when the particle is sphere and 6 for cylinders. For irregular shape, Hamilton and Crosser[137] proposed a generic model to include different shapes of irregular particles and derived the following correlation:

$$k_{nf} = k_f \left[1 + \frac{3(k_s - k_f)\varphi/\Psi}{k_s + k_f\left(\frac{3}{\Psi} - 1\right) - (k_s - k_f)\varphi}\right]. \quad (61)$$

The parameter Ψ represents the shape factor. For a sphere particle shape, $\Psi = 1$ and the above expression will be reduced to the Maxwell's expression whereas $\Psi = 5$ for cylindrical particle shapes. However, Bruggeman[136] proposed another model based on homogenous spherical solid–fluid mixture with no limitations to the volume fraction. This model supplies prediction slightly better than those discussed previously and can be presented in the following correlation:

$$k_{nf} = 0.25[k_s(3\varphi - 1) + (2 - 3\varphi)k_f + \sqrt{\Delta}], \quad (62)$$

where

$$\Delta = [(3\varphi - 1)k_s + (2 - 3\varphi)k_f]^2 + 8k_s k_f.$$

Another model was derived by Nan et al[138] based on very long aspect ratios of particle sizes and assumption of ($k_s \gg k_f$) which is appropriate for very high thermal conductivity particles such as CNT, SWCNT, and so forth. This model is represented by the following expression:

$$k_{nf} = k_f \left[1 + \frac{k_s \varphi}{3k_f}\right]. \quad (63)$$

This expression cannot be applied for general nanofluids since it is only derived for high-thermal conductivity nanoparticles.

Khanafer and Vafai[126] developed a model from experimental data of Al_2O_3 and CuO particles mixed with water base fluid. The derived expression is a statistical expression of thermal conductivity of nanofluid at ambient conditions which is given by:

$$k_{nf} = k_f \left[1 + 1.0112\varphi + 2.4375\varphi\frac{23.5}{\alpha} + 0.0248\frac{k_s\varphi}{k_f}\right]. \quad (64)$$

The parameter α in the above equation represents the particle radius (in nm). This formula introduces adversely relation between the thermal conductivity of nanoparticles and base fluids and also there is no explanation about how to define the particle size for nonspherical particles.

Yu and Choi[139] introduced an expression for the thermal conductivity of nonspherical particles suspended in a base fluid based on the Interfacial Layer concept. Their mode is written for the heterogeneous mixture in the following formulation:

$$k_{nf} = k_f \left[1 + \frac{3\varphi(k_s - k_f)\left(1 + \frac{\delta\alpha}{\alpha}\right)^3}{(k_s + 2k_f) - \varphi(k_s - k_f)(1 + \delta\alpha/\alpha)^3}\right]. \quad (65)$$

The values $\delta\alpha$ and α are empirical parameters which are assumed to be 2 and less than 5 nm, respectively, in their study. However, the nonlinear behavior of the thermal conductivity observed with nanofluids is not accurately predicted by this model. Others models are presented in more details in Michaelides.[134] The previous discussion clarifies that the thermal conductivity of nanofluids depends strongly on different parameters: both conductivities of fluid and solid particles, mixture temperature, a volume fraction value, and size dimensions of particles.

TABLE 10 Effects of nanoparticles (NP) used in literatures and their outcomes

References	Limitations	N.P. type	Base fluid type	Volume fraction (φ)	Achievements
Sokhansefat et al[147]	Single-phase model and three inlet temperatures.	Al_2O_3	Synthetic oil	1, 3, 5	Considerable increase in heat transfer coefficient with increasing nanoparticle volume fraction.
Paul et al[148]	One inlet temperature, laminar, and turbulent flow.	Al_2O_3	Ionic liquids	0.18, 0.36, 0.9	0.9% of φ enhanced the thermal conductivity by about 11% and heat capacity by 49%.
Zadeh et al[149]	Using single-phase and two-phase models.	Al_2O_3	Synthetic oil	0, 1, 2, 3, 4, 5	11.5% and 36% increase in the heat transfer coefficient using 5% of φ for models 1 and 2, respectively.
Mwesigye et al[150]	Single-phase model, different Re numbers, and different inlet temperatures.	Al_2O_3	Synthetic oil	0-4, 0-6, 0-8	The heat transfer performance increased by 35%, 54%, and 76% with increasing φ, respectively. The maximum efficiency enhancement was 7.6% recorded at the smallest temperature and minimum Re number.
Mwesigye et al[151]	Single-phase model, different Re numbers, and different inlet temperatures.	CuO	Syltherm 800	1-6	38% improvement in the heat transfer performance and 15% increase in the thermal efficiency.
Basbous et al[152]	Single-phase model and different inlet temperatures.	Al_2O_3	Syltherm 800	1, 3, 5	18% enhancement in convective heat transfer coefficient and 10% reduction in thermal loss at the largest volume fraction.
Abu-Hamdeh and Almitani[111]	Single-phase model.	Al_2O_3, Fe_3O_4, ZnO	Water	1-4	5.5%-9.01%, 6.2%-12.3%, and 7.2%-14.4% improvements in convection heat transfer coefficient with ZnO-water, Fe_3O_4-water, and Al_2O_3-water, respectively.
Basbous et al[153]	Single-phase model, different Re numbers, and different inlet temperatures.	Cu, CuO, Ag, Al_2O_3	Syltherm 800	5	36% enhancement in convective heat transfer coefficient and 21% reduction in overall thermal loss coefficient using Ag-Syltherm 800 nanofluid.
Bellos et al[154]	Single-phase model and different inlet temperatures.	Al_2O_3	Thermal oil	2	4.25% improvement in the thermal efficiency.
Kaloudis et al[57]	Both models, the receiver was subjected under constant wall temperature.	Al_2O_3	Syltherm 800	0-4	10% enhancement obtained in the collector efficiency at φ of 4%. Better results obtained by the two-phase model.
Toghyani et al[155]	Single-phase model, different flow rates, different DNI, and different inlet temperatures.	CuO, SiO_2, TiO_2, Al_2O_3	Therminol-55	2-5.5	The increase in overall exergy efficiency was 3%, 6%, 9%, and 11% when using CuO, TiO_2, SiO_2, and Al_2O_3, respectively.
Ghasemi and Ranjbar[215]	Single-phase model, uniform heat flux, and different Re numbers.	CuO, Al_2O_3	Water	0.5, 1.5, 3	The heat transfer coefficient increased up to 35% for CuO and 28% for Al_2O_3 at volume fraction

(Continues)

TABLE 10 (Continued)

References	Limitations	N.P. type	Base fluid type	Volume fraction (φ)	Achievements
					of 3%. However, the friction factor of Al_2O_3 was smaller than that of CuO.
Ferraro et al[211]	Single-phase model, different flow rates, different DNI, and different inlet temperatures.	Al_2O_3	Synthetic oil	5	A slight improvement in thermal efficiency and higher pumping power.
Wang et al[216]	Single-phase model, different DNIs, different inlet velocities, and inlet temperatures.	Al_2O_3	Synthetic oil	0, 0.01, 0.03, 0.05	The absorber deformation decreases moderately from 2.11 mm to 0.54 mm by increasing the φ from 0% to 0.05%.
Mwesigye et al[214]	Single-phase model, different flow rates, and different inlet temperatures.	Cu	TherminolVP-1	0, 1, 2, 4, 6	Heat transfer enhanced by 8%, 18%, and 32% at φ of 2%, 4%, and 6%, respectively. Moreover, the system thermal efficiency increased by 12.5% as the φ increased from 0% to 6% and the entropy generation rate decreased from 20% to 30%.
Alashkar and Gadalla[217]	Single-phase model, different flow rates, different DNI, and different inlet temperatures.	Al_2O_3, Cu, SWCNT	Syltherm 800	1-5	The candidate 5% Cu led to increase the annual energy from 163 to 167 GW and net savings from 4.58 to 4.69 million $.
Abid et al[212]	Single-phase model, different flow rates, different DNI, various ambient temperatures, and different inlet temperatures.	Al_2O_3, Fe_2O_3	Water	Wt.: 2-2.5	0.65% enhancement in thermal efficiency using Al_2O_3-water and 0.59% when using Fe_2O_3-water.
Mwesigye and Meyer[101]	Single-phase model, different flow rates, and different inlet temperatures.	Al_2O_3, Ag, Cu	TherminolVP-1	0, 1, 2, 4, 6	The maximum enhancement in the thermal efficiency was 13.9% recorded by silver-Therminol while Al_2O_3-Therminol provided the smallest enhancement 7.2% at the maximum solar concentration ratio of 113.
Bellos and Tzivanidis[218]	Single-phase model, different flow rates, and different inlet temperatures.	Al_2O_3, CuO	Syltherm 800	4	The thermal efficiency increased by 1.26% using CuO-Syltherm 800 and 1.13% using Al_2O_3-Syltherm 800.
Kasaeian et al[146]	Using glass-glass absorber tube.	MWCNT, nanosilica	Ethylene glycol (EG)	0.1, 0.2, 0.3	Compared with the base fluid, the thermal efficiency increased by 30.4% with an increase of 15.7 K in the outlet temperature using MWCNT/EG. For nanosilica/EG, the efficiency increase was 14% with an increase of 7.7 K at the outlet temperature.

(Continues)

TABLE 10 (Continued)

References	Limitations	N.P. type	Base fluid type	Volume fraction (φ)	Achievements
Paul et al[219]	Measuring the thermal properties at different temperatures.	Al_2O_3	Ionic liquids	0.5, 1.0, 2.5	Using 2.5 wt% of nanoparticles led to an enhancement of thermal conductivity by about 11% for [C4mim][NTf2], while the heat capacity enhancement reached up to 62% for [C4mpyrr][NTf2].
Khakrah et al[220]	Single-phase model, different flow rates, wind velocities, and different orientations.	Al_2O_3	Synthetic oil	1, 3, 5	The thermal efficiency when using φ of 5% enhanced by 12.4% and 14.3% for rotated and horizontal reflector's orientations.
Allouhi et al[221]	Single-phase model, different DNIs, and different wind velocities.	Al_2O_3, CuO, TiO_2	Syltherm 800	3, 5	The thermal energy enhances by 1.46, 1.25, and 1.40 using Al_2O_3, CuO, and TiO_2, respectively. The maximum exergy efficiency was about 9.05% by using 3% of CuO.
Aguilar et al[222]	Measuring the thermal properties at different temperatures.	NiO	Biphenyl and diphenyl oxide	wt%: (1, 5, 10)10^{-4}	An increase in the heat transfer coefficient up to 50% and thermal conductivity up to 96%.
Alashkar and Gadalla[223]	With/without storage system.	Cu, Ag	TherminolVP-1, Syltherm 800	1-5	The better performance was obtained when using 4% Ag-TherminolVP-1 nanofluid.
Bellos et al[224]	Single model, different inlet temperatures, and single flow rate.	CuO	Syltherm 800, Molten salt	6	40% Nu number improvement using CuO-Syltherm 800 and up to 13% when using CuO-molten salt.
Mwesigye et al[213]	Single-phase model, different flow rates, and different inlet temperatures.	SWCNT	TherminolVP-1	0.25, 0.5, 1, 2, 2.5	234% enhancement in the heat transfer performance and 4.4 increase in thermal efficiency at 2.5% volume fraction.
Khakrah et al[225]	Single-phase model, different inlet temperatures, and different wind speeds.	Al_2O_3	Synthetic oil	0-5	19% increase in the relative exergy efficiency at 5% φ. However, changing the wind speed affected the nanofluid behavior.
Kasaiean et al[226]	Different DNIs, different incident angles, and different inlet temperatures.	MWCNT, CuO	Ethylene glycol (EG)	0.3, 6	15% increase in convection heat transfer coefficient using 6% MWCNT-EG.
Ebrahimi-Moghadam et al[227]	Different inlet temperatures, Re numbers, and particle diameters.	Al_2O_3	Ethylene glycol (EG)	0.01-0.1	Using nanofluids caused a reduction in the thermal entropy generation and rising the hydraulic entropy generation.
Razmmand et al[228]	Two-phase model.	Ag, Al, Au, Ni, TiO_2	Water	0.1, 0.3, 0.5, 1, 2	Heat flux at the critical length when using Al-H_2O and Au-H_2O was increased by 2.3 and 2.7 times, respectively, compared with base fluid.

(Continues)

TABLE 10 (Continued)

References	Limitations	N.P. type	Base fluid type	Volume fraction (φ)	Achievements
Korres et al[229]	Single-phase model and different inlet temperatures in laminar flow.	CuO	Syltherm 800	5	2.76% enhancement in the thermal efficiency and 2.6% improvement in the exergy efficiency.
Abed et al[230]	Single-phase model, different Re numbers, and uniform heat flux distribution.	TiO_2, Al_2O_3, CuO, Cu	Water	2, 4, 6	Using 6% volume fraction led to enhance the performance evaluation criteria (PEC) by 1.214, 1.2, 1.18, and 1.155 when using TiO_2, Al_2O_3, CuO, and Cu, respectively.
Peng et al[115]	Experimental and two-phase model numerical studies using different Re numbers.	Cu, CNT	Gallium (Ga)	2, 5, 8, 10	The force heat transfer coefficient enhanced by 34.5% and 45.2% when using Cu-Ga and CNT-Ga, respectively.
Bozorg et al[231]	Single-phase model and porous in annular space, different Re number, and different inlet temperatures.	Al_2O_3	Synthetic oil	1.5, 3	By using 3% nanofluid and porous in annular, the heat transfer coefficient increased by 7% and 20%, whereas the thermal efficiency has raised by 5% and 14%, while the pressure drop increased by 42.5% and 42%, respectively.

6.2 | History of investigations using nanofluids in PTCs

To the best of the author's knowledge, there are a few experimental studies, which used nanoparticles in PTCs analysis, and the majority of them used water as the base working fluid. Chaudhari et al,[140] Subramani et al,[141] and Bretado et al[142] used Al_2O_3 with water in a PTC system. According to their results, the maximum thermal efficiency was enhanced up to 24%. While Coccia et al[143] examined (Fe_2O_3, SiO_2, TiO_2, ZnO, Al_2O_3, and Au) immersed in water for different volume fractions. As per their findings, there was no marked enhancement in the thermal efficiency compared with the base fluid.

The usage of Al_2O_3 and Fe_2O_3 nanoparticles in water with different concentrations (0.20%, 0.25%, and 0.30%) was recently studied by Rehan et al.[144] The authors reported an increase in the thermal efficiency by 13% with Al_2O_3 and 11% with Fe_2O_3 mixed with water. Moreover, Subramani et al[145] tested the usage of TiO_2/water nanofluid in the PTC using different volume fractions (0.05%, 0.10%, and 0.20%). The authors reported an 8.66% increase in the thermal efficiency for the highest concentration (0.20%). Recently, Natividade et al[102] studied a promising new type of nanoparticles called multilayer graphene suspended in water as a base fluid, with different flow rates and two-volume fractions (0.00045% and 0.00068%). It was noticed that a significant improvement in thermal efficiency was obtained with increasing the volume fraction where it was 31% with volume fraction of 0.00045% whereas it reached up to 76% with the largest volume fraction compared with the base fluid.

On the other hand, the experimental investigation using ethylene glycol (EG) as a base fluid was conducted by Kasaeian et al[146] using MWCNT and nanosilica nanoparticles with volume fractions of 0.1%, 0.2%, and 0.3%. The preparation of nanofluids was done by dispersing the nanoparticles inside the based fluid using a magnetic stirrer for 5 hours at 900 rpm in order to avoid the effect of particle agglomeration and using ultrasonic bath after that with power of 60 W from 0.25 hour in order to avoid the particles destruction. The authors found that the thermal efficiency at 0.3% concentration was 17% higher than that obtained by the base working fluid. The summarized review of previous investigations illustrating the use of nanofluids in PTCs of numerical studies and main findings is listed in Table 10.

TABLE 11 Thermal properties of particles used in previous studies

Type	T (K)	ρ (kg/m^3)	C_p (J/kg K)	k (W/m K)	Size (nm)	References
BH + SiO_2	300	2400	968.9	1.38	100	Okonkwo et al[157]
OLE + TiO_2	300	1120	2406	0.78	70	Okonkwo et al[157]
GO + Co_3O_4	293	3296	627.5	692.77	–	Minea et al[113]
Ag + MgO	293	7035	554.5	242	–	Minea et al[113]

6.3 | Hybrid nanofluids in the PTC applications

All investigations presented previously for PTC systems have concentrated on single nanofluids, that is, mixtures that include one type of nanoparticles suspended in a single base fluid. The hybrid nanofluids concept is basically achieved by adding at least two types of nanoparticles in a single or a combination of base fluids. In fact, mixing two or more metallic or nonmetallic particles until reaching the homogeneous phase is definitely promising technical approach to enhance thermo-physical properties, hydrodynamic behavior and accordingly the thermal characteristics compared with the single nanofluid. Researchers started paying attention to this technology since 2013. The major application of hybrid nanofluids is renewable energy applications, and in particular solar collectors. However, using this technology in solar applications whether numerically or experimentally is extremely rare. This is due to the difficulty of describing numerically the thermal properties of hybrid nanofluids and implementing this technology in the realistic systems (Minea et al[113]). The thermo-physical properties of hybrid nanofluids are discussed deeply in Babar and Ali.[156] However, the thermal properties of some hybrid nanoparticles that are found in previous studies are presented in Table 11.

Regarding the experimental and numerical investigations in PTC systems using hybrid nanofluids, Bellos and Tzivanidis[158] compared numerically the performance of single nanofluids (Al_2O_3 and TiO_2) with volume fraction of 3% and hybrid nanofluid (1.5% Al_2O_3 + 1.5% TiO_2). Results showed that up to 1.8% improvements in the thermal efficiency when using hybrid nanofluids while only 0.7% with single nanofluid. Menbari et al,[159] Menbari and Alemrajabi,[160] and Menbari et al[161] studied experimentally the effect of (γ-Al_2O_3 + CuO) suspended in hybrid base fluids of water and EG with different volume fractions, different solar irradiance and different flow rates. They pointed out that the thermal efficiency was higher in the case of dispersing hybrid nanoparticles than using single nanoparticle. It was also noticed that the larger enhancement in the thermal efficiency was marked when using water as a base fluid since the mixture of water-EG has a disadvantage of boiling and freezing temperature which is higher than those of pure water. As per their findings, the maximum thermal efficiency obtained was 48.03% using the largest volume fraction for hybrid nanoparticles with water whereas the minimum thermal efficiency recorded was 29.97% using the smallest volume fraction of hybrid nanoparticles with water-EG base fluid. Okonkwo et al[157] investigated numerically the behavior of new hybrid particles (green-synthesized) OLE-TiO_2 and BH-SiO_2 with water as base fluid using 3% volume fraction under different fluid inlet temperatures and different flow rates. Results showed that the thermal efficiency was enhanced by 0.073% and 0.077% when using OLE-TiO_2 and BH-SiO_2, respectively, with increasing in heat transfer coefficient by 128% and 138%. Other types of hybrid nanofluids (Ag + MgO), (Al_2O_3 + Cu), and (GO + Co_3O_4) have been numerically investigated by Minea et al[113] with both single base fluid (water, EG) and hybrid base fluid (water + EG) in the laminar flow regime. The authors reported an increase in the convection heat transfer coefficient between 115% and 125% when using (GO + Co_3O_4) and base fluid of (water + EG).

7 | THE EFFECT OF INSERTING SWIRL GENERATORS ON THE THERMAL PERFORMANCE

The use of swirl generators inside the receiver tube is a passive technique can be used to enhance the convection heat transfer rate. These devices could be shaped as twisted tapes, fins, coils, wires, and spiral grooved tubes etc. The flow across such devices has important features, such as an intense mixing between flow in the near-wall region and main-stream, a reduction in the thickness of the thermal boundary layer, and an increment in the tangential velocity component. Such techniques improve the thermal efficiency of PTC, minimize the cost, reduce the thermal gradient of the absorber tube and improve the overall system reliability subsequently.

A wide range of insert types have been studied in the past. Kasperski and Nemś[162] investigated the effect of multiple-fin arrays inside the solar receiver on the

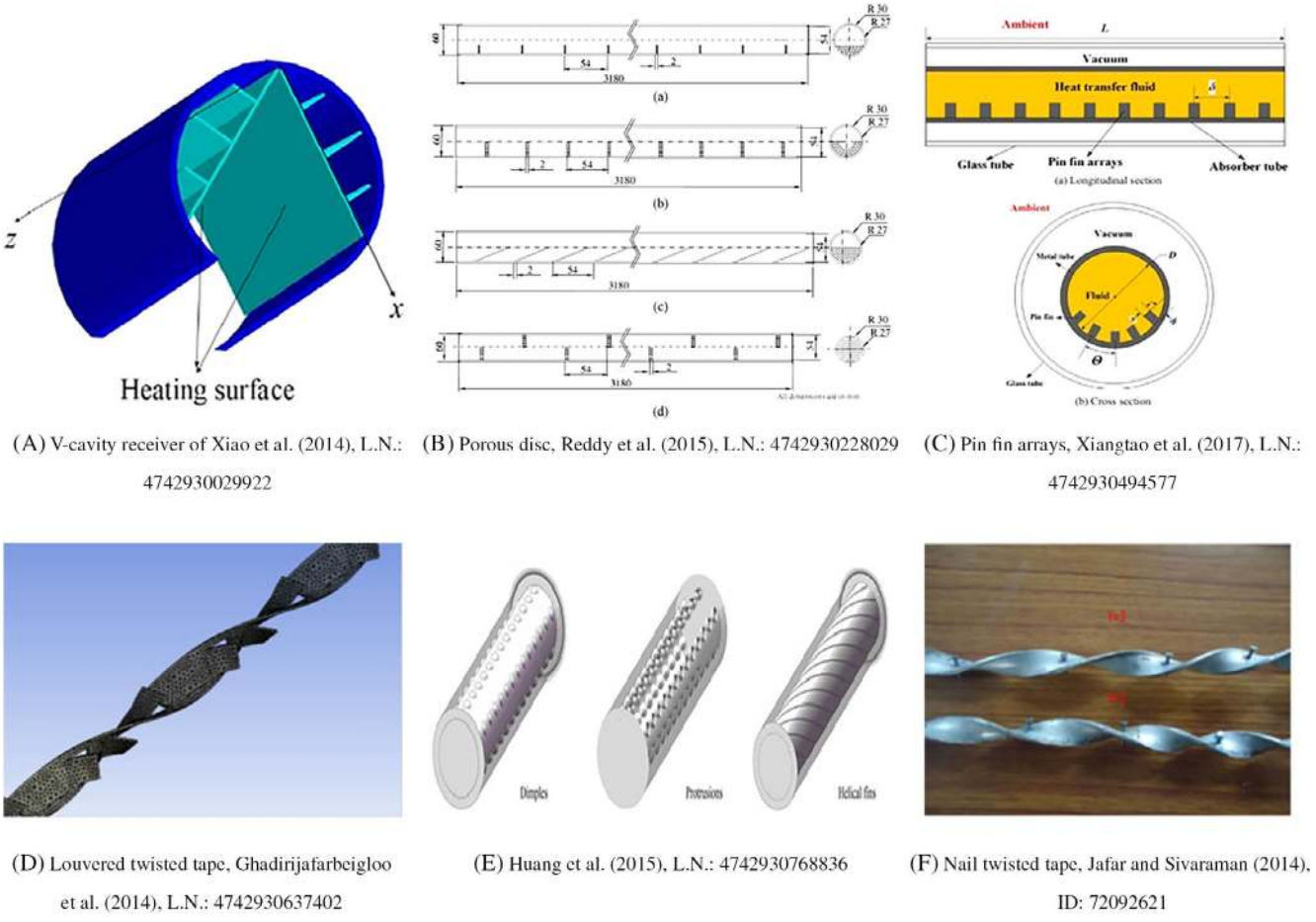

(A) V-cavity receiver of Xiao et al. (2014), L.N.: 4742930029922

(B) Porous disc, Reddy et al. (2015), L.N.: 4742930228029

(C) Pin fin arrays, Xiangtao et al. (2017), L.N.: 4742930494577

(D) Louvered twisted tape, Ghadirijafarbeigloo et al. (2014), L.N.: 4742930637402

(E) Huang et al. (2015), L.N.: 4742930768836

(F) Nail twisted tape, Jafar and Sivaraman (2014), ID: 72092621

FIGURE 14 Parabolic trough receiver with different inserting types [Colour figure can be viewed at wileyonlinelibrary.com]

thermo-hydraulic efficiency of the PTC compared with the smooth receiver. Up to 14% efficiency enhancement resulted in the case of half-pipe finned arrangement when there is no limitation of the ambient velocity. Song et al[163] studied numerically the effect of helical screw-tape with a core rod inside the receiver of the PTC on the thermal performance. Results proved that the usage of the helical screw-tape decreased the maximum temperature and heat losses by a small amount (less than those predicted by the tubular tube by six times at 0.11 kg/s and inlet temperature of 373 K). On the other hand, the pressure drop increased with increasing the mass flow rate by four times in the typical receiver while the pressure drops increase by 23 times in the case of using the helical screw tape insert.

Mwesigye et al[164] studied numerically a new type of insert called a twisted type with wall-detached inside the solar receiver. Results revealed that the temperature gradient of the absorber tube in the circumferential direction was reduced by 68% and the thermal efficiency was increased by 5% to 10% at a twist ratio of greater than 1 due to the presence of twisted tapes. Furthermore, the largest reduction in the entropy generation was about 58.8%. Chang et al[165] investigated numerically a new type of inserts in which they used concentric and eccentric rod tabulators in different positions with molten salt as a base fluid. The normalized Nusselt number resulted from the simulations increased from 1.1 to 7.42 times with respect to the typical solar receiver. Bellos and Tzivanidis (2018b)[166] used a star-design as a tabulator inside the solar receiver with different dimensions of star configurations. According to results obtained based on the optimum star configuration, up to 60% enhancement in the heat transfer coefficient and 14% reduction in thermal losses whereas up to 900% increase in the pressure drop. Recently, Liu et al[167] studied numerically conical strip inserts in the PTC system considering the effect of the geometrical parameters including a central angle, pitch ratio, and hollow diameter of inserts additional to different flow conditions. Results clarified that using this type of inserts led to an increase in the Nusselt number by 45% to 203% with a large reduction in both thermal losses and entropy generation reached to 82.1% and 74.2%, respectively. Moreover, the overall enhancement in

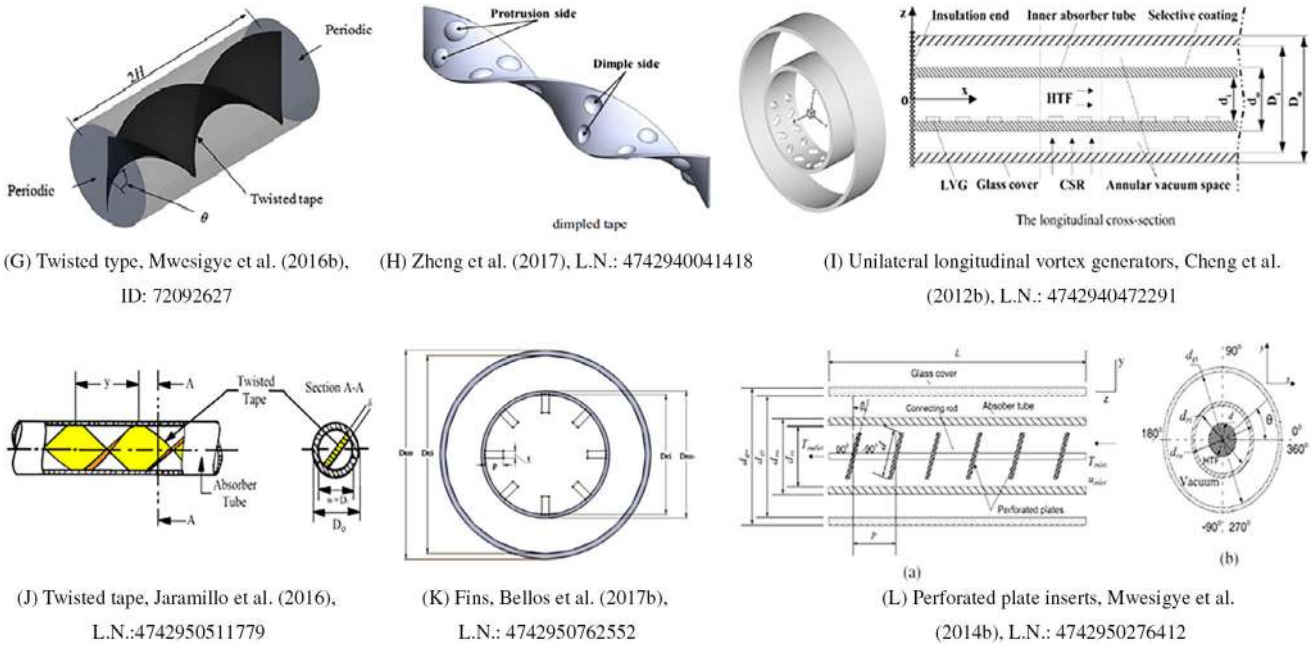

(G) Twisted type, Mwesigye et al. (2016b), ID: 72092627

(H) Zheng et al. (2017), L.N.: 4742940041418

(I) Unilateral longitudinal vortex generators, Cheng et al. (2012b), L.N.: 4742940472291

(J) Twisted tape, Jaramillo et al. (2016), L.N.:4742950511779

(K) Fins, Bellos et al. (2017b), L.N.: 4742950762552

(L) Perforated plate inserts, Mwesigye et al. (2014b), L.N.: 4742950276412

FIGURE 14 (Continued)

thermal efficiency and exergetic efficiency increased by 0.02% to 5.04% and 5.7%, respectively.

A large number of papers in the literature presented different types of inserts, some of them are shown in Figure 14. Besides, many types of swirl generators are individually investigated in previous studies taking into account the effect of geometrical arrangements of inserts, various rotating positions of inserts, different flow conditions, various ambient conditions, and a wide range of solar irradiations. Table 12 presents all abbreviations that are used in Table 13 which summarize the previous works and their main achievements.

8 | EFFECTS OF THE COLLECTOR DESIGN ON THE THERMAL PERFORMANCE

The structure of the solar receiver is very important factor that should be taken into account to improve the thermal performance. A new structure of a PTC was presented by Bader et al[201] in which the mirrored solar collector was made from pneumatic polymer which was mounted on a frames made from precast concrete. Results showed that the maximum solar concentrating ratio was 151. Wang et al[202] studied numerically the reliability of the collector by employing a secondary homogenizing reflector (HR). They reported that the absorber cylinder with the new configuration could be uniformly heated. This was accompanied with a slight decrease of about 4% efficiency due to the optical losses where a significant drop was noticed at the highest operating temperature. Behar et al[23] proposed new structure components such as reflectors and receivers rather than using the typical ones. The new collector was examined under different conditions and it was found that, at the large operating temperatures, there was a small divergence in the estimation of the heat losses. Increasing the concentration ratio of PTC is one of the most important solutions that make this technique more economic and competitive compared with other solar systems. Considering this advantage, Sanchez and Rosengarten[88] proposed a new type of PTC using a second-stage flat mirror. The concentration ratio increased up to 80%. Additionally, the heat flux distribution became more uniformly around the receiver. Fuqiang et al[203] numerically tested a new design of a PTC in which the tube was designed as an asymmetric outward corrugated convex. Two very important features were observed: the heat transfer enhancement improved while the thermal strain in the absorber receiver decreased. To study the effect of nocircular solar receivers, Bellos et al[154] numerically tested the effects of absorber geometry (sign wave) on the thermal efficiency of the IST-PTC with three different HTFs. According to their findings, the thermal efficiency improved by 4.55% compared with the typical configuration. Another new design was numerically investigated by Wang et al,[204] in which the length, aperture width and the diameter of a collector were designed to change gradually along the mean flow direction. The new design

TABLE 12 The abbreviations used in Table 13

W.R.	Width ratio	C.W.	Coiled wire	Nu_0	Nusselt number of the smooth tube
Re	Reynolds number	Lpm	Litter per minute	Th.Pe.	Thermal performance
T.R.	Twisted ratio	P.D.	Pressure drop	H.T.E.	Heat transfer enhancement
Nu	Nusselt number	H.L.	Heat losses	H.T.C.	Heat transfer coefficient
F.F.	Friction factor	T_{in}	Inlet temperature	Th.E.F.	Thermal efficiency factor
T.T.	Twisted tape	F.th.	Fin thickness	H	Height of metal foam in tube
H.T.	Heat transfer	F.L.	Fin length	F_0	Friction factor of the smooth tube
M.F.R.	Mass flow rate	E.G.	Entropy generation	d/D	Ring diameter/inner receiver diameter
Pr.	Prantle number	I.S.I.	incident solar irradiation	PEC	Performance evaluation criteria
I.A.	Incidence angle	Th.L.	Thermal losses	Th.E.I.	Thermal enhancement index
V	Velocity	Th.E.	Thermal efficiency	δ	Distance between two fins
A.R.	Aspect ratio	C.R.	Clearance ratio	Exe. Per	Exergetic performance
I.T.	Insert type	λ	Tip-to-base ratio of fin	Q/d	Fin distance/inner receiver diameter

proposed enhancement in the methanol conversion rate by 8.35% to 15.85% larger than this proposed by the typical design.

Recently, Bitam et al[205] studied numerically a new design of S-curved/sinusoidal absorber receiver. They found that the Nusselt number and thermal efficiency increased by 63% and 3%, respectively, as compared with the traditional design, whereas the friction factor increased by 40.8%. In the same year, Liang et al[206] proposed experimentally a new PTC with a cavity receiver. The receiver is connected to two inclined fins which act to absorb the energy concentrated. The idea is to avoid the possible nonuniform distribution of the flow in such applications. The maximum thermal efficiency was 48%. Peralta and Gleckman[207] designed experimentally a new support structure of the PTC system using lumber material. They examined the new design numerically and they expected that the mean intercept factor is greater than 95%. Li et al[208] proposed a novel design of the absorber receiver in the shape of a linear cavity with a lunate channel depending on the effect of the black cavity. The new design provided better behavior in terms of thermal performance, in particular the temperature distribution, compared with the typical receiver.

Another novel design of the solar receiver, proposed by Wang et al,[209] is covered with infrared reflectors (IR) on the upper part of the solar receiver from both sides. Authors concluded that the maximum reduction in thermal loss at the absorber temperature of 600°C was 43.8% whereas the thermal efficiency enhancement was 16.7%. Investigating the effect of the focal line is also taken into consideration by Kulahli et al[210] in which they proposed a new design for the parabolic trough with a changing focal length in the axial direction. The maximum enhancement in the thermal efficiency was 0.21% and 0.63% improvement in the thermal gain compared with the conventional design. Some of the aforementioned new designs are listed below in Figure 15.

9 | FURTHER DISCUSSIONS

Enhancement in PTC systems performance can be achieved using numerous technologies, as illustrated in the preceding discussions. These technologies can enhance the thermal and hydraulic performances, or they can improve the PTC optical characteristics, which in turn leads to higher thermal energy production, lower thermal losses, lower thermal stresses, optimized tracking systems, reduction in the manufacturing cost, optimized rim angle and collector shape parameters, and so forth. As clearly noticed, the previous studies aimed to improve the optical efficiency are fewer than those aimed to enhance the thermal performance. These technologies are extensively investigated numerically whereas the experimental works are relatively rare.

The usage of nanofluid technology is an effective approach to gradually improve the PTC thermal efficiency. Both metallic and nonmetallic nanoparticles can be suspended into the base fluids with different volume fractions or different weight percentage. Even though some studies (such as Ferraro et al[211] and Abid et al[212]) did not observe significant improvement with nanofluids, the bulk of the available literature seems to indicate that nanofluids can indeed improve the thermal performance of PTC systems. The maximum enhancement reported to date in the heat transfer coefficient was approximately

TABLE 13 The effect of insert types relative to the tubular tube in recent investigations

				Enhancements by inserting swirl generators compared with the typical receiver							
References	**Examined parameters**		**Typical output**	**Enhancement**	**Technique 1**	**Enhancement**	**Technique 2**	**Enhancement**	**Technique 3**	**Enhancement**	**Technique 4**
Reddy and Satyanarayana[168]	Re: (3-25.1)10^4 λ: 0-0.75 0.8-6.8 kg/s		H.T.C.& P.D. (Pa)	490-2200 Up to 1850	Trapezoidal fins	500-2300 Up to 2400	Circular fins	490-2200 Up to 1600	Triangular fins	–	–
Reddy et al[169]	Re: (3-25.1)10^4 A.R.: 0-2.2 Pr: 8.11		Nu: 229-1286	Nu: 302-1412	Porous fins	Nu: 263-1357	Solid fins	–	–	–	–
Kumar and Reddy[170]	Re: 31 845-254 765 Pr: 8.11, I.A.: 30°-60°		Nu number	Nu: 64.3%	Top porous discs	–	–	–	–	–	–
Sundar and Sharma[171]	Re: (10-22)10^3 TR: 0-83		H.T. & F.F.	H.T. (%) 22.76-30.30	0.5% Al_2O_3	H.T. & F.F. 33.51-42.17% 1.01-1.26	T.T. of 5 T. R.	–	–	–	–
Cheng et al[172]	Re: (3.8-38)10^4 I.S.I.: 100-1000 W/m^2		Nu & F.F. & Th.L. (%) & (PEC)	160 & 276.4 & 13.39% & 1.18	Milt-longitudinal vortexes	–	–	–	–	–	–
Kasperski and Nemś[162]	(0.002-0.1) m^3/s		Heat (W): 58.5	135.5, 148	Long. fins, Diff. height fins	179.6, 236.5, 255.5	Ring shape, wood-grain, wavy fins	423	Fully finned	434	Half-pipe finned
Wang et al[173]	H: 0-1 (m) V: 0-27 (m/s)		Nu (times) & F.F. (times) & (PEC)	10-12, 400-700, 1.1-1.5	Metal foam ($H = 0.75$ top)	5-10, 10-20, 1.4-3.2	Metal foam ($H = 0.25$ bottom)	–	–	–	–
Soo and Benito[174]	Heat transfer fluid: air, helium, CO_2), IT: helical coil, TT, dimple, porous foam		Th.E. (%), power (W), P.D. (kPa)	80.4%, 16.5, 5.26	Dimple & helium	–	–	–	–	–	–
Ghadirijafarbeigloo et al[175]	Re: (5-30)10^3 TR: 2.67-5.33		Nu (%) F.F. (%)	Nu: 37%	T.T.	Nu & F.F. 150% & 210%	Louvered T.T.	–	–	–	–
Waghole et al[176]	Re: 500-6000 TR: 0.577-1.732	H.T. (times) F.F. (times) Th.E. (%)	1.25-2.1, 1-1.75, 135%-205%	T.T. and 0.1% of silver	–	–	–	–		–	–
Xiao et al[177]	Re: 117.6-480.3.	H.L. (W)	26.6	V-cavity receiver	16.3	V-cavity with fins	–	–		–	–
Jafar and Sivaraman[178]	Re: 710-2130	Nu (%)	16%	T.T. & 0.3% of Al_2O_3	20%	Nail. T.T. & 0.3% of Al_2O_3	–	–		–	–
Mwesigye et al[32]	Re:		10 200-738 000 T_{in}: 400-650 K		133.5, 1.05, 95, −52.7	Perforated plate	–	–	–	–	

(Continues)

TABLE 13 (Continued)

References	Examined parameters		Typical output	Enhancements by inserting swirl generators compared with the typical receiver							
				Enhancement	Technique 1	Enhancement	Technique 2	Enhancement	Technique 3	Enhancement	Technique 4
				Nu & F.F. & Th.E.F. & E.G.							
–	–										
Huang et al[179]	Re: (1-2)10^4	PEC	1.23-1.37	Dimples	1.125-1.225	Helical fins	1.13-1.41	Protrusions		–	–
Reddy et al[180]	100-1000 L/h	Th.E. (%): 57.21-66.96	58.98%-67.59%	Bottom insert	59.41%-67.78%	U-shaped	60.5%-67.43%	Inclined insert		61.18-69.03%	Alternative insert
Chang et al[181]	T.R.: 2.5-41.7 C.R.: 0-1 Re: 7485-30 553	Nu (times) & F.F. (times)	2.9 & 1.24	T.T.	–	–	–	–		–	–
Şahin et al[182]	Re: (3-17)10^3	H.T.E. (times)	1.95	C.W. pitch = 45 mm	2.07	Pitch = 30 mm	2.28	Pitch = 15 mm		–	–
Jaramillo et al[183]	T.R.: 1-5 (1-6) Lpm	Th.E. (%) & F.F. (times)	Up to 9% & 26%	T.T.	–	–	–	–		–	–
Mwesigye et al[164]	Re: 10×10^3-14×10^5 T.R.: 0.5-2.0 W.R.: 0.53-0.91	H.T.E., F.F., Th.E. (%), & E.G.	1.05-2.69, 1.6-14.5, 5%-10% & −58.8%	T.T. with wall-detached	–	–	–	–		–	–
Amina et al[184]	Re: (25.7-257) 10^3	Nu (times) & F.F. (times)	1.3-1.8 & 1.66	Triangular fins	1.3-1.8 & 1.57	Rectangular fins	Nu: 150%	Fins & 0.01 of nanofluid		–	–
Xiangtao et al[185]	N: 1, 3, 5, 9 Re: (2-11.25) 10^3 δ/L: 0.1-0.025	Nu (%) & Th. Pe. (%)	9% & 12%	Arrays of pin fins	–	–	–	–	–		–
Ghasemi and Ranjbar[186]	Re: (3-25.1)10^4	Nu: 229-1286	374.63-1766	Porous rings	–	–	–	–	–		–
Zhu et al[187]	Re: (7.2-21.6) 10^4	Nu (%), F.F. (%), H.L. (%), E.G. (%)	261%-310%, 382%-405%, −17.5%-33.1%, −30.2%-81.8%	Wavy-tape	–	–	–	–	–		–
Zheng et al[188]	Re: (1-10) 10^3	H.T.C. (%) & E.G. (%)	25.53% & −29.1%	Dimpled T.T.	58.96% in H.T.C. & 5.05% in F.F.	Dimpled T.T. & Al_2O_3	–	–	–		–
Bellos et al[189]	50-250 Lpm		1.483 & 2.65	Fins	–	–	–	–	–		–

(Continues)

TABLE 13 (Continued)

References	Examined parameters		Typical output	Enhancements by inserting swirl generators compared with the typical receiver							
				Enhancement	Technique 1	Enhancement	Technique 2	Enhancement	Technique 3	Enhancement	Technique 4
	F.th.: 2, 4, 6 mm F.L.: 5-20 mm	Th.E. I. & Nu (times)									
Bellos et al[190]	Fin L: 0-15 mm	Exe. Per. (%) & Th.E. (%)	42.7% & 70.82%	Longitudinal fins with helium	40.76% & 70.54%	Longitudinal fins with air	41.97% & 69.93%	Longitudinal fins with Co2	–		–
Bellos et al[191]	Re: (1-14)10^4 T_{in}: 300-650 K	Th.E. (%): 68.24	68.62%	6% CuO-Oil	68.8%	Thermal oil-finned tube	69.02%	Nanofluid-finned tube	–		–
Bellos et al[192]	Different fin positions	Th.E. (%): 68.24	68.40%, 68.50%	One fin, two fins	68.59%, 68.63%	Three fins, four fins	68.71%, 68.74%	Five fins, six fins	68.78%, 68.80%		Seven fins, eight fins
Bellos et al[193]	Different cylindrical insert positions	Th.E. (%): 67.7	+0.119%	One cylindrical rod	+0.387%	Two cylindrical rods	+0.589%	Three cylindrical rods	+0.656%		Four cylindrical rods
Bilal et al[194]	T_{in}: 29°C-38°C (2.5-20) Lpm I.S.I.: 600-950 W/m^2	Nu (%)	56%-75%	C.R. (0.6%) of Fe_3O_4	59%-73%	T.T.	63%-87%	T.T. and C.R. (0.6%) of Fe_3O_4	–		–
Okonkwo et al[195]	40-200 Lpm, T_{in}: 350-650 K	Exergy enhancement 16.39 (%)	16.41%	Al_2O_3-oil	16.42%	Al_2O_3-Oil in finned tube	16.41%	Al_2O_3-oil + T. T.	16.51%		Al_2O_3-oil in Con.Div. tube
Kurşun[196]	Re: 2×10^4-8×10^4 T_{in}: 300-600 K	Nu (%)	25%	Flat fins	75%	Sinusoidal fins	–	–	–		–
Malekan et al[197]	Re: 3×10^4-25×10^4 Particle size: 10, 20	Th.E.F. (%)	1.35%	CuO-oil	4%	CuO-Oil + fins	–	–	–		–
Isravel et al[198]	Re: (7-12)10^3	Nu (%)	5%-40%	T.T.	11%-101%	Rings attached T.T.	7%-77%	Modified rings attached T.T.	–		–

(Continues)

TABLE 13 (Continued)

References	Examined parameters		Typical output	Enhancements by inserting swirl generators compared with the typical receiver							
				Enhancement	Technique 1	Enhancement	Technique 2	Enhancement	Technique 3	Enhancement	Technique 4
Liu et al[199]	Different ribs insert positions	Nu (%)	1.41%-2.98%	Ribs in (SADIR)	1.58%-3.21%	Ribs in (SCSIR)	–	–	–	–	–
Valizade et al[200]	20-100 Lph Re: 500-1800	Th.E. (%)	28.84%	Free-porous	49.42%	Semi-porous	60.23%	Full-porous	–	–	–

234%, as described by Mwesigye et al[213] that used MWCNT/therminol VP – 1 nanofluid. Moreover, the maximum improvement in the thermal efficiency was approximately 30.4%, as reported by Kasaeian et al[146] when using 0.3% of MWCNT/GE nanofluids. Another important finding due to the presence of nanofluid was large reduction in the entropy generation: up to 20% to 30% when using 6% Cu-Therminol oil (Mwesigye et al [2016a]).[214] There is no doubt that increasing the nanoparticle volume fraction would increase the heat transfer performance and reduce the thermal losses on the absorber tube, but at the same time the nanofluid stability will also be affected, leading to agglomeration and clustering of nanoparticles resulting in greatly enhancement in the pumping power required to force the flow through the absorber tube and accordingly reducing the collector efficiency. Therefore, the nanoparticle volume fraction or weight concentration should be optimized for effective thermal and hydraulic performances of PTCs.

Another main approach that can be employed to effectively enhance the thermal performance of the absorber receiver is inserting swirl generators or other flow-modifying inserts (tabulators) inside the HCE with different shapes and different positions. In comparison with the nanofluid approach, using tabulators is more cost-effective, and their actual implementation rather simple. The usage of inserting tabulators acts at enhancing the thermal properties of HTF and improving the turbulence performance inside the absorber tube which in turn leading to significantly improve the thermal performance. However, the maximum enhancement reported to date in the heat transfer coefficient was approximately 375%, when using three segmental rings as proposed by Ghasemi and Ranjbar.[186] Moreover, using circular fins inside the HCE enhanced the heat transfer coefficient by 360% compared with the typical performance (Reddy and Satyanarayana[168]), while using half-pipe finned also contributed to enhancing the thermal efficiency of the PTC by 13% as reported by Kasperski and Nemś.[162] On the other hand, the main challenge associated with this method is the potential pressure shocks due to the presence of swirl generators or tabulators, which could lead to glass envelope breakage.

The third possible technology which may be employed to improve the thermal performance of PTC is to combine the previous two technologies, nanofluids and flow-modifying inserts, in the same system. For example, Amina et al[184] reported a 150% enhancement in heat transfer coefficient when using fins with nanofluids. In another study, the exergy enhancement achieved was approximately 16.51% when using twisted tape with Al_2O_3-thermal oil nanofluid (Okonkwo et al[195]). For this

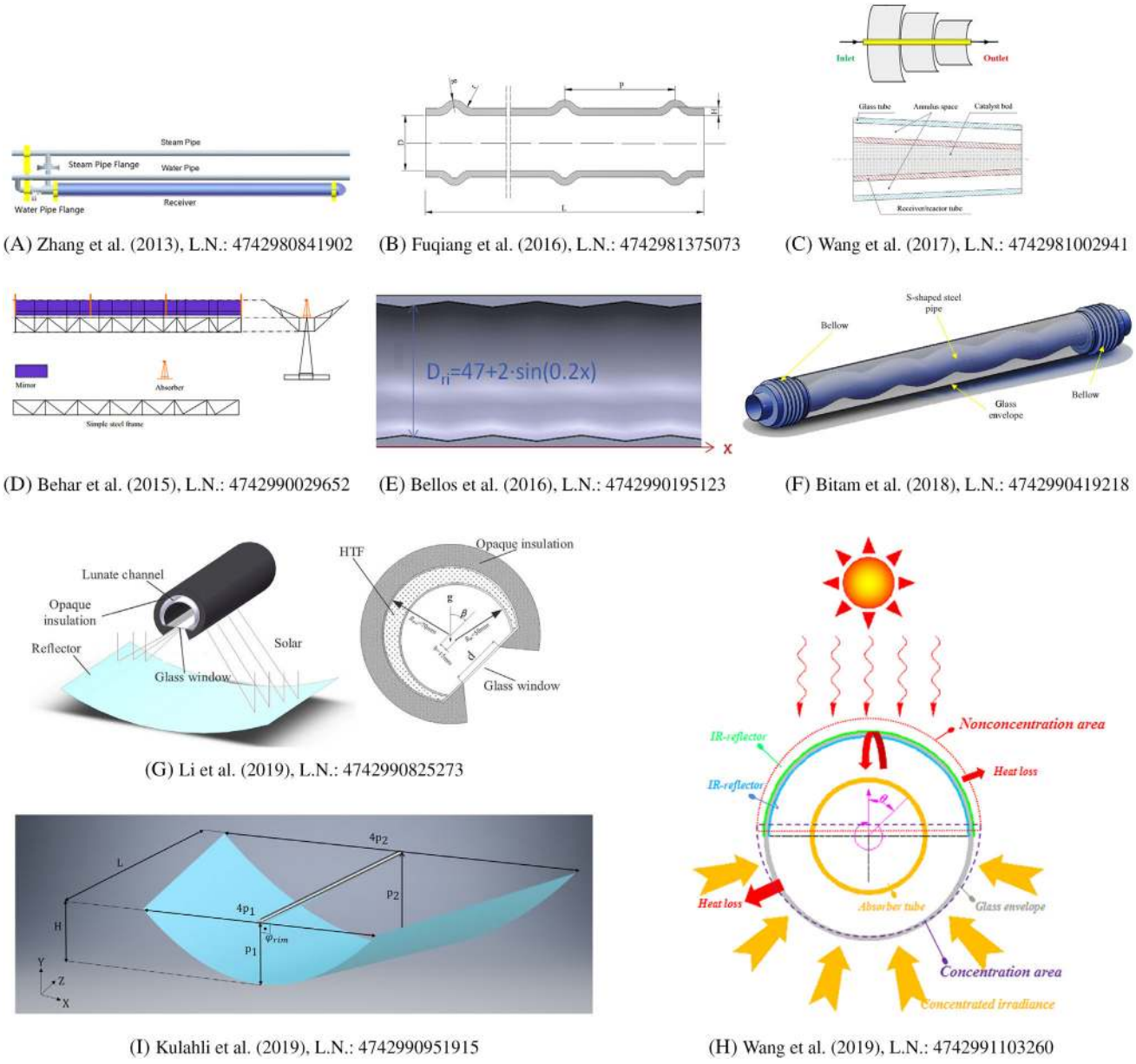

(A) Zhang et al. (2013), L.N.: 4742980841902 (B) Fuqiang et al. (2016), L.N.: 4742981375073 (C) Wang et al. (2017), L.N.: 4742981002941

(D) Behar et al. (2015), L.N.: 4742990029652 (E) Bellos et al. (2016), L.N.: 4742990195123 (F) Bitam et al. (2018), L.N.: 4742990419218

(G) Li et al. (2019), L.N.: 4742990825273

(I) Kulahli et al. (2019), L.N.: 4742990951915 (H) Wang et al. (2019), L.N.: 4742991103260

FIGURE 15 Novel designs of collector structures in literature [Colour figure can be viewed at wileyonlinelibrary.com]

method to be effective, clearly the nanofluid and the flow-modifying insert have to be optimized simultaneously and synergistically.

As regards PTC systems performance enhancement, in conclusion, areas that require further investigation include:

- The optimization of the volume fraction or weight concentration of nanoparticles to fine-tune the performance of nanofluids, as well as investigations on the long-term stability of nanofluids.
- Notwithstanding their potential superior performance, hybrid nanofluids have received little attention, both experimentally and numerically, so that more studies are clearly needed to duly assess their potential. Using hybrid nanofluid instead of mono fluid (single fluid) is expected to double the thermal efficiency of the PTC, Bellos and Tzivanidis.[158] Therefore, this is a large room of research for the scientific society that has to pay attention and examine different cases of nanofluids; metallic–metallic nanofluids, metallic–nonmetallic nanofluids, and nonmetallic–nonmetallic nanofluids. Examining multiple base fluids with hybrid nanofluids is also needed. Besides, experimental studies are extremely needed in order to be used for validation in the numerical investigations.
- Very few studies have investigated the synergy between nanofluids and flow-modifying insert, so that

more studies are clearly needed to duly assess the potential of combining these two performance–enhancement technologies.

10 | CONCLUSIONS

PTC systems play a key role in solar thermal energy. Numerous technologies and different techniques have been investigated to improve the overall performance of the PTC optically, thermally and hydraulically, using experiments, simulations, or analytical approaches. As previously discussed, PTC systems performance–enhancement approaches can be basically categorized into two main families: technologies used to improve the thermal performance, and technologies used to enhance the optical characteristics. The investigations focused on enhancing the thermal performance are currently more numerous than those addressing the optical performance; probably due to the fact that the tools needed to investigate the thermal characteristics are more extensively available.

In this article, research investigations performed experimentally and numerically to improve the thermal and the optical performance of PTC systems have been reviewed. It is clear that experimental studies are less numerous in comparison with numerical investigations, because of the cost associated with experiments, particularly when carried out at representative scale. Advantages of numerical simulations, in comparison with experiments, include the possibility to run cost-effective parametric studies, and the possibility to focus on aspects that are difficult to duly investigate experimentally, such as the nonuniform heat flux distribution on solar absorber or conjugate heat transfer.

Based on the available literature, it can be concluded that the utilization of nanofluids for improving thermal properties is promising but still an emerging field. The knowledge gap in the literature is still considerable in terms of testing different types of nanoparticles with different volume fractions and different base fluids for conjugated heat transfer problems. Moreover, there are still some open questions about the thermal–physical properties of nanofluids which thus require further research. Furthermore, investigating hybrid nanofluids is still restricted to investigations. More contributions are needed, notably testing the effect of metallic with metallic nanoparticles, metallic with nonmetallic nanoparticles and nonmetallic with nonmetallic nanoparticles with/without hybrid base fluids. Even though a lot of data is available in literature related to the improvement of thermal performance using swirl generators (or other flow-modifying devices) and nanoparticles, there is yet a rather large void when it comes to the use of both nanoparticles and swirl generators together. Studies related to the testing of the combined effect of these are much needed and should be the focus of further research. The use of hybrid nanofluids with swirl generators offers good potential since different inserts could be investigated with numerous types of hybrid nanofluids.

ACKNOWLEDGEMENTS

The authors would like to thank the Department of Mechanical, Aerospace and Civil Engineering (MACE), University of Manchester for the financial support. The authors would also like to thank the U.K. Department of Business, Energy and Industrial Strategy (BEIS) for the financial support through Newton institutional links fund (Engineering Sustainable Solar Energy and Thermocline Alternatives-ESSEnTiAl, Grant ID 332271136). Authors would like to greatly thank Dr. Andrea Cioncolini, Prof. Hector Iacovides, Dr. Adel Nasser, and Dr. Tarek Abdel-Malak Meakhail for their support.

ORCID

Nabeel Abed https://orcid.org/0000-0001-5868-1767
Imran Afgan https://orcid.org/0000-0002-8082-299X

ENDNOTE

[1] Adapted from https://www.dlr.de/dlr/en/desktopdefault.aspx/tabid-10202/334_read-1557/year-2011/#/gallery/3281, accessed October 12, 2018.

REFERENCES

1. Blanco MJ, Miller S. *Introduction to Concentrating Solar Thermal (CST) Technologies. Advances in Concentrating Solar Thermal Research and Technology*. Amsterdam, Netherlands: Elsevier, Inc.; 2017.
2. Philibert C, Frankl P. *International Energy Agency. Technology Roadmap: Concentrating Solar Power*. Paris, France: IEA/OECD; 2010.
3. Kreith F, Goswami DY. *Handbook of Energy Efficiency and Renewable Energy*. Milton Park, UK: Taylor & Francis; 2007.
4. Price H, Lüpfert E, Kearney D, et al. Advances in parabolic trough solar power technology. *J Solar Energy Eng*. 2002;124(2):109-125.
5. Hachicha AA, Rodríguez I, Capdevila R, Oliva A. Heat transfer analysis and numerical simulation of a parabolic trough solar collector. *Appl Energy*. 2013;111:581-592.
6. Nahhas, Tamar, Xavier Py, Sophie Grégoire, Christian Cristofari, Minh D. Pham, Catherine Bessada, and Régis Olives. Materials and thermal storage systems by sensible heat for thermodynamic electro-solar plants. Thèse de doctorat: Energétique et Génie des Procédés, Perpignan, France; 2017.
7. Jebasingh VK, Herbert GMJ. A review of solar parabolic trough collector. *Renew Sustain Energy Rev*. 2016;54:1085-1091.
8. Abdulhamed AJ, Adam NM, Ab-Kadir MZA, Hairuddin AA. Review of solar parabolic-trough collector geometrical and

thermal analyses, performance, and applications. *Renew Sustain Energy Rev*. 2018;91:822-831.
9. Bellos E, Tzivanidis C. Alternative designs of parabolic trough solar collectors. *Progr Energy Combust Sci*. 2019;71:81-117.
10. Larrain T, Escobar R, Vergara J. Performance model to assist solar thermal power plant siting in northern Chile based on backup fuel consumption. *Renew Energy*. 2010;35(8):1632-1643.
11. Jafari MH, Jahangiri MS, Shafii MB, Hakim SA. A new desalination system using a combination of heat pipe, evacuated tube and parabolic trough collector. *Energ Conver Manage*. 2015;99:141-150.
12. Raja NS, Vijay S. Desalination of water using parabolic trough collector. *Mater Today Proc*. 2019;21:375-379.
13. Bigoni R, Kötzsch S, Sorlini S, Egli T. Solar water disinfection by a parabolic trough concentrator (ptc): flow-cytometric analysis of bacterial inactivation. *J Clean Prod*. 2014;67:62-71.
14. Fadar EA, Mimet A, Azzabakh A, Pérez-García M, Castaing J. Study of a new solar adsorption refrigerator powered by a parabolic trough collector. *Appl Therm Eng*. 2009;29:1267-1270.
15. Al-Alili A, Hwang Y, Radermacher R. A hybrid solar air conditioner: experimental investigation. *Int J Refrig*. 2014;39:117-124.
16. Hewett R, Gee R, May EK. *Solar Process Heat Technology in Action: The Process Hot Water System at the California Correctional Institution at Tehachapi*. Golden, CO: National Renewable Energy Laboratory; 1991.
17. Larson DL. Operational evaluation of the grid-connected Coolidge solar thermal electric power plant. *Solar Energy*. 1987;38(1):11-24.
18. Noman M, Wasim A, Ali M, et al. An investigation of a solar cooker with parabolic trough concentrator. *Case Studies Therm Eng*. 2019;14:100436.
19. Larcher M, Rommel M, Bohren A, Frank E, Minder S. Characterization of a parabolic trough collector for process heat applications. *Energy Procedia*. 2014;57:2804-2811.
20. Kizilkan O, Kabul A, Dincer I. Development and performance assessment of a parabolic trough solar collector-based integrated system for an ice-cream factory. *Energy*. 2016;100:167-176.
21. Duffie JA, Beckman WA. *Solar Engineering of Thermal Processes*. Hoboken, NJ: Wiley; 2013.
22. Gaul HW, Rabl A. *Incidence Angle Modifier and Average Optical Efficiency of Parabolic Trough Collectors*. Golden, CO: Solar Energy Research Institute; 1979.
23. Behar O, Mohammedi K, Khellaf A. A novel parabolic trough solar collector model - validation with experimental data and comparison to engineering equation solver (EES). *Energ Conver Manage*. 2015;106:268-281.
24. Wirz M, Petit J, Haselbacher A, Steinfeld A. Potential improvements in the optical and thermal efficiencies of parabolic trough concentrators. *Solar Energy*. 2014;107:398-414.
25. Yazdanpanahi J, Sarhaddi F, Mahdavi AM. Experimental investigation of exergy efficiency of a solar photovoltaic thermal (pvt) water collector based on exergy losses. *Solar Energy*. 2015;118:197-208.
26. Petela R. Exergy of undiluted thermal radiation. *Solar Energy*. 2003;74(6):469-488.
27. Bhowmik NC, Mullick SC. Calculation of tubular absorber heat loss factor. *Solar Energy*. 1985;35(3):219-225.
28. Swinbank WC. Long-wave radiation from clear skies. *Q J Roy Meteorol Soc*. 1963;89:339-348.
29. Incropera FP, DeWitt DP. *Fundamentals of Heat and Mass Transfer*. New York: J. Wiley, 2002.
30. Petukhov BS. "Heat Transfer and Friction in Turbulent Pipe Flow with Variable Physical Properties." *Advances in Heat Transfer*. 1970;6:503-564.
31. Gnielinski V. New equations for heat and mass transfer in turbulent pipe and channel flow. *Int Chem Eng*. 1976;16:359-368.
32. Mwesigye A, Meyer JP, Bello-Ochende T. Heat transfer and thermodynamic performance of a parabolic trough receiver with centrally placed perforated plate inserts. *Appl Energy*. 2014;136:989-1003.
33. Dudley VE, Kolb GJ, Mahoney AR, Mancini TR, Matthews CW, Sloan M, Kearney D. Test Results: Segs Ls-2 Solar Collector. Albuquerque, NM: Dept. of Energy, Sandia Laboratories, 1994.
34. Xu L, Wang Z, Yuan G, Li X, Ruan Y. A new dynamic test method for thermal performance of all-glass evacuated solar air collectors. *Solar Energy*. 2012;86(5):1222-1231.
35. Lei D, Li Q, Wang Z, Li J, Li J. An experimental study of thermal characterization of parabolic trough receivers. *Energ Conver Manage*. 2013;69:107-115.
36. Coccia G, Di NG, Sotte M. Design, manufacture, and test of a prototype for a parabolic trough collector for industrial process heat. *Renew Energy*. 2015;74:727-736.
37. Li M, Xu C, Xu J, Zhang P, Qiongfen Y. A new study on the end loss effect for parabolic trough solar collectors. *Energy*. 2015;82:382-394.
38. Wu Y-T, Liu S-W, Xiong Y-X, Ma C-F, Ding Y-L. Experimental study on the heat transfer characteristics of a low melting point salt in a parabolic trough solar collector system. *Appl Therm Eng*. 2015;89:748-754.
39. Geete A, Kothari S, Sahu R, Likhar P, Saini A, Singh A. Experimental analysis on fabricated parabolic solar collector with various flowing fluids and pipe materials. *Int J Renew Energy Res*. 2016;6(4):1454-1463.
40. Kumaresan G, Sridhar R, Velraj R. Performance studies of a solar parabolic trough collector with a thermal energy storage system. *Energy Technol Resour Reser Demands Impact Conserv Manage Policy*. 2012;47(1):395-402.
41. Sivaram PM, Nallusamy N, Suresh M. Experimental and numerical investigation on solar parabolic trough collector integrated with thermal energy storage unit. *Int J Energy Res*. 2016;40(11):1564-1575.
42. Kumar and Kumar. Thermal performance of solar parabolic trough collector at variable flow rates: an experimental investigation. *Int J Ambient Energy*. 2016;39:1-36. https://doi.org/10.1080/01430750.2016.1269673.
43. Tajik J-AM, Saedodin S, Aminy M. Experimental investigation on the effect of partially metal foam inside the absorber of parabolic trough solar collector. *Int J Eng Trans B Appl*. 2017;30(2):1286-1292.
44. Agagna B, Smaili A, Falcoz Q, Behar O. Experimental and numerical study of parabolic trough solar collector of Microsol-R tests platform. *Exp Therm Fluid Sci*. 2018;98:251-266.
45. Mouaky A, Alami MA, Laadel NE, Bennouna EG. Simulation and experimental validation of a parabolic trough plant for solar thermal applications under the semi-arid climate conditions. *Solar Energy*. 2019;194:969-985.

46. Wang R, Wanjun Q, Hong H, Sun J, Jin H. Experimental performance of 300 Kwth prototype of parabolic trough collector with rotatable Axis and irreversibility analysis. *Energy*. 2018; 161:595-609.
47. Bakos GC. Design and construction of a two-axis sun tracking system for parabolic trough collector (PTC) efficiency improvement. *Renew Energy*. 2006;31(15):2411-2421.
48. Jeter, Sheldon M. "*Optical and Thermal Effects in Linear Solar Concentrating Collectors*". Atlanta, GA: Georgia Institute of Technology, (1979). http://hdl.handle.net/1853/32784.
49. Jeter SM. Calculation of the concentrated flux density distribution in parabolic trough collectors by a Semifinite formulation. *Solar Energy*. 1986;37(5):335-345.
50. Thomas A, Guven HM. Effect of optical errors on flux distribution around the absorber tube of a parabolic trough concentrator. *Energ Conver Manage*. 1994;35(7):575-582.
51. Grena R. Optical simulation of a parabolic solar trough collector. *Int J Sustain Energy*. 2009;29(1):19-36.
52. Yang B, Zhao J, Xu T, Zhu Q. Calculation of the concentrated flux density distribution in parabolic trough solar concentrators by Monte Carlo ray-trace method (2010). Symposium on photonics and optoelectronics. IEEE; 2010. p. 1–4.
53. He Y-L, Xiao J, Cheng Z-D, Tao Y-B. A Mcrt and Fvm coupled simulation method for energy conversion process in parabolic trough solar collector. *Renew Energy*. 2011;36(3):976-985.
54. Cheng ZD, He YL, Cui FQ, Xu RJ, Tao YB. Numerical simulation of a parabolic trough solar collector with nonuniform solar flux conditions by coupling FVM and MCRT method. *Solar Energy*. 2012;86(6):1770-1784.
55. Cheng ZD, He YL, Cui FQ. A new modelling method and unified code with MCRT for concentrating solar collectors and its applications. *Appl Energy*. 2013;101:686-698.
56. Zhao D, Xu E, Yu Q, Lei D. The simulation model of flux density distribution on an absorber tube. *Energy Procedia*. 2015; 69:250-258.
57. Kaloudis E, Papanicolaou E, Belessiotis V. Numerical simulations of a parabolic trough solar collector with Nanofluid using a two-phase model. *Renew Energy*. 2016;97:218-229.
58. Liang H, You S, Zhang H. Comparison of three optical models and analysis of geometric parameters for parabolic trough solar collectors. *Energy*. 2016;96:37-47.
59. Liang H, Fan M, You S, et al. A Monte Carlo method and finite volume method coupled optical simulation method for parabolic trough solar collectors. *Appl Energy*. 2017;201:60-68.
60. Houcine A, Maatallah T, Alimi SE, Nasrallah SB. Optical Modeling and investigation of Sun tracking parabolic trough solar collector basing on Ray tracing 3dimensions-4rays. *Sustain Cities Soc*. 2017;35:786-798.
61. Hoseinzadeh H, Kasaeian A, Behshad SM. Geometric optimization of parabolic trough solar collector based on the local concentration ratio using the Monte Carlo method. *Energ Conver Manage*. 2018;175:278-287.
62. Cheng Z-D, Zhao X-R, He Y-L. Novel optical efficiency formulas for parabolic trough solar collectors: computing method and applications. *Appl Energy*. 2018;224:682-697.
63. Khanna S, Kedare SB, Singh S. Analytical expression for circumferential and axial distribution of absorbed flux on a bent absorber tube of solar parabolic trough concentrator. *Solar Energy*. 2013;92:26-40.
64. Mwesigye A, Bello-Ochende T, Meyer JP. Minimum entropy generation due to heat transfer and fluid friction in a parabolic trough receiver with non-uniform heat flux at different rim angles and concentration ratios. *Energy*. 2014;73:606-617.
65. Khanna S, Singh S, Kedare SB. Explicit expressions for temperature distribution and deflection in absorber tube of solar parabolic trough concentrator. *Solar Energy*. 2015;114: 289-302.
66. Khanna S, Sharma V. Explicit analytical expression for solar flux distribution on an Undeflected absorber tube of parabolic trough concentrator considering Sun-shape and optical errors. *J Solar Energy Eng*. 2016;138(1):011010.
67. Forristall RE. *Heat Transfer Analysis and Modeling of a Parabolic Trough Solar Receiver Implemented in Engineering Equation Solver*. Golden, CO: National Renewable Energy Laboratory; 2003 (Internet resource).
68. Tao YB, He YL. Numerical study on coupled fluid flow and heat transfer process in parabolic trough solar collector tube. *Solar Energy*. 2010;84(10):1863-1872.
69. Huang W, Hu P, Chen Z. Performance simulation of a parabolic trough solar collector. *Solar Energy*. 2012;86(2):746-755.
70. Lu J, Ding J, Yang J, Yang X. Nonuniform heat transfer model and performance of parabolic trough solar receiver. *Energy*. 2013;59:666-675.
71. Cheng, Z.-D, Y.-L He, K Wang, B.-C Du, and F.Q Cui. "A detailed parameter study on the comprehensive characteristics and performance of a parabolic trough solar collector system." *Appl Therm Eng* 63.1 (2014): 278–289.
72. Wu Z, Li S, Yuan G, Lei D, Wang Z. Three-dimensional numerical study of heat transfer characteristics of parabolic trough receiver. *Appl Energy*. 2014;113:902-911.
73. Okafor IF, Dirker J, Meyer JP. Influence of non-uniform heat flux distributions on the secondary flow, convective heat transfer and friction factors for a parabolic trough solar collector type absorber tube. *Renew Energy*. 2017;108:287-302.
74. Ray S, Tripathy AK, Sahoo SS, Bindra H. Performance analysis of receiver of parabolic trough solar collector: effect of selective coating, vacuum and Semitransparent glass cover. *Int J of Energy Res*. 2018;42(13):4235-4249.
75. Tripathy AK, Ray S, Sahoo SS, Chakrabarty S. Structural analysis of absorber tube used in parabolic trough solar collector and effect of materials on its bending: a computational study. *Solar Energy*. 2018;163:471-485.
76. Donga RK, Kumar S. Thermal performance of parabolic trough collector with absorber tube misalignment and slope error. *Solar Energy*. 2019;184:249-259.
77. Zou B, Jiang Y, Yang Y, Yang H. Impacts of non-ideal optical factors on the performance of parabolic trough solar collectors. *Energy*. 2019;183:1150-1165.
78. Xu L, Sun F, Ma L, et al. Analysis of optical and thermal factors' effects on the transient performance of parabolic trough solar collectors. *Solar Energy*. 2019;179:195-209.
79. García S, Sánchez-Mora H, Polo-Labarrios MA, Cázares-Ramírez RI. Modeling and simulation to determine the thermal efficiency of a parabolic solar trough collector system. *Case Stud Therm Eng*. 2019;16:100523.
80. Khandelwal DK, Ravi KK, Kaushik SC. Heat transfer analysis of receiver for large aperture parabolic trough solar collector. *Int J Energy Res*. 2019;43(9):4295-4311.

81. Norouzi AM, Siavashi M, Khaliji OMH. Efficiency enhancement of the parabolic trough solar collector using the rotating absorber tube and nanoparticles. *Renew Energy*. 2020;145: 569-584.
82. Burkholder F, Kutscher CF. *Heat Loss Testing of Schott's 2008 Ptr70 Parabolic Trough Receiver*. Golden, CO: National Renewable Energy Laboratory; 2009.
83. Odeh SD, Morrison GL, Behnia M. Modelling of parabolic trough direct steam generation solar collectors. *Solar Energy*. 1998;62(6):395-406.
84. Gong G, Huang X, Wang J, Hao M. An optimized model and test of the China's first high temperature parabolic trough solar receiver. *Solar Energy*. 2010;84(12):2230-2245.
85. Roesle M, Coskun V, Steinfeld A. Numerical analysis of heat loss from a parabolic trough absorber tube with active vacuum system. *J Solar Energy Eng*. 2011;133(3):031015.
86. Yaghoubi M, Ahmadi F, Bandehee M. Analysis of heat losses of absorber tubes of parabolic through collector of shiraz (Iran) solar power plant. *J Clean Energy Technol*. 2013;1: 33-37.
87. Zhang L, Yu Z, Fan L, et al. An experimental investigation of the heat losses of a U-type solar heat pipe receiver of a parabolic trough collector-based natural circulation steam generation system. *Renew Energy*. 2013;57:262-268.
88. Sanchez D, Rosengarten G. Improving the concentration ratio of parabolic troughs using a second-stage flat mirror. *Appl Energy*. 2015;159:620-632.
89. Osorio JD, Rivera-Alvarez A. Performance analysis of parabolic trough collectors with double glass envelope. *Renew Energy*. 2019;130:1092-1107.
90. Montes MJ, Abańades A, Martińez-Val JM. Thermofluidynamic model and comparative analysis of parabolic trough collectors using oil, water/steam, or molten salt as heat transfer fluids. *J Solar Energy Eng*. 2010;132(2):21001.
91. Ouagued M, Khellaf A. Simulation of the temperature and heat gain by solar parabolic trough collector in Algeria. *Int J Math Comput Phys Electr Comput Eng*. 2012;6(7):746-752.
92. Ouagued M, Khellaf A, Loukarfi L. Estimation of the temperature, heat gain and heat loss by solar parabolic trough collector under Algerian climate using different thermal oils. *Energ Conver Manage*. 2013;75:191-201.
93. Biencinto M, Bayón R, Rojas E, González L. Simulation and assessment of operation strategies for solar thermal power plants with a thermocline storage tank. *Solar Energy*. 2014; 103:456-472.
94. Good P, Zanganeh G, Ambrosetti G, Barbato MC, Pedretti A, Steinfeld A. Towards a commercial parabolic trough CSP system using air as heat transfer fluid. *Energy Procedia*. 2014;49:381-385.
95. Wang Y, Liu Q, Lei J, Jin H. A three-dimensional simulation of a parabolic trough solar collector system using molten salt as heat transfer fluid. *Appl Therm Eng*. 2014;70(1):462-476.
96. Selvakumar P, Somasundaram P, Thangavel P. Performance study on evacuated tube solar collector using Therminol D-12 as heat transfer fluid coupled with parabolic trough. *Energ Conver Manage*. 2014;85:505-510.
97. Qiu Y, Li M-J, He Y-L, Tao W-Q. Thermal performance analysis of a parabolic trough solar collector using supercritical Co2 as heat transfer fluid under non-uniform solar flux. *Appl Therm Eng*. 2017;115:1255-1265.
98. Tahtah, Reda, Ali Bouchoucha, Cherifa Abid, Mahfoud Kadja, and Fouzia Benkafada. Experimental Study of Heat Transfer in Parabolic Trough Solar Receiver: Using Two Different Heat Transfer Fluids. (2017).
99. Bellos E, Tzivanidis C, Antonopoulos KA. A detailed working fluid investigation for solar parabolic trough collectors. *Appl Therm Eng*. 2017;114:374-386.
100. Aguilar R, Valenzuela L, Avila-Marin AL, Garcia-Ybarra PL. Simplified heat transfer model for parabolic trough solar collectors using supercritical Co2. *Energ Conver Manage*. 2019; 196:807-820.
101. Mwesigye A, Meyer JP. Optimal thermal and thermodynamic performance of a solar parabolic trough receiver with different Nanofluids and at different concentration ratios. *Appl Energy*. 2017;193:393-413.
102. Natividade PSG, de Moraes MG, Avallone E, Bandarra FEP, Gelamo RV, Gonçalves JCSI. Experimental analysis applied to an evacuated tube solar collector equipped with parabolic concentrator using multilayer Graphene-based Nanofluids. *Renew Energy*. 2019;138:152-160.
103. Al-damook A, Alfellag MA, Khalil WH. Three-dimensional computational comparison of mini-pinned heat sinks using different nanofluids: Part two—energy and exergy characteristics. *Heat Transfer—Asian Res*. 2020;49:441-460.
104. Turkyilmazoglu M. Condensation of laminar film over curved vertical walls using single and two-phase Nanofluid models. *Eur J Mech B Fluids*. 2017;65:184-191.
105. Sharafeldin MA, Gyula G. Evacuated tube solar collector performance using Ceo2/water Nanofluid. *J Clean Prod*. 2018; 185:347-356.
106. Nelson AT, Rittman DR, White JT, Dunwoody JT, Kato M, McClellan KJ. An evaluation of the thermophysical properties of stoichiometric CeO_2 in comparison to UO_2 and PuO_2. *J Am Ceram Soc*. 2014;97(11):3652-3659.
107. Myers, P.D, R Kamal, D.Y Goswami, P.D Myers, T.E Alam, R Kamal, D.Y Goswami, E Stefanakos, T.E Alam, and E Stefanakos. "Nitrate salts doped with Cuo nanoparticles for thermal energy storage with improved heat transfer." *Appl Energy* 165 (2016): 225–233.
108. Al-damook A, Alfellag MA, Khalil WH. Three-dimensional computational comparison of mini pinned heat sinks using different nanofluids: part one-the hydraulic-thermal characteristics. *Heat Transfer Asian Res*. 2019;49:591-613.
109. Pak BC, Cho YI. Hydrodynamic and heat transfer study of dispersed fluids with submicron metallic oxide particles. *Exp Heat Transf*. 1998;11(2):151-170.
110. Sadeghi G, Safarzadeh H, Ameri M. Experimental and numerical investigations on performance of evacuated tube solar collectors with parabolic concentrator, applying synthesized Cu_2O/distilled water Nanofluid. *Energy Sustain Dev*. 2019;48:88-106.
111. Abu-Hamdeh NH, Almitani KH. Solar liquid desiccant regeneration and Nanofluids in evaporative cooling for greenhouse food production in Saudi Arabia. *Solar Energy*. 2016;134: 202-210.
112. Huminic G, Huminic A. Numerical study on heat transfer characteristics of Thermosyphon heat pipes using nanofluids. *Energ Conver Manage*. 2013;76:393-399.
113. Minea AA, El-Maghlany WM. Influence of hybrid nanofluids on the performance of parabolic trough collectors in solar

thermal systems: recent findings and numerical comparison. *Renew Energy*. 2018;120:350-364.
114. Sundar SL, Singh MK, Ferro MC, Sousa ACM. Experimental investigation of the thermal transport properties of graphene oxide/Co_3O_4 hybrid Nanofluids. *Int Commun Heat Mass Transf*. 2017;84:1-10.
115. Peng H, Guo W, Li M. Thermal-hydraulic and thermodynamic performances of liquid metal based nanofluid in parabolic trough solar receiver tube. *Energy*. 2019;192:116564.
116. Khan WA, Khan ZH, Rahi M. Fluid flow and heat transfer of carbon nanotubes along a flat plate with Navier slip boundary. *Appl Nanosci*. 2014;4(5):633-641.
117. Ghadikolaei SS, Kh H, Hatami M, Ganji DD, Armin M. Investigation for squeezing flow of ethylene glycol ($C_2H_6O_2$) carbon nanotubes (CNTS) in rotating stretching channel with nonlinear thermal radiation. *J Mol Liq*. 2018;263:10-21.
118. Xuan Y, Roetzel W. Conceptions for heat transfer correlation of nanofluids. *Int J Heat Mass Transf*. 2000;43(19):3701-3707.
119. O'Hanley H, Buongiorno J, McKrell T, Lin-wen H. Measurement and model validation of nanofluid specific heat capacity with differential scanning calorimetry. *Adv Mech Eng*. 2012;4:181079.
120. Einstein A. Eine neue bestimmung der moleküldimensionen. *Ann Phys*. 1906;324(2):289-306.
121. Einstein A. Eine neue bestimung der molekuldimensionen. *Ann Phys*. 1911;34:591-592.
122. Brinkman HC. The viscosity of concentrated suspensions and solutions. *J Chem Phys*. 1952;20.4:571.
123. Batchelor GK. The effect of Brownian motion on the bulk stress in a suspension of spherical particles. *J Fluid Mech*. 1977;83(1):97-117.
124. Happel J. Viscosity of suspensions of uniform spheres. *J Appl Phys*. 1957;28(11):1288-1292.
125. Buongiorno J. Convective transport in nanofluids. *Trans Am Soc Mech Eng J Heat Transf*. 2006;128(3):240-250.
126. Khanafer K, Vafai K. A critical synthesis of thermophysical characteristics of nanofluids. *Int J Heat Mass Transf*. 2011;54:4410-4428.
127. Wang X, Xu X, Choi SUS. Thermal conductivity of nanoparticle-fluid mixture. *J Thermophys Heat Transf*. 1999;13(4):474-480.
128. Maiga SE, Palm SJ, Nguyen CT, Roy G, Galanis N. Heat transfer enhancement by using nanofluids in forced convection flows. *Int J Heat Fluid Flow*. 2005;26(4):530-546.
129. Chen H, Ding Y, He Y, Tan C. Rheological behaviour of ethylene glycol based titania nanofluids. *Chem Phys Lett*. 2007;444:333-337.
130. Mooney M. The viscosity of a concentrated suspension of spherical particles. *J Colloid Sci*. 1951;6(2):162-170.
131. Tseng WJ, Chen C-N. Effect of polymeric dispersant on rheological behavior of nickel-Terpineol suspensions. *Mater Sci Eng A*. 2003;347(1):145-153.
132. Tseng WJ, Lin KC. Rheology and colloidal structure of aqueous Tio2 nanoparticle suspensions. *Mater Sci Eng A*. 2003;355:186-192.
133. Nguyen, C.T, F Desgranges, G Roy, N Galanis, T Maré, S Boucher, and Mintsa H. Angue. "Temperature and particle-size dependent viscosity data for water-based nanofluids—hysteresis phenomenon." *Int J Heat Fluid Flow* 28.6 (2007): 1492–1506.
134. Michaelides, Efstathios. Nanofluidics: Thermodynamic and Transport Properties., (2016).
135. Maxwell JC. *A Treatise on Electricity and Magnetism*. 2nd ed. Oxford, UK: Clarendon; 1881.
136. Bruggeman DAG. Berechnung Verschiedener Physikalischer Konstanten Von Heterogenen Substanzen. I. Dielektrizitätskonstanten Und Leitfähigkeiten Der Mischkörper Aus Isotropen Substanzen. *Ann Phys*. 1935;416(7):636-664.
137. Hamilton RL, Crosser OK. Thermal conductivity of heterogeneous two-component systems. *Ind Eng Chem Fundam*. 1962;1(3):187-191.
138. Nan CW, Shi Z, Lin Y. A simple model for thermal conductivity of carbon nanotube-based composites. *Chem Phys Lett*. 2003;375:666-669.
139. Yu W, Choi SUS. The role of interfacial layers in the enhanced thermal conductivity of Nanofluids: a renovated Hamilton-crosser model. *J Nanopart Res*. 2004;6(4):355-361.
140. Chaudhari KS, Walke PV, Wankhede US, Shelke RS. An experimental investigation of a nanofluid (Al2O3+H2O) based parabolic trough solar collectors. *Br J Appl Sci Technol*. 2015;9(6):551-557.
141. Subramani J, Nagarajan PK, Somchai W, El-Agouz SA, Sathyamurthy R. Experimental study on the thermal performance and heat transfer characteristics of solar parabolic trough collector using Al_2O_3 nanofluids. *Environ Prog Sustain Energy*. 2018;37(3):1149-1159.
142. Bretado d RMS, Rivera-Solorio CI, García-Cuéllar AJ. Thermal performance of a parabolic trough linear collector using Al_2O_3/H_2O nanofluids. *Renew Energy*. 2018;122:665-673.
143. Coccia G, Di NG, Colla L, Fedele L, Scattolini M. Adoption of Nanofluids in low-enthalpy parabolic trough solar collectors: numerical simulation of the yearly yield. *Energ Conver Manage*. 2016;118:306-319.
144. Rehan MA, Ali M, Sheikh NA, et al. Experimental performance analysis of low concentration ratio solar parabolic trough collectors with Nanofluids in winter conditions. *Renew Energy*. 2018;118:742-751.
145. Subramani J, Nagarajan PK, Mahian O, Sathyamurthy R. Efficiency and heat transfer improvements in a parabolic trough solar collector using TiO2 nanofluids under turbulent flow regime. *Renew Energy*. 2018;119:19-31.
146. Kasaeian A, Daneshazarian R, Rezaei R, Pourfayaz F, Kasaeian G. Experimental investigation on the thermal behavior of nanofluid direct absorption in a trough collector. *J Clean Prod*. 2017;158:276-284.
147. Sokhansefat T, Kasaeian AB, Kowsary F. Heat transfer enhancement in parabolic trough collector tube using Al_2O_3 synthetic oil nanofluid. *Renew Sustain Energy Rev*. 2014;33:636-644.
148. Paul TC, Morshed AKMM, Fox EB, Khan JA. Thermal performance of Al_2O_3 nanoparticle enhanced ionic liquids (Neils) for concentrated solar power (CSP) applications. *Int J Heat Mass Transf*. 2015;85:585-594.
149. Zadeh M, Sokhansefat PT, Kasaeian AB, Kowsary F, Akbarzadeh A. Hybrid optimization algorithm for thermal

analysis in a solar parabolic trough collector based on Nanofluid. *Energy*. 2015;82:857-864.
150. Mwesigye A, Huan Z, Meyer JP. Thermodynamic optimisation of the performance of a parabolic trough receiver using synthetic oil-Al_2O_3 nanofluid. *Appl Energy*. 2015;156:398-412.
151. Mwesigye, A, Z Huan, and J.P Meyer. "Thermal Performance of a Receiver Tube for a High Concentration Ratio Parabolic Trough System and Potential for Improved Performance with Syltherm 800-Cuo Nanofluid." ASME International Mechanical Engineering Congress and Exposition, Proceedings (IMECE). (2015).
152. Basbous N, Taqi M, Belouaggadia N. Numerical study of a study of a parabolic trough collector using a nanofluid. *Asian J Curr Eng Math*. 2015;3:40-44.
153. Basbous, Nabil, Mohamed Taqi, and Moulay A. Janan. "Thermal Performances Analysis of a Parabolic Trough Solar Collector Using Different Nanofluids." (2016): 322–326.
154. Bellos E, Tzivanidis C, Antonopoulos KA, Gkinis G. Thermal enhancement of solar parabolic trough collectors by using Nanofluids and converging-diverging absorber tube. *Renew Energy*. 2016;94:213-222.
155. Toghyani S, Baniasadi E, Afshari E. Thermodynamic analysis and optimization of an integrated Rankine power cycle and Nano-fluid based parabolic trough solar collector. *Energ Conver Manage*. 2016;121:93-104.
156. Babar H, Ali HM. Towards hybrid Nanofluids: preparation, thermophysical properties, applications, and challenges. *J Mol Liq*. 2019;281:598-633.
157. Okonkwo EC, Abid M, Essien EA, Akhayere E, Ratlamwala TAH, Kavaz D. Thermal performance analysis of a parabolic trough collector using water-based green-synthesized nanofluids. *Solar Energy*. 2018;170:658-670.
158. Bellos E, Tzivanidis C. Thermal analysis of parabolic trough collector operating with mono and hybrid nanofluids. *Sustain Energy Technol Assess*. 2018;26:105-115.
159. Menbari A, Alemrajabi AA, Ghayeb Y. Experimental investigation of stability and extinction coefficient of Al_2O_3-Cuo binary nanoparticles dispersed in ethylene glycol-water mixture for low-temperature direct absorption solar collectors. *Energ Conver Manage*. 2016;108:501-510.
160. Menbari A, Alemrajabi AA. Analytical modeling and experimental investigation on optical properties of new class of nanofluids (Al_2O_3-Cuo binary Nanofluids) for direct absorption solar thermal energy. *Opt Mater*. 2016;52:116-125.
161. Menbari A, Alemrajabi AA, Rezaei A. Experimental investigation of thermal performance for direct absorption solar parabolic trough collector (dasptc) based on binary nanofluids. *Exp Therm Fluid Sci*. 2017;80:218-227.
162. Kasperski J, Nemś M. Investigation of thermo-hydraulic performance of concentrated solar air-heater with internal multiple-fin Array. *Appl Therm Eng*. 2013;58:411-419.
163. Song X, Dong G, Gao F, Diao X, Zheng L, Zhou F. A numerical study of parabolic trough receiver with nonuniform heat flux and helical screw-tape inserts. *Energy*. 2014;77:771-782.
164. Mwesigye A, Bello-Ochende T, Meyer JP. Heat transfer and entropy generation in a parabolic trough receiver with wall-detached twisted tape inserts. *Int J Therm Sci*. 2016;99:238-257.
165. Chang C, Sciacovelli A, Wu Z, et al. Enhanced heat transfer in a parabolic trough solar receiver by inserting rods and using molten salt as heat transfer fluid. *Appl Energy*. 2018;220:337-350.
166. Bellos E, Tzivanidis C. Investigation of a star flow insert in a parabolic trough solar collector. *Appl Energy*. 2018;224:86-102.
167. Liu P, Zheng N, Liu Z, Liu W. Thermal-hydraulic performance and entropy generation analysis of a parabolic trough receiver with conical strip inserts. *Energ Conver Manage*. 2019;179:30-45.
168. Reddy KS, Satyanarayana GV. Numerical study of porous finned receiver for solar parabolic trough concentrator. *Eng Appl Comput Fluid Mech*. 2008;2(2):172-184.
169. Reddy KS, Ravi Kumar K, Satyanarayana GV. Numerical investigation of energy-efficient receiver for solar parabolic trough concentrator. *Heat Transf Eng*. 2008;29(11):961-972.
170. Kumar K, Reddy KS. Thermal analysis of solar parabolic trough with porous disc receiver. *Appl Energy*. 2009;86(9):1804-1812.
171. Sundar LS, Sharma KV. Turbulent heat transfer and friction factor of Al2o3 Nanofluid in circular tube with twisted tape inserts. *Int J Heat Mass Transf*. 2010;53:1409-1416.
172. Cheng ZD, He YL, Cui FQ. Numerical study of heat transfer enhancement by unilateral longitudinal vortex generators inside parabolic trough solar receivers. *Int J Heat Mass Transf*. 2012;55:5631-5641.
173. Wang P, Liu DY, Xu C. Numerical study of heat transfer enhancement in the receiver tube of direct steam generation with parabolic trough by inserting metal foams. *Appl Energy*. 2013;102:449-460.
174. Soo TYC, Benito R. Enhancing heat transfer in air tubular absorbers for concentrated solar thermal applications. *Appl Therm Eng*. 2013;50(1):1076-1083.
175. Ghadirijafarbeigloo S, Zamzamian AH, Yaghoubi M. 3-d numerical simulation of heat transfer and turbulent flow in a receiver tube of solar parabolic trough concentrator with louvered twisted-tape inserts. *Energy Procedia*. 2014;49:373-380.
176. Waghole DR, Warkhedkar RM, Kulkarni VS, Shrivastva RK. Experimental investigations on heat transfer and friction factor of silver nanofliud in absorber/receiver of parabolic trough collector with twisted tape inserts. *Energy Procedia*. 2014;45:558-567.
177. Xiao X, Zhang P, Shao DD, Li M. Experimental and numerical heat transfer analysis of a V-cavity absorber for linear parabolic trough solar collector. *Energ Conver Manage*. 2014;86:49-59.
178. Jafar KS, Sivaraman B. Thermal performance of solar parabolic trough collector using nanofluids and the absorber with nail twisted Tapes inserts. *Int Energy J*. 2014;14(4):189-198.
179. Huang Z, Yu GL, Li ZY, Tao WQ. Numerical study on heat transfer enhancement in a receiver tube of parabolic trough solar collector with dimples, protrusions and helical fins. *Energy Procedia*. 2015;69:1306-1316.
180. Reddy KS, Ravi KK, Ajay CS. Experimental investigation of porous disc enhanced receiver for solar parabolic trough collector. *Renew Energy*. 2015;77:308-319.
181. Chang C, Xu C, Wu ZY, Li X, Zhang QQ, Wang ZF. Heat transfer enhancement and performance of solar thermal absorber tubes with circumferentially non-uniform heat flux. *Energy Procedia*. 2015;69:320-327.

182. Şahin HM, Baysal EŞ, Dal AR, Şahin N. Investigation of heat transfer enhancement in a new type heat exchanger using solar parabolic trough systems. *Int J Hydrogen Energy*. 2015;40 (44):15254-15266.
183. Jaramillo OA, Mónica B, Velazquez-Lucho KM, Robles M. Parabolic trough solar collector for low enthalpy processes: an analysis of the efficiency enhancement by using twisted tape inserts. *Renew Energy*. 2016;93:125-141.
184. Amina B, Miloud A, Samir L, Abdelylah B, Solano JP. Heat transfer enhancement in a parabolic trough solar receiver using longitudinal fins and Nanofluids. *J Therm Sci*. 2016;25 (5):410-417.
185. Xiangtao G, Wang F, Wang H, Tan J, Lai Q, Han H. Heat transfer enhancement analysis of tube receiver for parabolic trough solar collector with pin fin arrays inserting. *Solar Energy*. 2017;144:185-202.
186. Ghasemi S, Akbar RA. Numerical thermal study on effect of porous rings on performance of solar parabolic trough collector. *Appl Therm Eng*. 2017;118:807-816.
187. Zhu X, Zhu L, Zhao J. Wavy-tape insert designed for managing highly concentrated solar energy on absorber tube of parabolic trough receiver. *Energy*. 2017;141:1146-1155.
188. Zheng L, Xie Y, Zhang D. Numerical investigation on heat transfer performance and flow characteristics in circular tubes with dimpled twisted Tapes using Al_2O_3-water Nanofluid. *Int J Heat Mass Transf*. 2017;111:962-981.
189. Bellos E, Tzivanidis C, Tsimpoukis D. Thermal enhancement of parabolic trough collector with internally finned absorbers. *Solar Energy*. 2017;157:514-531.
190. Bellos E, Tzivanidis C, Daniil I, Antonopoulos KA. The impact of internal longitudinal fins in parabolic trough collectors operating with gases. *Energ Conver Manage*. 2017;135: 35-54.
191. Bellos E, Tzivanidis C, Tsimpoukis D. Enhancing the performance of parabolic trough collectors using nanofluids and turbulators. *Renew Sustain Energy Rev*. 2018;91:358-375.
192. Bellos E, Tzivanidis C, Tsimpoukis D. Optimum number of internal fins in parabolic trough collectors. *Appl Therm Eng*. 2018;137:669-677.
193. Bellos E, Daniil I, Tzivanidis C. Multiple cylindrical inserts for parabolic trough solar collector. *Appl Therm Eng*. 2018;143: 80-89.
194. Bilal FR, Arunachala UC, Sandeep HM. Experimental validation of energy parameters in parabolic trough collector with plain absorber and analysis of heat transfer enhancement techniques. *J Phys Conf Ser*. 2018;953(1):10.
195. Okonkwo EC, Abid M, Ratlamwala TAH. Effects of synthetic oil Nanofluids and absorber geometries on the Exergetic performance of the parabolic trough collector. *Int J Energy Res*. 2018;42(11):3559-3574.
196. Kurşun B. Thermal performance assessment of internal longitudinal fins with sinusoidal lateral surfaces in parabolic trough receiver tubes. *Renew Energy*. 2019;140:816-827.
197. Malekan M, Khosravi A, Syri S. Heat transfer modeling of a parabolic trough solar collector with working fluid of Fe_3O_4 and CuO/therminol 66 nanofluids under magnetic field. *Appl Therm Eng*. 2019;163:114435.
198. Isravel S, Raja RM, Saravanan S, Vijayan V. Thermal augmentation in parabolic trough collector solar water heater using rings attached twisted Tapes. *Mater Today Proc*. 2019;21: 127-129.
199. Liu P, Lv J, Shan F, Liu Z, Liu W. Effects of rib arrangements on the performance of a parabolic trough receiver with ribbed absorber tube. *Appl Therm Eng*. 2019;156:1-13.
200. Valizade M, Heyhat MM, Maerefat M. Experimental study of the thermal behavior of direct absorption parabolic trough collector by applying copper metal foam as volumetric solar absorption. *Renew Energy*. 2020;145:261-269.
201. Bader R, Haueter P, Pedretti A, Steinfeld A. Optical design of a novel two-stage solar trough concentrator based on pneumatic polymeric structures. *J Solar Energy Eng*. 2009;131(3): 31007.
202. Wang K, He YL, Cheng ZD. A design method and numerical study for a new type parabolic trough solar collector with uniform solar flux distribution. *Sci China Technol Sci*. 2014;57(3): 531-540.
203. Fuqiang W, Qingzhi L, Huaizhi H, Tan J. Parabolic trough receiver with corrugated tube for improving heat transfer and thermal deformation characteristics. *Appl Energy*. 2016;164: 411-424.
204. Wang Y, Liu Q, Sun J, Lei J, Yi J, Jin H. A new solar receiver/reactor structure for hydrogen production. *Energ Conver Manage*. 2017;133:118-126.
205. Bitam EW, Demagh Y, Hachicha AA, Benmoussa H, Kabar Y. Numerical investigation of a novel sinusoidal tube receiver for parabolic trough technology. *Appl Energy*. 2018;218:494-510.
206. Liang H, Zhu C, Fan M, You S, Zhang H, Xia J. Study on the thermal performance of a novel cavity receiver for parabolic trough solar collectors. *Appl Energy*. 2018;222:790-798.
207. Peralta NR, Gleckman P. The engineering design of a high-performance parabolic trough collector using lumber for the support structure. *Solar Energy*. 2019;191:382-399.
208. Li X, Chang H, Zheng Y, Shu S, Duan C. Thermal performance analysis of a novel linear cavity receiver for parabolic trough solar collectors. *Appl Energy*. 2019;237:431-439.
209. Wang Q, Hu M, Yang H, et al. Performance evaluation and analyses of novel parabolic trough evacuated collector tubes with spectrum-selective glass envelope. *Renew Energy*. 2019; 138:793-804.
210. Kulahli MC, Akbulut ÖS, Etemoglu AB. Numerical simulation of a parabolic trough collector containing a novel parabolic reflector with varying focal length. *Appl Therm Eng*. 2019;161:114210.
211. Ferraro, V, J Settino, M A. Cucumo, and D Kaliakatsos. Parabolic Trough System Operating with Nanofluids: Comparison with the Conventional Working Fluids and Influence on the System Performance; 2016.
212. Abid M, Ratlamwala TAH, Atikol U. Solar assisted multi-generation system using nanofluids: a comparative analysis. *Int J Hydrogen Energy*. 2017;42(33):21429-21442.
213. Mwesigye A, Yılmaz İH, Meyer JP. Numerical analysis of the thermal and thermodynamic performance of a parabolic trough solar collector using SWCNTS-Therminol®vp-1 nanofluid. *Renew Energy*. 2018;119:844-862.
214. Mwesigye A, Huan Z, Meyer JP. Thermal performance and entropy generation analysis of a high concentration ratio parabolic trough solar collector with cu-Therminol®vp-1 Nanofluid. *Energ Conver Manage*. 2016;120:449-465.

215. Ghasemi SE, Ranjbar AA. Thermal performance analysis of solar parabolic trough collector using nanofluid as working fluid: a CFD modelling study. *J Mol Liq*. 2016;222:159-166.
216. Wang Y, Xu J, Liu Q, Chen Y, Liu H. Performance analysis of a parabolic trough solar collector using Al_2O_3/synthetic oil nanofluid. *Appl Therm Eng*. 2016;107:469-478.
217. Alashkar A, Gadalla M. Thermo-economic analysis of an integrated solar power generation system using nanofluids. *Appl Energy*. 2017;191:469-491.
218. Bellos E, Tzivanidis C. Parametric investigation of nanofluids utilization in parabolic trough collectors. *Therm Sci Eng Progr*. 2017;2:71-79.
219. Paul TC, Khan JA, Morshed AKMM, Fox EB. Enhanced Thermophysical properties of Neils as heat transfer fluids for solar thermal applications. *Appl Therm Eng*. 2017;110:1-9.
220. Khakrah H, Shamloo A, Hannani SK. Determination of parabolic trough solar collector efficiency using nanofluid: a comprehensive numerical study. *J Solar Energy Eng Trans ASME*. 2017;139.5:051006.
221. Allouhi A, Benzakour AM, Saidur R, Kousksou T, Jamil A. Energy and exergy analyses of a parabolic trough collector operated with nanofluids for medium and high temperature applications. *Energ Conver Manage*. 2018;155:201-217.
222. Aguilar T, Navas J, Gallardo JJ, et al. Investigation of enhanced thermal properties in Nio-based nanofluids for concentrating solar power applications: a molecular dynamics and experimental analysis. *Appl Energy*. 2018;211:677-688.
223. Alashkar A, Gadalla M. Performance analysis of an integrated solar-based power generation plant using nanofluids. *Int J Energy Res*. 2018;42(9):2875-2900.
224. Bellos E, Tzivanidis C, Tsimpoukis D. Thermal, hydraulic and Exergetic evaluation of a parabolic trough collector operating with thermal oil and molten salt based nanofluids. *Energ Conver Manage*. 2018;156:388-402.
225. Khakrah H, Shamloo A, Kazemzadeh HS. Exergy analysis of parabolic trough solar collectors using Al_2O_3/synthetic oil nanofluid. *Solar Energy*. 2018;173:1236-1247.
226. Kasaiean A, Sameti M, Daneshazarian R, Noori Z, Adamian A, Ming T. Heat transfer network for a parabolic trough collector as a heat collecting element using nanofluid. *Renew Energy*. 2018;123:439-449.
227. Ebrahimi-Moghadam A, Mohseni-Gharyehsafa B, Farzaneh-Gord M. Using artificial neural network and quadratic algorithm for minimizing entropy generation of Al_2O_3-Eg/w nanofluid flow inside parabolic trough solar collector. *Renew Energy*. 2018;129:473-485.
228. Razmmand F, Mehdipour R, Mousavi SM. A numerical investigation on the effect of nanofluids on heat transfer of the solar parabolic trough collectors. *Appl Therm Eng*. 2019;152:624-633.
229. Korres D, Bellos E, Tzivanidis C. Investigation of a nanofluid-based compound parabolic trough solar collector under laminar flow conditions. *Appl Therm Eng*. 2019;149:366-376.
230. Abed, N., Afgan, I., Nasser, A., Iacovides, H., Cioncolini, A. and Meakhail, T. Numerical investigations of parabolic trough collectors using different nanofluids. Proceedings of 5th International Conference on Energy Engineering, December 24–26, 2019, Aswan-Egypt.
231. Bozorg MV, Hossein DM, Hong K, Xiong Q. CFD study of heat transfer and fluid flow in a parabolic trough solar receiver with internal annular porous structure and synthetic oil-Al_2O_3 nanofluid. *Renew Energy*. 2020;145:2598-2614.

How to cite this article: Abed N, Afgan I. An extensive review of various technologies for enhancing the thermal and optical performances of parabolic trough collectors. *Int J Energy Res*. 2020; 1–46. https://doi.org/10.1002/er.5271